ABSTRACT

Title of Thesis:	MODELING CONTROL STRATEGIES OF A HIGH-PERFORMANCE ENERGY RECOVERY VENTILATOR IN NIST'S NET ZERO ENERGY RESIDENTIAL TEST FACILITY
	Andrew MacLean Shore, Master of Science in Mechanical Engineering, 2025
Thesis Directed By:	Research Professor Yunho Hwang, Ph.D. Department of Mechanical Engineering

With the acceleration of climate change causing increased global temperatures, reduced polar ice caps, and more severe weather, reducing carbon emissions is more important than ever. Residential buildings are responsible for 57 % of the greenhouse gas emissions in the building sector. This sector provides a clear opportunity to reduce emissions and energy consumption. Net Zero Energy Buildings (NZEB) are a more recent answer to this need where the building generates more energy over a year than it consumes through renewable sources. NIST's Net Zero Energy Residential Test Facility (NZERTF) was constructed and instrumented to serve as a test bed for NZEB research at the residential scale. This facility has a previously uncharacterized Energy Recovery Ventilator with opportunities to implement a bypass mode to avoid

any heat exchange between the fresh and stale air streams. This bypass mode allows for free cooling in the shoulder seasons by using cooler outdoor air to cool the inside of the building. To test the energy savings potential for temperature-based and enthalpic-free cooling control schemes, a TRNSYS model was updated and tuned to accommodate more recent building performance and shifting operation patterns. These updates included heat pump performance curves, adjustments to HVAC airflow modeling, moisture capacitance models, and a complete evaluation of the ERV's fan power and sensible and latent effectiveness. This model was run for annual simulations without bypass mode, with bypass mode enabled based on the outdoor temperature, and with bypass mode based on the outdoor enthalpy. The temperature-based control required an additional 2.4 % of heat pump energy relative to the baseline along with a slight degradation in thermal comfort. The enthalpic control saved 0.2 % and maintained a similar thermal comfort to the no bypass mode case. These bypass controls do not offer significant opportunities for this facility in this climate zone but could be implemented in lower-humidity climates or more extensive facilities with more substantial sensible loads. I plan to continue this work by testing the enthalpy bypass control at the NZERTF, characterizing, modeling, and testing bypass options with the ventilator's HRV core, and by integrating CONTAM into the TRNSYS model to improve the airflow modeling for more accurate zone level conditions.

MODELING CONTROL STRATEGIES OF A HIGH-PERFORMANCE ENERGY RECOVERY VENTILATOR IN NIST'S NET ZERO ENERGY RESIDENTIAL TEST FACILITY

by

Andrew MacLean Shore

Thesis submitted to the Faculty of the Graduate School of the
University of Maryland, College Park, in partial fulfillment
of the requirements for the degree of
Master of Science
2025

Advisory Committee:
Research Professor Dr. Yunho Hwang, Chair
Dr. Bao Yang
Dr. Damena Agonafer
Dr. William Healy

Acknowledgments

I would like to thank my advisor, Dr. Yunho Hwang for his guidance, advice, and perspective as I have planned my coursework and developed this research over the past 2.5 years. I also greatly appreciate the time and effort that my committee members, Dr. Bao Yang, Dr. Damena Agonafer, and Dr. William Healy, each gave to evaluate my work. I have learned a great deal from each of you.

I greatly appreciate my colleagues at NIST who supported me through this research. Dr. Behrang Hamadani provided constant support and encouragement. Brian Dougherty offered his vast knowledge and experience with the NZERTF, was willing to discuss the TRNSYS model, and made the facility accessible for testing. Thank you to Dr. Harrison Skye for the nudge into learning the TRNSYS model and Dongsoo Jang for helping to familiarize myself with the original NZERTF model. I have learned a tremendous amount from each of you which has given me a new skill to assist with research on NZEBs.

A quick recognition to Muhammad Tauha Ali for their MATLAB SI Psychrometric chart plotting tool that likely saved me countless hours trying to effectively plot thousands of points onto a psychrometric chart.

Most importantly, I want to recognize and thank my family and friends who have supported me and cheered me on along the way. My wife, Allison Rollins, has been my biggest supporter offering her unwavering love, kindness, and patience as I worked on my thesis. Her empathy, compassion, and grace are everything to me and kept me sane through grad school. I love you.

Table of Contents

List of Tables

List of Figures

Nomenclature

ASHRAE: American Society of Heat, Refrigeration, and Air Conditioning Engineers

BAS: Building Automation System

CFM: Cubic Feet per minute

DHW: Domestic Hot Water

DOAS: Dedicated Outdoor Air System

EMS: Energy Management System

ERV: Energy Recovery Ventilator

HRV: Heat Recovery Ventilator

HVAC: Heating Ventilation and Air Conditioning

LED: Light Emitting Diode

NIST: National Institute of Standards and Technology

NZEB: Net Zero Energy Building

NZERTF: Net Zero Energy Residential Test Facility

PV: Photovoltaic

SHW: Solar Hot Water

TRNSYS: Transient System Simulation Tool

Chapter 1: Introduction

Earth's global temperature has increased by 1.5 degrees Celsius in the last one hundred years [1]. The planet's temperature has also risen more rapidly in the last 30 years than at any point in the last one hundred and fifty years [2]. A significant factor in the rapid global climate change is a marked increase in greenhouse gas emissions, particularly carbon dioxide (CO_2), coinciding with the industrial revolution. In 1911 the atmospheric concentration of CO_2 reached a peak of 300 ppm for the first time in the 800,000 years of cataloged atmospheric carbon dioxide ice core measurements [3]. The atmosphere's concentration has only risen – from 320 ppm to 425 ppm in the last 70 years [3].

The increased global temperature due to higher atmospheric greenhouse gas concentrations also leads to a variety of climate issues. These include the arctic ice shrinking by 12 % per decade [4], increased precipitation [2], ocean level rise [5], and more natural disasters [6]. As the climate becomes more extreme, not only are the natural environments threatened, but so are human populations in equatorial and polar regions more heavily impacted by climate change [7]. With all these climate concerns, mitigating carbon emissions is critical socially and environmentally.

1.1. *Background*

Over 80 % of United States energy comes from fossil fuels in the form of petroleum, natural gas, and coal (see Figure 1) [8]. The building energy sector is a

significant energy consumer and carbon emitter, using 28 % of annual end-use energy in the United States every year as shown in Figure 2. More than half of that energy is consumed in residential homes with about 50 % of home energy use coming from fossil fuels like natural gas for space heating and water heating. The residential fossil fuel use is equivalent to 339 million metric tons of CO_2 per year or 57 % of United States building greenhouse gas (GHG) emissions [9].

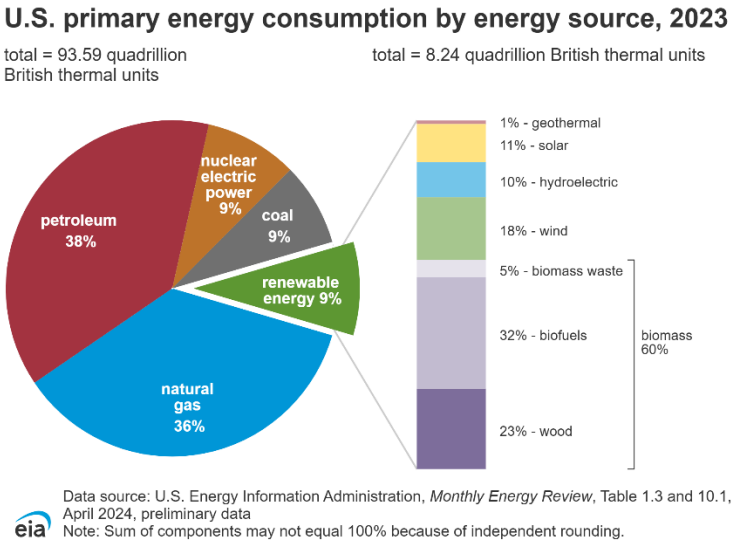

Figure 1. United States Primary Energy Consumption in 2023 [8].

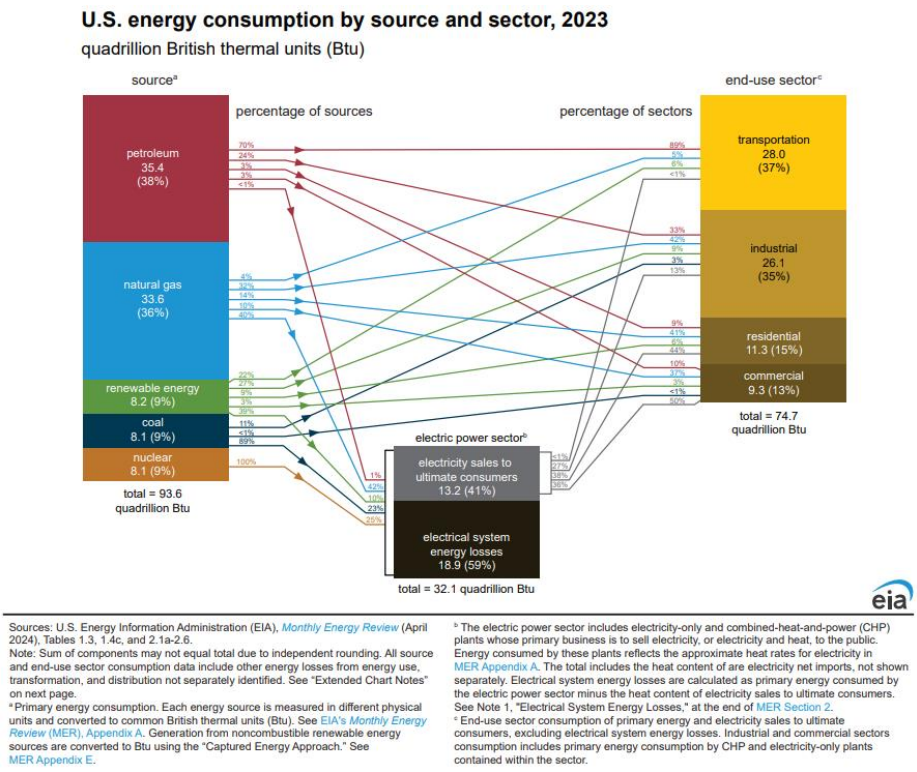

Figure 2. United States energy consumption diagram from source energy to sector energy in 2023 [8]**.**

Reducing fossil fuel use in residential settings could assist in reducing the country's total GHG emissions tremendously. We have already noticed a decrease in total residential energy use relative to population growth. This is mostly due to minimum appliance energy efficiency standards as instituted by laws like the United States Energy Independence and Security Act of 2007 [10] or localities adopting improved building energy codes like IECC or ASHRAE standards necessitating technological advances (e.g., improving from incandescent lamps to fluorescent lamps to light emitting diode lamps). These laws and codes aim at common energy efficiency improvements like improved insulation or more efficient equipment to

assist in reducing the total energy demand. While this initiative does reduce site energy use, it does not provide the potential to eliminate carbon emissions. From a site energy perspective, building electrification is a necessary step that requires shifting from combustion heating systems to electrical heating systems. The best option at this time is some form of a heat pump system that typically provides about three times as much heating or cooling energy as electricity put into the system [2].

Electrification is a critical step for reducing emissions, but if the electricity's source energy is still mostly coming from fossil fuel combustion Rankine Cycle or heat engine power plants, then our residential energy use is still reliant on fossil fuels. Instead, we can begin to look at renewable energy sources. In the case of a single-family home, on-site solar power installed onto the building's roof is a natural solution as there is plenty of areas to install a photovoltaic (PV) system to power a low-load building for an entire year [11], [12], [13], [14].

Integrating all these measures together results in one particularly appealing option: net-zero energy or positive energy buildings. The goal of these buildings is to generate just as much or more energy through on site sources like solar or wind energy as they consume for operating the building over the course of one year. Increasing the proportion of these homes in the residential building stock has the potential to significantly reduce energy consumption and greenhouse gas emissions in the United States [15], [16]. As such, in 2024 the United States Department of Energy released a blueprint to completely remove carbon emissions from the building sector

with an emphasis on further improving building energy efficiency and reducing site carbon emissions [17].

1.2. *Net-Zero Energy Buildings*

While not a prevalent design in United States residential single housing stock, NZEBs are swiftly increasing in construction across the country. NZEB construction projects doubled from 2018 to 2020 alone and the rate of construction has been increasing at a constant rate [18]. Additionally, considerations for NZEBs are being added to standards like the American Society of Heating Refrigeration and Air Conditioning Engineers' (ASHRAE) newest standard for residential buildings, 90.2 – 2024, or Standard 228 for evaluating net zero energy and net zero carbon buildings [19], [20]. Standard 90.2 requires reduced infiltration and minimum building envelope standards if renewable on-site energy is being utilized as an emphasis on reducing the building's thermal load. This standard also requires energy storage capacity if renewable energy is used on-site. Energy storage can save further energy by reducing grid reliance when renewable energy generation drops off, e.g. PV array no longer produces energy after the sun sets.

As mentioned in section 1.1, these buildings have two main methods of achieving net zero energy: reduce the loads required in the home and provide an on-site energy source, typically through renewable energy. Load reduction can be accomplished in several different ways including improving the building envelope to lower the building's overall heat transfer (UA) and infiltration, improving equipment

efficiency like using a heat pump for heating, ventilation, and air conditioning (HVAC) and domestic hot water (DHW) supply, using light-emitting diode (LED) lighting, and installing high-efficiency appliances [21]. Adding all these components together can result in a building design that, when solar energy is also utilized, can easily become net-zero energy [12], [13]. This solar energy can be in the form of both PV arrays for electricity production and solar thermal collectors for DHW preheating.

Along with greatly reducing the site energy, the building will also be fully electrified and only pull electricity from the grid when solar power is insufficient. As the grid becomes less dependent on fossil fuels, the building will also have an even smaller carbon footprint.

1.2.1 NZEB Residential Control Strategies

The building operation must be taken into consideration to more reliably achieve net-zero energy use. Optimum control of the space conditioning is necessary to limit thermal loads and, therefore, heat pump energy use [14], [22]. On a commercial scale, a Building Automation System (BAS) or Energy Automation System (EMS) is typically used to ensure that energy use and human comfort are appropriately managed. This system autonomously follows a schedule to reduce energy use for the given temperature set points, lighting schedule, etc. On a residential scale, this sort of system is not as pervasive. 72.5 % of single-family residences include a thermostat with one temperature sensor in the home, and one-third of those thermostats aren’t programmable at all [23]. These thermostats

generally turn on or off the heating or cooling source and fan (if applicable) with little other automated control. Additionally, most residences utilize single air volume equipment with only one fan speed and one compressor speed for vapor compression cycles. But when used, smart thermostats and more accessible IoT devices are proving to be effective options to improve control of various rooms or zones in a residential home while also saving energy [24].

1.2.2 NIST's Net-Zero Energy Residential Test Facility

Starting in 2013, the National Institute of Standards and Technology began operating and testing the performance of its Net Zero Energy Residential Test Facility (NZERTF). The NZERTF is a 4-bedroom, 3-bathroom residential house designed to achieve net zero energy use over the course of one year. It includes a data acquisition and control system to measure and simulate the use of a residential home by two adults and two children without any real people living in the home. This setup allows for repeatable and reliable measurements. The controls include the usage of appliances, lights, plug loads, water, and HVAC systems on a set schedule. NIST's team showed that reaching net zero energy was achievable [13] over the course of two separate twelve-month studies from July 1, 2013 to June 30, 2014 [25] and February 1, 2015 to January 31, 2016 [26]. The team also found a few specific control strategies that helped to further reduce energy consumption in the second twelve-month study. These strategies included a temperature and humidity-based HVAC control scheme without any timing-based control which reduced operation time and

reduced the heat recovery ventilator fan run time to minimally meet ASHRAE Standard 62.2 compliance [13].

Figure 3. Photograph of NIST's Net Zero Energy Residential Test Facility.

With the data from these two test years, Balke and Leyde both modeled this building in TRNSYS [27], [28] for their theses. It has also been modeled in EnergyPlus by Kneifel et al. [29], [30] While not a direct replacement for field measurements, this software has allowed for various equipment and control options to be evaluated in the home more quickly [14], [22]. This is particularly helpful when considering a significant piece of equipment (like a heat pump) or a complex control change. Some of these findings include the energy savings associated with a ground-source heat pump over an air-source heat pump, tradeoffs between thermal comfort with dedicated dehumidification for the heat pump versus dehumidification with the heat pump, and the energy savings benefits of using an energy recovery ventilator instead of a heat recovery ventilator or no heat recovery [14], [22].

The building's HVAC system is highly customizable with a wide variety of equipment available to control including a variable speed air-source heat pump option, a two-stage air-source heat pump with dehumidifying setting, and electrical resistance emergency heat, a dedicated whole-house dehumidifier, a standard duct system with 36 controllable dampers, a small duct high-velocity system, whole house humidifiers, and a recovery ventilator that can have either a heat recovery or energy recovery core inserted. The building's thermostat and humidistat can interface and control any of this equipment while simultaneously accessing temperatures and humidities throughout the house. For example, the first floor living room temperature and humidity sensors can be utilized for a zone while the temperature and humidity sensors in the owner's bedroom on the second floor can be used for a second zone. The thermostat will dictate when the two-stage air source heat pump will either be off, first-stage heating or cooling, second-stage heating or cooling, electric heat, or dehumidify based on the measured temperatures and humidities in the two rooms. Dampers assigned to each zone will open or close depending on if the zone's temperature and humidity is satisfied. The temperature and humidity settings can be changed throughout the day and each stage of heating/cooling also has a specific deadband to limit cycling the heat pump.

1.3. *Energy Recovery Ventilation*

A well-designed NZEB's envelope is typically very tight to minimize thermal load due to outdoor air infiltration [13]. Mechanical ventilation is required as

specified by ASHRAE Standard 62.2 [31] to maintain sufficient indoor air quality for occupants in these buildings. This constant ventilation adds an additional thermal load to the space conditioning system. To reduce the added load of bringing in outdoor air, various systems can be used to pre-condition the outdoor air and limit the energy required for space conditioning.

On the commercial scale, a Dedicated Outdoor Air System (DOAS) can be used to bring in the necessary outdoor air for an entire building. This system preconditions the air with either a vapor compression cycle or a heater. Adding either a heat or energy wheel upstream can assist in preconditioning the outdoor air. This wheel slowly rotates as return air is exhausted through one half of the wheel and outdoor air is supplied through the other half (see Figure 4). A heat wheel allows for efficient sensible heat exchange, while the energy wheel also includes a desiccant so that latent exchange can occur and reduce the latent load.

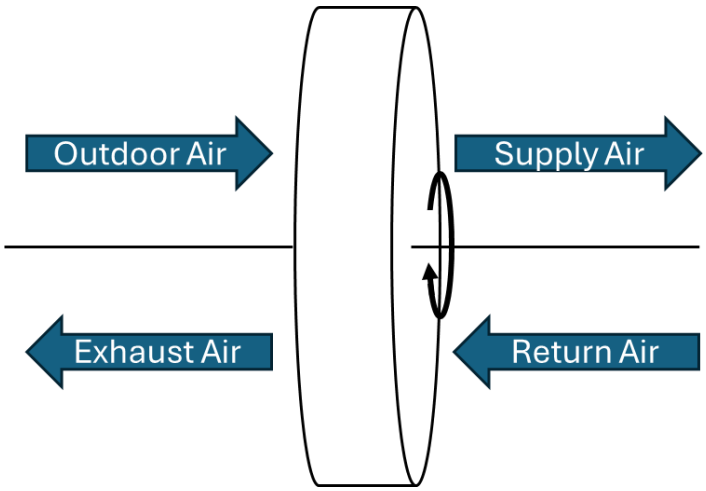

Figure 4. Heat or Energy Recovery Wheel. Fresh and Exhaust Air is exchanged via a rotating wheel.

For residential applications, Heat Recovery Ventilation (HRV) systems, shown in Figure 5, can be used to reduce the space conditioning sensible load by blowing the outdoor air and the return air through a fixed membrane for sensible heat exchange. This equipment prevents the air streams from interacting but allows for sensible heat transfer to occur. Its ability to reduce heat pump load greatly depends on the climate zone. An HRV performs very well in dry climates where there is little opportunity to introduce latent loads into the home, but its benefits are reduced in more humid environments [14]. The total cooling season load may increase due to the added humidity from outdoor conditions using an HRV in a mixed-humid climate, but this is generally offset by the significant heating season savings. [32]. An Energy Recovery Ventilation (ERV) takes this a step further by either adding a desiccant to the core like the energy wheel or using a membrane that only allows moisture to travel between the air streams. These alterations allow for a latent energy exchange where moisture is either added or removed to the outdoor air depending on the humidity ratios of the outdoor and return air streams. Reducing the latent load further reduces energy use [33].

Running an ERV can lead to upwards of 30 % savings in space conditioning in more extreme climate zones, but less in more temperate regions [22], [34], [35]. In particularly cold zones, a defrost cycle is required to ensure the ERV core does not freeze, which limits the high potential for savings [34]. Additionally, the ERV introduces a slightly higher heating load than an HRV during heating season as the latent exchange limits the sensible exchange [28]. More temperate climate zones

show less energy savings due to a smaller temperature or enthalpy difference between the setpoint and outdoor [14], [35], [36]. Another limitation to energy savings includes a reduction in space conditioning operation due to occupancy-based control as seen in schools or office buildings [37], [38]. The system's effectiveness is also dictated by several factors including the climate zone (dry bulb and wet bulb temperatures), air flow rate, and design temperature [39]. All these factors lead to the need for a control scheme to be considered for optimized ERV operation.

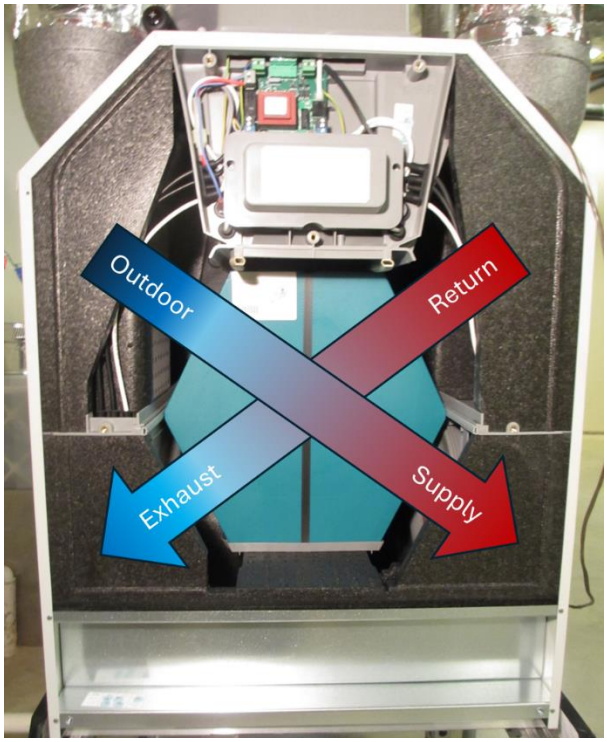

Figure 5. Inside of Heat or Energy Recovery Ventilator with fresh air and exhaust air streams exchanging sensible heat (and latent heat for energy recovery) without the air streams mixing.

1.3.1 Residential NZEB ERV Control

For residential low-load homes, the expectation is that a mechanical ventilation system will run to meet ASHRAE 62.2. This can be achieved by either constantly running or running intermittently to achieve the necessary air change rate each hour. But, as mentioned in 1.3, running an ERV constantly can still add a cooling load at certain times during swing seasons [33]. This load can be either sensible or latent depending on the climate and weather conditions. This means that both the temperature and humidity would ideally be tracked to determine the best times to minimize sensible or latent heat recovery.

1.3.2 Residential Free Cooling

More complex control schemes for an HRV or ERV are necessary to reduce the cooling load if the outdoor enthalpy decreases to below the return air enthalpy while in the cooling season. Under these conditions, the enthalpy of the outdoor air increases as it moves through the ERV core resulting in a more significant cooling load. These are the times when we can take advantage of "free cooling" or disabling vapor compression cooling and ventilating the space with the available cooler outdoor air by bypassing the energy recovery system. Naturally, free cooling opportunities are very dependent on the local climate and how the controls are handled. It has been well documented that the implementation of temperature or enthalpy-based controls for free-cooling significantly impacts the sensible and latent loads introduced to the house. A temperature-based control carries a risk given that it is not considering the

added latent loads that may be directly added to the house. In these cases, especially in humid climates, the humid outdoor air can increase the latent load by over 10 % [36]. With the increase in latent load, most of the benefits of free cooling are negated seeing a net savings in cooling demand of maybe 1 % or 2 %. However, free cooling is much more beneficial in cooler climates resulting in potentially 20 % savings on cooling load relative to constant operation of the ERV [37], [40]. Increasing the flow rate during free cooling and utilizing equipment with both a sensible core and an enthalpy core can be even more beneficial and potentially yield up to 40 % in colder climates [40].

Each building is unique in terms of its envelope, climate, ERV equipment, and control scheme. Varying any of these parameters leads to a significant change in savings potential. This is apparent in the above works, [37], [40], where [37] utilized a temperature-based ERV control to determine when to bypass energy recovery while [40] considered both the temperature and the humidity for the outdoor, indoor, and supply air streams. These findings suggest a bigger potential when including humidity-based controls in the scheme, but this has not been done for a low-load residential home in ASHRAE climate zone 4A like the NZERTF.

1.4. *Research Objectives*

The benefits of using an ERV are well understood under a range of conditions. However, there are times when an ERV introduces a thermal load into the home. This increased load typically occurs during swing seasons when cooling is needed during

the day, but the outdoor temperature is below the cooling setpoint at night. In fact, up to a third of the cooling time, the ERV introduces additional cooling load due to these effects [41]. There are significant opportunities for free cooling when the outdoor air can cool the home without a vapor compression cycle, in climates with warm weather. Free cooling tests have been run at the NZERTF, but scheduling conflicts have prevented a full measurement period throughout the cooling season.

A temperature-based and enthalpy-based control will be evaluated with a TRNSYS model of the National Institute of Standards and Technology's Net-Zero Energy Residential Test Facility (NZERTF). The baseline energy model will be discussed in Chapter 2. Neither the current ERV installed at the NZERTF nor the current thermostat logic have been characterized in the TRNSYS model. The model will be updated to accommodate these newer components of the facility as discussed in 2.2. In section 2.3 these components will be tuned using real-time data from the facility to better inform these potential control strategies. Chapter 3 will investigate a temperature-based control algorithm for free cooling that was implemented for approximately one month in the early summer of 2024 and will be used to further tune the model. A potential enthalpy-based control scheme will be investigated and simulated in Chapter 4 before comparing the temperature and enthalpy-based controls in Chapter 5. These controls will help to inform optimized performance of a residential low-load home in climate zone 4A [42] to minimize energy use while ensuring environmental quality with low humidity and sufficient outdoor air.

Chapter 2: NZERTF Energy Model

NIST's NZERTF has two years of real-time data showing the facility's energy use performance. This has allowed students to tune a TRNSYS model for future use. However, this model has not been updated with more recent house operations like the updated thermostat controls or to accommodate new equipment like the building's mechanical ventilation system with heat or energy recovery options. The base model is summarized below with updates to the model Types summarized in the section 2.2 and tuning adjustments described in the section 2.3.

2.1 Base Model Summary

Leyde and Balke both used the NZERTF year 1 dataset to create and tune a TRNSYS model for the NZERTF [27], [28]. Wu et. al. continued work with this model by evaluating theoretical HVAC configurations at the NZERTF as well as evaluating the impact of different climates [14], [22]. In this section, I will summarize this TRNSYS model and note any sections where adjustments must be made when tuning the system.

2.1.1 Building Envelope

The NZERTF was designed with a very tight building envelope that includes robust thermal insulation and minimal infiltration. The building model was previously created in TRNBuild based on the architectural drawings for a Type 56 multizone building. This software automatically calculates the thermal resistance of the walls

and develops an effective UA. Balke described how the UA value, thermal capacitance, and moisture capacitance of each floor were adjusted based on performance relative to the first 12-month study [28].

The thermal and moisture capacitance values were calculated based on ASHRAE handbook calculations, which considered the building materials of the home. The thermal capacitance was later increased based on real performance during the first 12-month study to approach values typically associated with a fully furnished home, unlike the test facility. The moisture capacitance was modeled with a simple capacitance model that considers only the mass of water in the air and the building material in the zone with the least diffusion resistance. In this house, the gypsum board was selected as the material with the lowest diffusion resistance. The resulting values for each zone are shown below in Table 1.

Table 1. Summary of Key Building Envelope Values

Zone	UA (kW/K)	Thermal Capacitance (kJ/K)	Moisture Capacitance Ratio
1 (basement)	0.201	11951	2.2
2 (first floor)		12000	2.2
3 (second floor)		9638	2.2
4 (attic)		147	1

The building is also modeled with an equivalent infiltration area of 244 cm^2 which is divided between the first floor (zone 2) and second floor (zone 3) based on the ratio of each zone to the total volume of zones 2 and 3. This leakage area results in an average of between 0.03 h^{-1} to 0.07 h^{-1} air volume changes in the facility. This

matches the blower door test done at the facility about 13 years ago that yielded an equivalent air change rate of 0.03 h^{-1}.

2.1.2 Loads & Schedule

The NZERTF is not occupied by any actual people. Instead, a family of four is simulated through the control of appliance electronics, solenoid valves for water use, and heat lamps and humidifiers to emulate human sensible loads and latent heat loads. Each load and emulation are detailed in the following sections. The base schedule for the two initial year-long studies was based on typical homeowner appliance, plug load, and water usage as described by Omar and Bushby [43].

2.1.2.1 Occupancy

The standard schedule that was used in the year 1 and year 2 test periods is outlined in Omar and Bushby [43]. The two parents in the virtual family go to work each weekday and the two children leave for school. Over the weekend the entire family remains in the home. The NZERTF building control allocates a resistance heat lamp on the first and second floors for each occupant. Parent A is in the owner's bedroom or kitchen, Parent B is in the owner's bedroom or the dining room, Child A is in bedroom 2 or the living room, and Child B is in bedroom 3 or the dining room. The corresponding heat lamps turns off or on to emulate occupancy on each floor. The TRNSYS model only considers the location of each virtual family member based on the zone or floor of the building. Two humidifiers are also located in the kitchen that emulate the latent loads generated by both the occupants and cooking in the

kitchen. They run on a set schedule to draw the appropriate volume of water corresponding to the latent load.

2.1.2.2 Electrical Loads

The electrical loads for the house are controlled via a relay panel that turns the relevant load on or off. These loads include the oven and stove, dishwasher, washing machine, dryer, emulators for appliances (TV, Bluetooth, kitchen appliances), and lighting. Details of their control and scheduling are outlined by Omar and Bushby [43]. These loads were divided into sensible and latent load contributions based on NREL's simulation protocols [44].

2.1.2.3 Water Use

The water use at the house is controlled by solenoid valve opening faucets in the kitchen sink, the owner's bedroom shower and bath, and the second-floor hall bathroom shower and sink. These valves open at prescribed times and close when the correct water mass has been measured on a scale. The standard schedule includes between 225 L and 300 L of water usage per day composed of a blend of hot and cold water.

2.1.3 HVAC

2.1.3.1 Air-source Heat Pump

The NZERTF has been predominantly conditioned using a 2-ton Aaon heat pump with a 2-stage compressor, 2 fan speeds, and electrical resistance emergency heat. The system comes with a dedicated dehumidification mode that can be run or

disabled with a separate whole-house dehumidification system in operation. For this work, I considered the heat pump system with its dedicated dehumidification option to manage humidity control. The TRNSYS model includes 3 type 922 heat pumps to emulate the Aaon performance. One handles stage 1 and stage 2 heating and cooling, another handles dedicated dehumidification mode, and the third handles emergency heat operation. The same low-speed and high-speed heating and cooling performance curves were used for all 3 models, but the nominal capacity, speed, and power draw data were adjusted for each. Details for these parameters are listed in Appendix I.

2.1.3.2 Air Distribution/Zoning

The building model is split into 4 zones divided by the floors of the house: basement, first floor, second floor, and attic. Zone 1 was assumed to only have air supplied from the HVAC system with no return air or interaction with other zones. Zone 4 is assumed to have no air supplied or returned from it and infiltration is also neglected. Zones 2 and 3 are where most of the HVAC supply is directed and all the HVAC and ERV return flow is from these two zones. The difference between supply and return flows for the two zones is assumed to move to the zone with a smaller net flow. The exact flows supplied to and returned from each zone are outlined below in Table 2.

Table 2. Fraction of Supply and Return Airflows for each Zone

Zone	Heat Pump Supply	Heat Pump Return	HRV Supply	HRV Return
1 (Basement)	0.12	0	0	0
2 (First Floor)	0.553	0.65	0.27	0.33
3 (Second Floor)	0.352	0.35	0.73	0.67
4 (Attic)	0	0	0	0

2.1.3.3 Thermostat Control

The TRNSYS model is based on the original thermostat control for the house. This thermostat considered both the temperature difference between the sensor and the setpoint as well as runtime at a given control stage. First-stage cooling turns on based on a 0.3 °C deadband and will run for 40 minutes before second-stage cooling can be called. The second stage of cooling has a deadband of 2.8 °C. First-stage heating has a 0.1 °C deadband and can run for up to 40 minutes before second-stage heating is called. Second-stage heating's deadband is 1.1 °C and must run for 40 minutes before third-stage emergency heating can be called if a deadband of 3.3 °C is reached. The dehumidification setpoint is 48 %, and the second-stage dehumidification turns on after 6 minutes of runtime for the first-stage dehumidification.

2.1.3.4 Mechanical Ventilation

The most recent energy model utilizes custom Type 1269 equipment to represent and control the ERV [22]. The rated sensible and latent effectiveness are 0.68 and 0.47 respectively. The rated fan power is 60 W at 195 $m^3 h^{-1}$, equivalent to approximately 115 CFM. The latent effectiveness was treated as constant.

Specification data comes from a Venmar AVS E15 ECM ERV. The system's sensible effectiveness and fan power are modeled as a quadratic function of mass flow rate, as outlined in Table 3 relative to the nominal effectiveness, fan power, and flow rate. The effectiveness is calculated as:

$$\varepsilon_{sensible} = \varepsilon_0 \left[c_0 + c_1 \frac{m}{m_0} + c_2 \left(\frac{m}{m_0} \right)^2 \right] \quad (1)$$

and the fan power is calculated in the same fashion:

$$P = P_0 \left[c_0 + c_1 \frac{m}{m_0} + c_2 \left(\frac{m}{m_0} \right)^2 \right] \quad (2)$$

Table 3. Base Model Effectiveness and Fan Power Coefficients

Coefficient	Sensible Effectiveness	Fan Power
c_0	1.103	0.3098
c_1	0.0162	-0.1082
c_2	-0.119	0.7972

2.1.4 Domestic Hot Water

The domestic hot water is partially run by renewable energy in the form of two flat plate solar thermal collectors to preheat the water that is stored in a preheater tank before being supplied to a heat pump water heater. This system does produce loads in the house, but it is not a major emphasis of the work.

2.1.4.1 Solar Hot Water

This solar hot water tank is a preheating tank for the main water heating system and serves as a method of reducing required electrical energy for water heating. It is an active indirect system. The two flat plate collectors are modeled

using two type 539 solar thermal collectors with a surface area of 2.2 m^2. A water-glycol solution is pumped through the collectors based on heating demand determined by a type 2 aquastat controller. The heated glycol solution is run through a heat exchanger and heats up the water in the solar water preheater tank. The flow from the solar hot water tank is also controlled by the aquastat so that heat exchange occurs only when necessary.

2.1.4.2 Water Heating

The model utilizes a heat pump water heater to supplement the solar water heating system and maintain the hot water setpoint. The type 938 heat pump has a total cooling capacity of 1,231 W, a sensible capacity of 1,169 W, and a heating capacity of 2,025 W, with a 794 W compressor. This heat pump water heater is controlled via a controller set to 71 °C to maintain the temperature in an 189 L tank. An auxiliary electrical resistance heater is also used in case the heat pump cannot meet demand. The heat pump will generate a small cooling effect in the basement which has the potential to reduce total cooling capacity needs in the building.

2.1.5 Solar Photovoltaic System

A 10.2 kW photovoltaic array is installed on the main roof of the home comprised of 2 strings of 16 320 W rated modules. The roof has an incline of 18.4 ° and results in a total system efficiency of 18.9 % over the array area. The two string inverters are in the attic or zone 4.

The model calculates the PV generation by using two Type 194a PV with inverter models to simulate the PV generation based on the modules and the incident irradiance fed in from the weather data. The inverter losses from the array are added to the zone 4 sensible gains based on the array power output and the inverter efficiency.

2.2 Updating Model

The NZERTF serves as a facility to validate net-zero energy usage in a residential building and test various equipment and control schema. This means that the house's configuration has shifted and changed over time. Included in this shift is an updated thermostat and a

2.2.1 Thermostat Control

The temperature and humidity control at the NZERTF has undergone several changes through the years. During the original 12-month studies, a commercial thermostat was utilized to control the house's HVAC system as described in 2.1.3.3.

About five years ago a custom thermostat control was built to allow for a wide variety of controls over the 36 dampers, air-source heat pump, and optionally the whole house dehumidifier instead of the heat pump's dedicated dehumidifier. The current thermostat operates based on temperature and humidity differentials without any maximum runtimes. However, there is a 2-minute delay between operating modes to minimize compressor cycling. The temperature dead bands are the same for heating and cooling, typically 0.5 °F / 0.222 °C for the first stage and 1.0 °F / 0.555

°C for the second stage. There is also an emergency electrical resistance third-stage heating with a typical deadband of 1.5 °F / 0.777 °C. The dehumidifier is enabled when the average relative humidity from the chosen group of sensors exceeds a maximum value, e.g., 53 %, and is disabled when the relative humidity is less than or equal to a cutoff value, e.g., 47 %. Second-stage dehumidification is not enabled. The fan is typically controlled in "Auto" mode, which only turns on if there is a cooling, heating, or dehumidification call.

2.2.2 ERV Specifications

A Zehnder ComfoAir 350-R ventilation system is installed at the NZERTF. It comes with two independent fans that adjust the flow rate for the fresh air and exhaust air streams from 29 CFM up to 219 CFM. The system has an effective heat recovery rate of 84 % as certified by the Passive House Institute. The unit comes with two core options. The first is an HRV core of polypropylene plastic channels that allow the fresh and exhaust air streams to remain separate while exchanging heat. It also has an ERV core composed of many layers of a semi-permeable membrane to allow for humidity and heat to be exchanged, but no air. I will be focusing on the ERV core in this thesis, taking advantage of the humidity exchange. This system does have a temperature-based bypass option to prevent heat exchange if the outdoor temperature is less than the desired comfort temperature (e.g. 23 °C) and the return air temperature is greater than the comfort temperature. This feature was not typically

utilized at the NZERTF as the climate temperature was set to 28 °C to reduce latent loads added during the humid summers.

A custom TRNSYS equipment Type 1269 is used in the base model to describe the ERV. Values have been adjusted from previous work, like in [28], to better model the Zehnder ComfoAir equipment. The baseline model uses the manufacturer-provided specification sheet to relate the air flow rate to fan power consumption as shown in Table 4. A constant heat recovery rate of 84 % was used for the un-tuned model based on the Passive House Institute certification. No humidity recovery rate or effectiveness was provided, so the same 0.47 value from the previous base model using the Venmar ERV system was used. Specifications also report frost protection for the heat exchanger with constant fresh air down to -15 °C. Each fan's power draw is a polynomial function with the flow rate as the input of the same form as in the equation 2. The sensible and latent effectiveness values are assumed constant due to a lack of further detail in the specification data. More detailed relationships to determine the sensible and latent effectiveness and fan power based on measured system performance are outlined in 2.3.4 and 2.3.5.

Table 4. Nominal ERV Specifications

Effectiveness		**Fan Power vs. Mass Flow**	
Sensible	Latent	P_0 (W)	19.01
0.84	0.47	m_0 (kg/h)	204.8
		c0	0.794
		c1	-1.555
		c2	-2.147
		c3	0.7225

2.2.3 Weather Data, Schedule Changes & Loads

While the schedule and load files created from the 2013-2014 model are incredibly useful for performing analyses when a typical family of four may reside in the home, the facility has been operated a little differently in the last few years as different subsystems are tested.

The weather data must be updated to properly tune and adjust for recent operations. We measure outdoor dry bulb air temperature, outdoor dewpoint, wind speed, and wind direction at the NZERTF and record this data every minute. The local Montgomery County Airport, KGAI, records the remaining model weather drivers: daily precipitation, total sky cover, and atmospheric pressure. All these parameters were tabulated, and the hourly average was used to generate the input weather files for 2024.

A few schedule adjustments occurred during the more recent operation of the facility. This includes an “All Days are Saturday” schedule where each day of the week repeats the Saturday schedule from the year 1 and year 2 datasets. This schedule occurred during the tuning period and the TRNSYS input files were created based on the recorded relay panel controls for the virtual family. In this schedule, the occupants move between the first and second floors but never leave the home. This means that more moisture is created in the home and some appliances run more often.

Exact electric load data was used to reflect the true electrical, sensible, and latent loads generated during turning periods. The sensible and latent load contributions from the measured electrical power draws of the appliances, lights, and

plug loads were calculated based on the coefficients provided by Wilson et al. [44] in the same fashion as the original schedule files were created from section 2.1.2.2.

The entire DHW system was not running in 2024. When adjusting the model, all water setpoints were set to below ambient to ensure that the system would not turn on. For tuning: assumed that if the water heater temperature was low, then no sensible or latent related water draws occurred at that time. However, the domestic hot water system and solar hot water systems did not run during this time. It's important to note that the DHW system will introduce additional loads to the home, but the tuning is being done to primarily ensure the ERV, heat pump, and ambient conditions are well modeled. The DHW water temperature was collected in the same fashion as the electrical load data, and it remained below 22 °C during the tuning periods confirming that the system was inactive. So, the DHW control temperatures were set to 20 °C. Combining the ambient temperature of the measured DHW water along with locking out the water heating controls allowed for the entire SHW/DHW system to be dormant in the model.

2.2.4 Model Performance

To compare to recent facility operation, I evaluated this updated model over 3 periods of operation in 2024 to validate the effects of the changes and check for any additional tuning that may be necessary. January 25 – January 30 and August 2 – August 5 periods were selected as they were the heating and cooling season counterparts with very similar thermostat and heat pump controls. February 3 –

February 9 was also selected as the thermostat system was offline for repairs. The building was effectively floating with no HVAC loads besides the ERV. The scheduled virtual family and appliance loads were the only sources of heat during this period, so it was an excellent opportunity to validate the thermal and moisture capacitance in the model.

The zone 2 temperature and humidity from the model are compared to the measured values in the basement (average of four sensors), living room sensor (input for thermostat control), and the owner's bedroom. Figure 6 compares the heating season period. The temperature tracks reasonably well during this time, but the humidity appears to be very reactive to outdoor conditions as the outdoor humidity increased rapidly during the annual hours of 580 – 610.

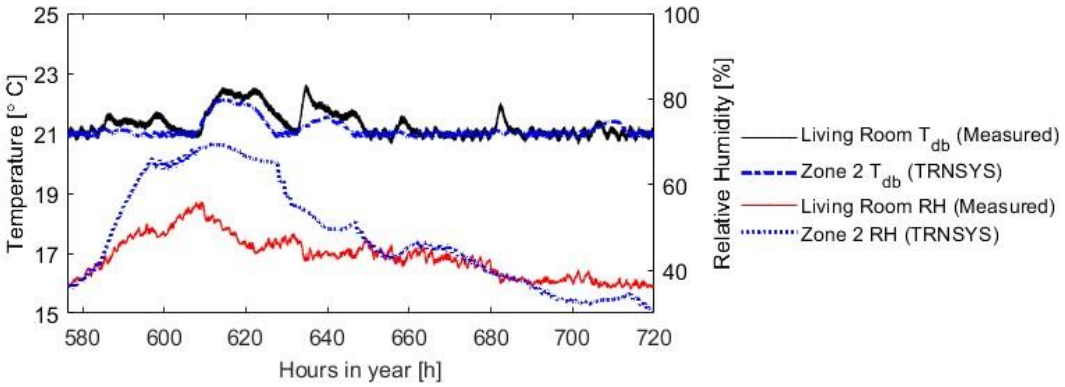

Figure 6. Measured temperature and relative humidity and Zone 2 tuned TRNSYS values for 01/24/2024 – 01/30/2024

Cooling season, seen in Figure 7, shows a significant discrepancy between zone 2 conditions and the actual measured conditions in the living room. This difference appears to be due to the heat pump operation – the current nominal heat

pump values or the performance curves are inaccurate causing the space to be overcooled when dehumidifying and providing insufficient dehumidification when in cooling mode.

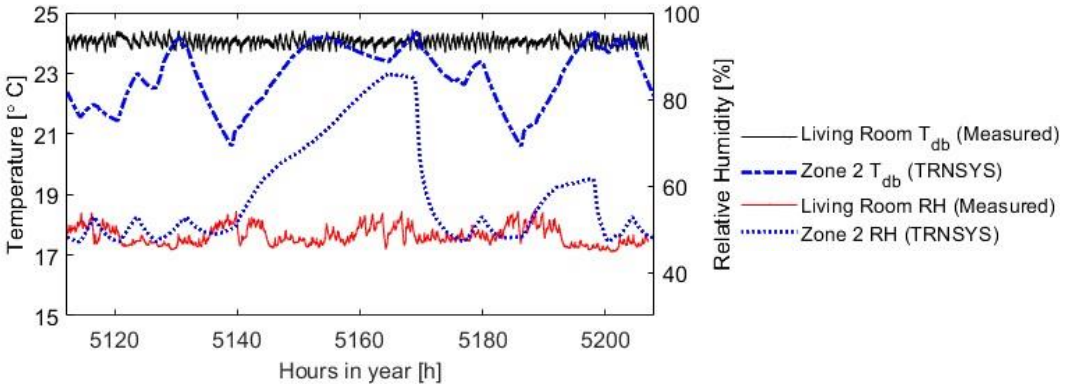

Figure 7. Measured temperature and relative humidity and Zone 2 tuned TRNSYS values for 08/02/2024 – 08/05/2024

The float period, shown in Figure 8, also demonstrates a few differences. The temperature drops off more rapidly than the building did, though that is likely due to the outdoor temperature used in the model being a true outdoor measurement while the outdoor air measurement of the ERV is taken in the intake duct. The measurement in the duct is affected by some preheating of the fresh air as it traverses the ductwork from outdoors to the ERV inlet.

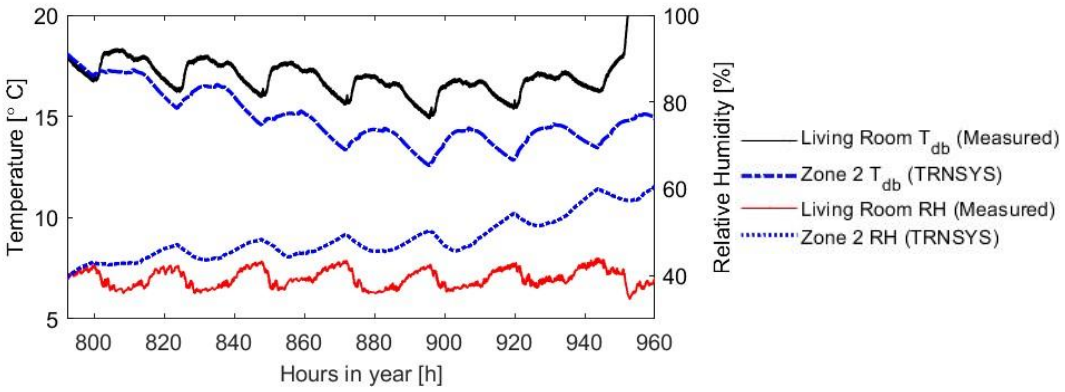

Figure 8. Measured temperature and relative humidity and Zone 2 tuned TRNSYS values for 02/03/2024 – 02/09/2024.

I also considered the variation in temperature and humidity between the floors of the house. This should assist in assessing the validity of the airflow fractions in each zone, the interactions between the zones, and the moisture capacitance of each zone. The less stratification in the house indicates that either the airflows are selected to intentionally prevent stratification and/or a net airflow between the zones reduces stratification. Each zone's rate of change for the measured value can also indicate the thermal or moisture capacitance. Figure 9 shows the temperature and relative humidity during the heating period of the 3 zones that interact with the HVAC system: zones 1, 2, and 3. The measured values indicate more temperature stratification, but less humidity stratification than is predicted by the updated model. In particular, the relative humidity in all the zones is much less reactive to outdoor conditions than the model predicts, suggesting that the moisture capacitance in the zones needs to be updated. The relative humidity in zones 1 and 2 is also much closer than what is modeled suggesting that the airflow fractions are also inaccurate.

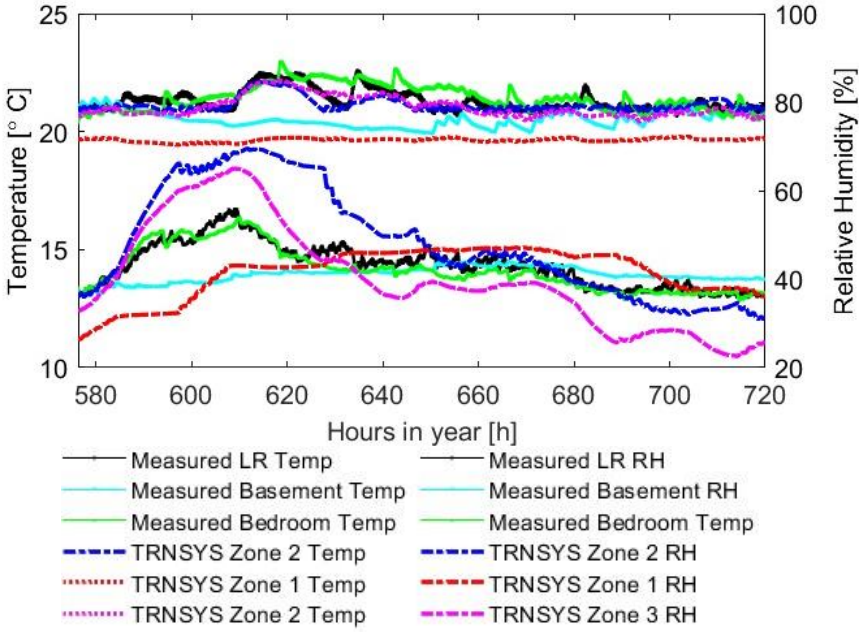

Figure 9. Comparison of Temperature and Relative Humidity across Zones 1, 2, and 3 for January 24 – January 30 tuning period with updated model.

The TRNSYS calculated ERV supply temperatures and humidity ratios do generally match well with the measurements during the heating season as shown in Figure 10a. This means that the sensible and latent effectiveness for this volumetric flow matches well with the nominal values given in 2.2.2. However, the humidity ratios in the cooling season deviate a bit more suggesting the possibility of the latent effectiveness having a weather dependence. Figure 10c indicates that when the return air is relatively consistent and not impacted by HVAC loads, the ERV supply air conditions are predicted well despite using nominal values.

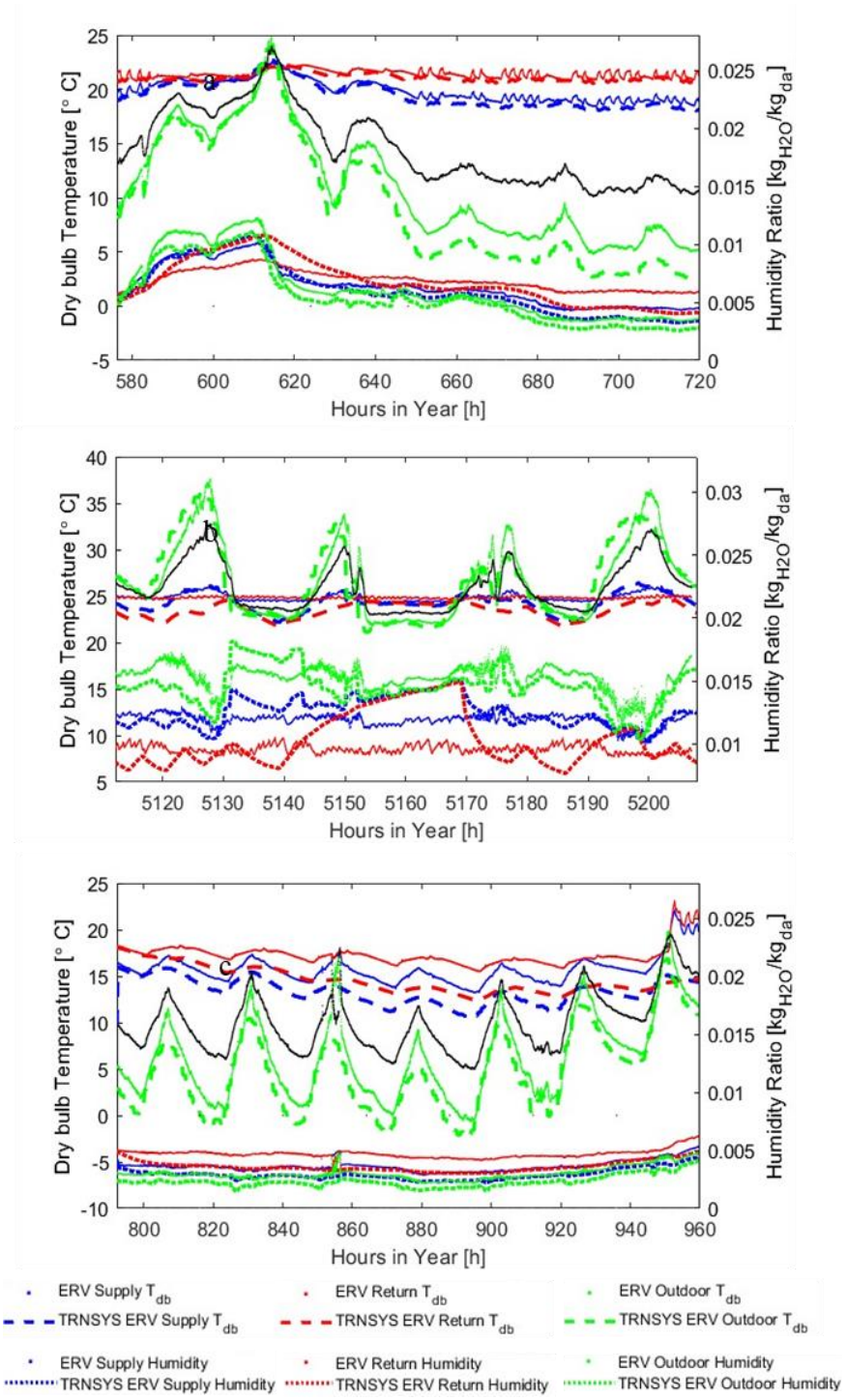

Figure 10. Measured ERV temperature (top of figure) and humidity ratio (bottom) conditions compared to the updated TRNSYS model for (a) 01/24/2024 – 01/30/2024, (b) 08/02/2024 – 08/05/2024, and (c) 02/03/2024 – 02/09/2024.

The inaccurate modeling of the zone conditions causes the ERV return air conditions to deviate. Since the return air conditions are one of the two main independent variables driving ERV heat exchange, any difference in return air conditions creates a significant difference between the sensible and latent loads added during these testing periods. The latent load has significant deviations in the heating period likely due to moisture capacitance and air flow differences (Figure 11a), while the poorly modeled heat pump operation in the cooling season (Figure 11b) results in oscillatory latent loads. The sensible load is generally replicated during the float period (Figure 11c), though it begins to drift away from real conditions due to the more rapid decrease in air temperature. As mentioned previously, this is mostly driven by the outdoor air temperature difference.

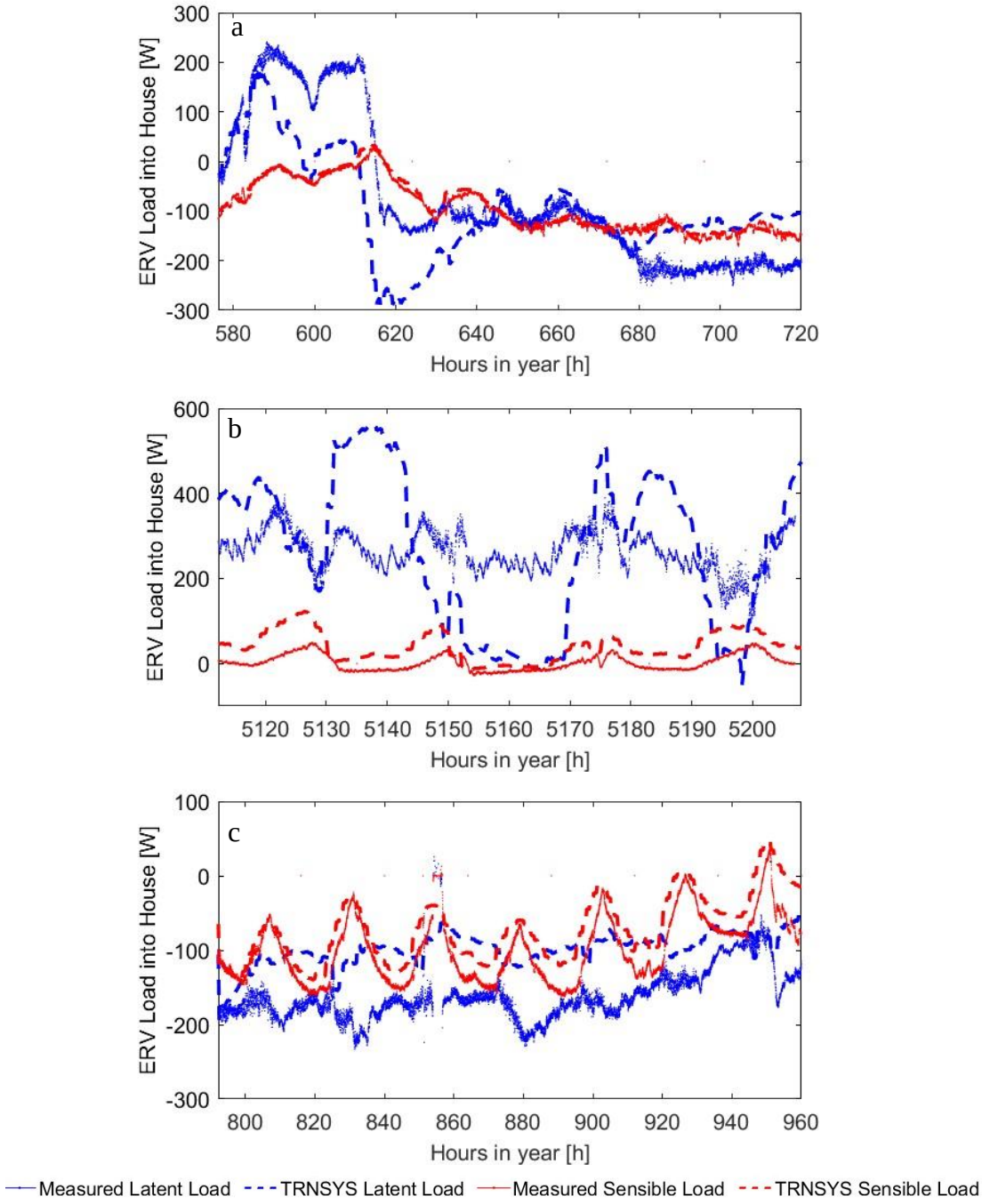

Figure 11. Comparison of measured sensible and latent ERV loads to updated TRNSYS model for (a) 01/24/2024 – 01/30/2024, (b) 08/02/2024 – 08/05/2024.

2.3 Tuning Model

Given the significant differences between actual building performance and simulations from the updated model, the model was tuned for several different parameters. The heat pump performance, HVAC airflow fractions, zone airflow interactions, moisture capacitance, and ERV effectiveness were all evaluated to improve the general building simulation and create a more accurate return air temperature to properly model the ERV performance. I evaluated this updated model over the same 3 periods of operation in 2024 to validate the effects of the changes and check for any additional tuning that may be necessary.

2.3.1 Heat Pump Performance Curves

The heat pump capacities and performance were not aligned with the actual performance during the heating and cooling seasons and the humidity control did not match actual performance. To compensate for these, the heat pump performance curves for dehumidification and first-stage heating and cooling were all evaluated based on 2024 performance using most of the 2024 cooling season (specifically April 11 to August 6).

The dehumidification mode is no longer accurately modeled, best shown by the cooling season zone condition evaluation period in Figure 7. The latent load for both the dehumidification mode and stage 1 cooling are on the order of 3,000 W and 2,000 W respectively as shown in Figure 12. Additionally, the sensible load during dehumidification mode averages only about 300 W. However, the original model

used a total dehumidification capacity of 5997 W with a sensible capacity of 4,177 W and stage 1 cooling only had a nominal latent capacity of less than 1,300 W. These values and the existing performance curves led to excessive sensible cooling during dehumidification mode and insufficient latent capacity for humidity control during stage 1 cooling.

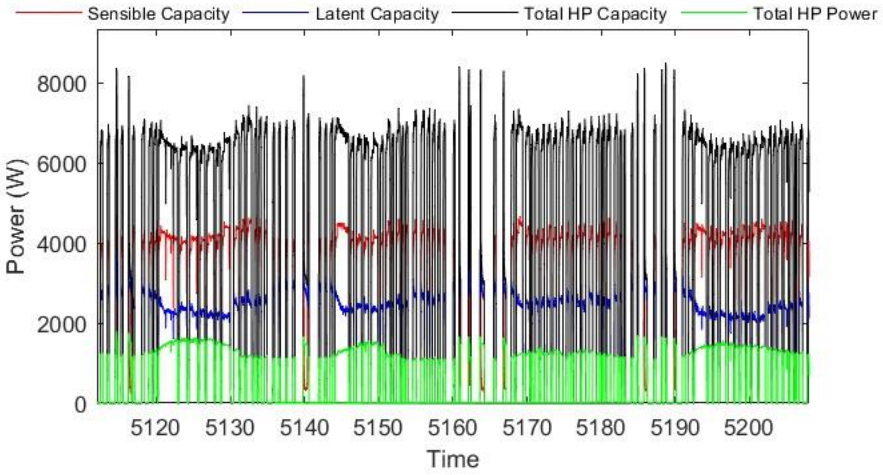

Figure 12. NZERTF heat pump capacity and power draw (August 2 - August 5).

Dehumidification mode is mainly driven by the indoor conditions, namely the indoor wet bulb temperature and the indoor dry bulb temperature focused on reducing the moisture from the inside of the building, its performance is. This mode typically operates at nighttime when the outdoor temperature is more consistent since there is no solar thermal load, and the main load is the increased moisture from the outdoors. Because of these factors, the total capacity of dehumidification, latent capacity, and power all increase as indoor dry bulb and wet bulb temperatures, shown in Figure 13, increase because those parameters indicate more moisture to be removed from the environment. The relative performance curves based on the multivariable regressions

shown below were used and calculated relative to the average total capacity of 3,006 W, sensible capacity of 286 W, and total power of 1,531 W. Second-stage dehumidification was not evaluated as the thermostat does not enable this stage. The resulting TRNSYS model performance curve equation fit is shown in Appendix II.

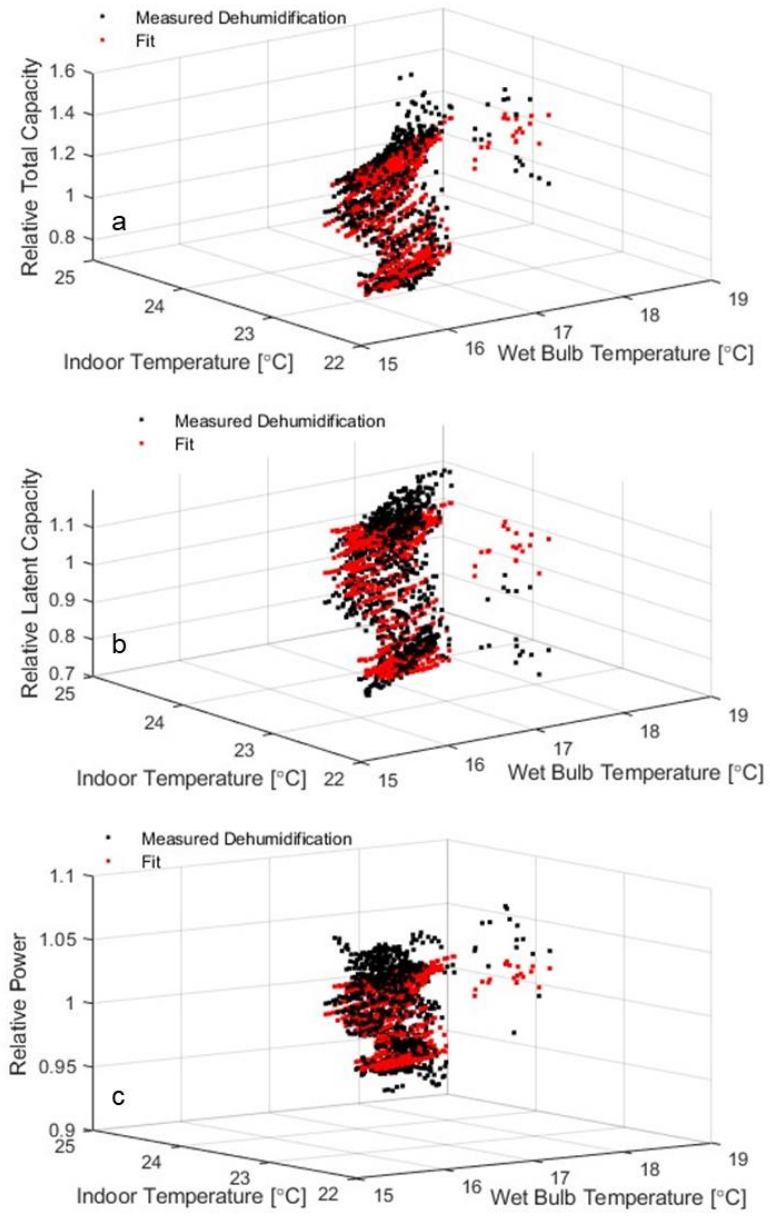

Figure 13. Dehumidification performance relative to nominal values for a) total cooling capacity as a function of outdoor temperature, b) latent cooling capacity as a function of indoor wet bulb temperature and outdoor temperature, and c) power draw as a function of outdoor temperature.

The stage 1 cooling performance is mostly driven by the outdoor temperature as would be expected for a vapor compression cycle since the indoor conditions are

reasonably stable compared to the outdoor conditions. These trends are confirmed by the relative performance curve fits shown in Figure 14. As the outdoor temperature increases, the cooling capacity (Figure 14a) decreases since the condenser temperature must increase. This leads to operating closer to the top of the vapor dome where the total latent heat decreases. The sensible capacity (Figure 14b) is lightly correlated with the outdoor conditions, likely limited by the condenser capacity. The indoor wet bulb is much more indicative of the sensible capacity since the wet bulb capacity informs the amount of moisture removal that the cooling coil can remove. The total power is impacted by the outdoor temperature, such as the total capacity. Since the condenser must operate at a higher temperature and pressure when the outdoor temperature is high, the compressor must do more work to reach this higher pressure. This is confirmed by the linear regression shown in Figure 14c. These fits were still valid for the initial TRNSYS equipment parameters of 5,425 W of total cooling capacity and 4,155 W of sensible capacity, but an updated nominal power draw of 1,351 W. The TRNSYS model low-speed cooling performance equation is shown in Appendix II.

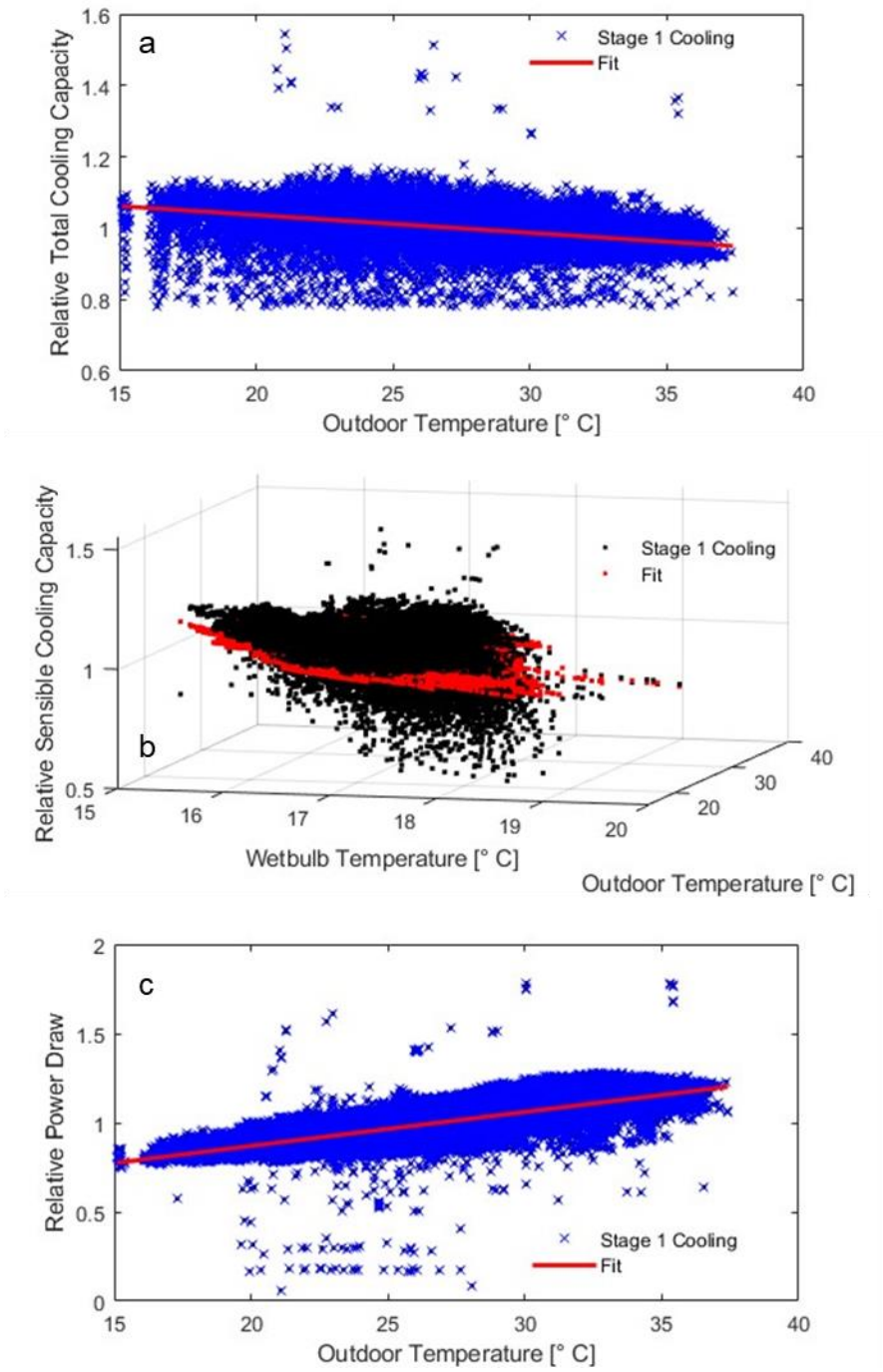

Figure 14. 1st stage cooling performance relative to nominal values for a) total cooling capacity as a function of outdoor temperature, b) sensible cooling capacity as a function of indoor wet bulb temperature and outdoor temperature, and c) power draw as a function of outdoor temperature.

First-stage heating was also analyzed based on the heating data from January 2024. Like with first-stage cooling, the first-stage heating capacity and power draw are mostly dependent on the outdoor temperature. This is primarily due to the pressure lift required of the compressor when operating in heating mode to move between the outdoor coil and indoor coil. Indoor conditions are stable relative to the significant temperature swings in the winter months. The heating capacity and power draw are shown plotted against outdoor dry bulb temperature in Figure 15. As expected, the heating capacity increases with outdoor temperature as less compressor lift is needed, and the mass flow rate increases at higher temperatures for a constant compressor volumetric flow. Therefore, the evaporator has more capacity to remove heat from the outdoor conditions. The same trend is observed with the heat pump power draw. The relative capacity and power curves are fit as a polynomial with the independent variable being the natural logarithm of outdoor temperature with a 10 K offset to keep the value greater than 0. This fit was developed to ensure that there was not a local maximum in the best fit artificially creating a higher capacity than the physical system would allow. These performance curves were updated relative to a new heating capacity of 7,034 W observed during first-stage heating with an average power draw of 1,379 W. The resulting TRNSYS model low-speed heating performance equation curve fit is shown in Appendix II.

These three modes constitute most of the operating time for the heat pump. These are also the three stages most likely to occur around or near any bypass mode operation, so they were the focus of this analysis.

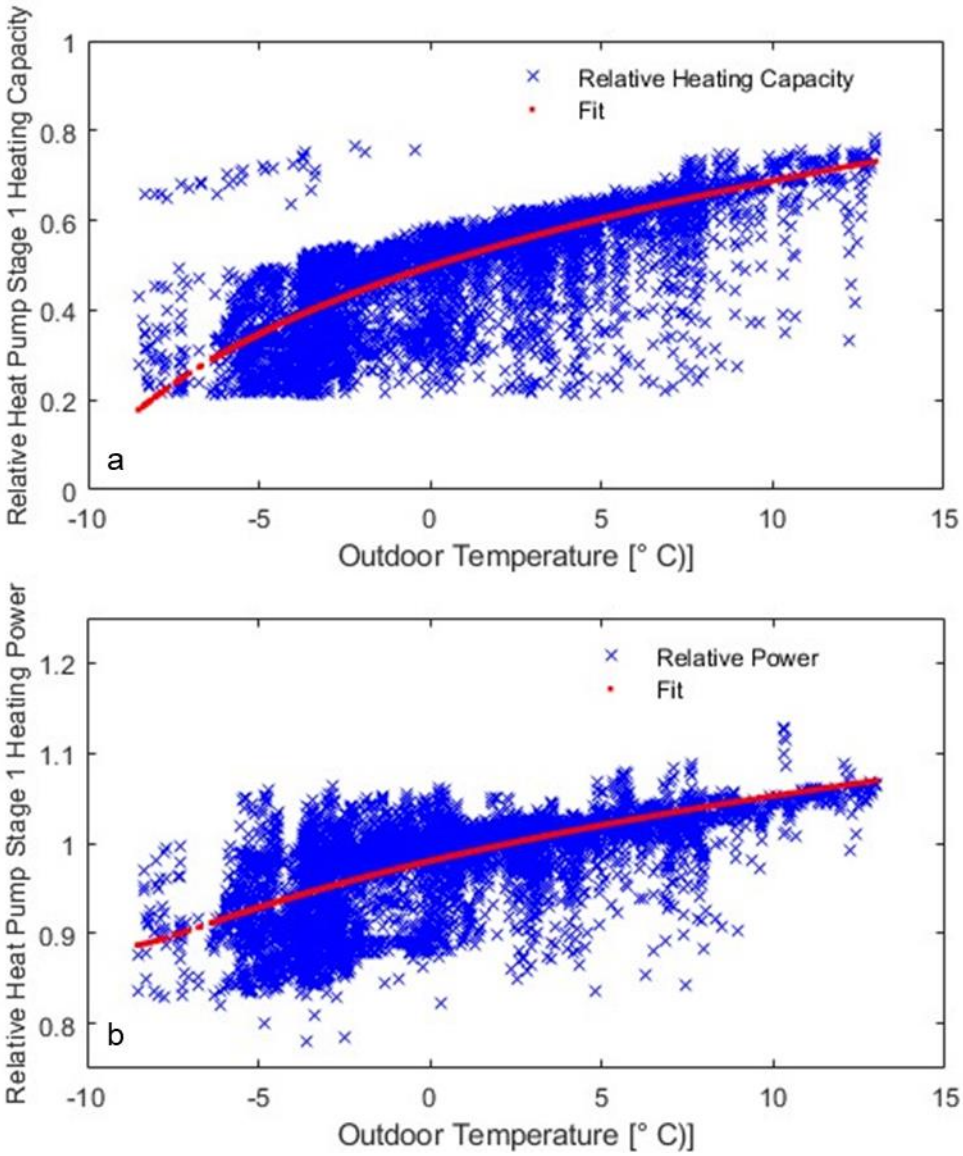

Figure 15. Stage 1 heating relative capacity (a) and relative power draw (b) plotted against outdoor temperature.

2.3.2 HVAC Airflow Changes

The heating and cooling season evaluation periods were nearly identical in terms of thermostat operation and control. But the air flow fractions have changed over time as the team has learned more about the facility. It was discovered that the

only difference between the settings for these two periods was the supply and return duct flows. This has been done to mitigate the temperature stratification observed in the summer while ensuring sufficient heating in lower zones during the winter.

Table 5. Ratio of Air Flow through HVAC Supply and Return Ducts by Zone

Zone	1/25 – 1/30 Duct Flow Ratios		8/2 – 8/5 Duct Flow Ratios	
	Supply	Return	Supply	Return
1	0.171	0	0.043	0
2	0.512	0.389	0.605	0.726
3	0.317	0.611	0.352	0.274

The original model only considered air flows between Zones 1 and 2. This method means that the overall energy use and loads in the house can be effectively modeled, but it limits the effectiveness of evaluating quickly changing weather patterns or loads in the building. Because interactions only happened between two Zones in the previous model, the net flow between zones was a simple subtraction of the net HVAC and ERV flows in Zone 3 from the net HVAC and ERV flows in Zone 2. By adding another zone, this could no longer be done. Instead, the fraction of air flow entering or leaving Zone 2 was divided between interactions with zones 1 and 3 based on the open area between the zones. There is approximately a 2 m^2 door at the top of the stairs into zone 1 from Zone 2 and a 9 m^2 overlook at the top of the stairs between 2 and 3. No effective area was included between Zones 3 and 4 as zone 4 is the attic and well-sealed from Zone 3. These areas mean that about 18 % of any surplus or deficit air flow to Zone 2 was pulled from or sent to Zone 1, and the remainder of the interaction was with Zone 3. While this is an imperfect model of

airflow interactions between the zones, it will suffice for the purposes of replicating the return air conditions for the ERV and the Zone 2 conditions for thermostat and heat pump operation that are critical for this study.

2.3.3 Building Model Adjustments

Along with heat pump operation and air flow interactions, the moisture capacitance of the building plays a significant role in affecting the indoor conditions. From experience, the basement plays a role in the other zone temperatures and humidities. Its impact is likely due to the concrete slab's significant thermal and moisture capacitance. The basement's simple moisture capacitance model was adjusted according to equation 3 below.

$$Moisture\ Capacitance\ Ratio = \frac{m_{H_2O,air} + \sum_{i=1}^{n} u_i m_{material\ i}}{m_{H_2O,air}} \quad 3$$

where m indicates the relevant mass and u_i is the corresponding material's isotherm of water sorption. Previous work included gypsum on the walls, but did not include the concrete slab. By incorporating concrete's isotherm of approximately 0.05 kg water per kg of concrete at the building's relative humidity setpoint of 50 %, Zone 1's moisture capacitance increased from 2.2 to 162.6 [45].

The difference between the measured and modeled moisture in Zones 2 and 3 also varies a significant amount. To account for this variation, a buffer storage capacitance model replaced the previously used simple model. This model incorporates the gradient of the sorptive isotherm relative to the relative humidity (updated to 0.075 kg water per kg of material per humidity [46]), the material

diffusion resistance, material density, and surface area of the various materials for the corresponding zone. In Zones 2 and 3, the gypsum walls have the smallest diffusion resistance and therefore the largest impact on water sorption. They were the focus in determining the key parameters of surface sorption, deeper material sorption, surface mass, deep water mass, coefficients for zone to surface storage and surface storage to deep storage (see Appendix I for parameter values). The detailed equations are outlined on page 6-146 of the TRNSYS modeling handbook volume 6 on Multizone Building modeling with Type 56 and TRNBuild [47].

2.3.4 Characterizing ERV Effectiveness and Heat Transfer

ASHRAE Handbook HVAC Systems and Equipment Chapter 26 Air-to-Air Energy Recovery Equipment, Section 2 [48] defines sensible effectiveness as change in sensible heat from outdoor air to supply air divided by the maximum potential sensible heat transfer, which is between the outdoor air and return air and limited by the minimum airflow in the ERV:

$$\varepsilon_{sensible} = \frac{\dot{m_{supply}}(c_{p,outdoor}T_{outdoor} - c_{p,supply}T_{supply})}{\dot{m_{min}}(c_{p,outdoor}T_{outdoor} - c_{p,return}T_{return})} \quad 4$$

The latent effectiveness is calculated the same way using the latent heat of vaporization and the humidity ratio of the moist air:

$$\varepsilon_{latent} = \frac{\dot{m_{supply}}(h_{fg,outdoor}W_{outdoor} - h_{fg,supply}W_{supply})}{\dot{m_{min}}(h_{fg,outdoor}W_{outdoor} - h_{fg,return}W_{return})} \quad 5$$

We measure the dry bulb and dewpoint of the air at the outdoor inlet air, fresh supply air, house return air, and exhaust air every minute at the facility. This provides

granular data to calculate the psychrometric properties of the air and determine the total load added by the ERV and its effectiveness under a wide range of conditions. Unfortunately, direct calculation of the effectiveness leads to asymptotic behavior as the outdoor conditions approach the return conditions as seen in Figure 16. This leads to artifacts in the data that make it challenging to effectively capture the actual effectiveness by direct calculation even after separating the data into different weather conditions like cold and humid vs. cold and dry conditions.

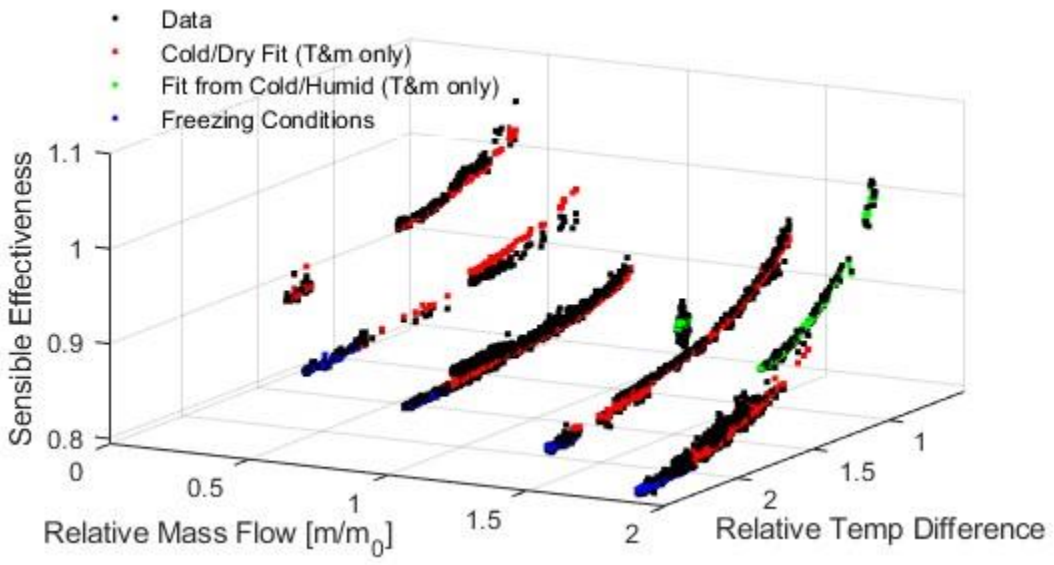

Figure 16. Relationship between the ERV's calculated sensible effectiveness, relative mass flow rate, and difference in outdoor and return dry bulb temperatures relative to 10 °C.

Instead, I calculated the actual sensible and latent heat transfers against the maximum potential sensible and latent heat transfers as a function of mass flow rate. Knowing that the relationship between the actual heat transfer and the maximum potential follows the form shown below:

$$q = \varepsilon q_{MAX} \quad (6)$$

then the effectiveness can be described as a function of mass flow and optionally, a dimensionless outdoor weather condition, if necessary:

$$q = \varepsilon\left(\frac{m}{m_0}, \frac{T_{outdoor} - T_{supply}}{10\ °C}, \frac{W_{outdoor} - W_{supply}}{0.001\frac{kg_{H_2O}}{kg_{da}}}\right) q_{MAX} \quad (7)$$

I then fit a polynomial curve to the relationship in equation 7. The effectiveness as a function of mass flow and outdoor conditions is given by dividing q_{MAX} out of the polynomial fit resulting in a polynomial fit in the same form as shown in equation 1.

This methodology was performed for the sensible effectiveness, shown in Figure 17, and latent effectiveness, shown in Figure 18. Data was pulled over a sample of dates including in April 2024, August 2024, and 3 straight weeks of measurements in February 2025 where the volumetric flow rate was adjusted across five different flow rates: 15 %, 35 %, 50 %, 75 %, and 100 % of maximum flow rate. These relative flow rates correspond to approximately 35 CFM, 65 CFM, 100 CFM, 135 CFM, and 175 CFM. The sampling dates allowed for a wide variety of weather patterns to be considered from freezing conditions, cold and dry conditions, cold and humid, and hot and humid conditions. Despite the range of weather conditions in this sampling period, the sensible effectiveness is driven by the mass flow rate across the heat exchanger. However, the latent effectiveness is impacted based on the temperature and humidity conditions. The latent effectiveness is generally much

greater (around 0.61 at a nominal flow rate of 100 CFM) under humid conditions and only about 0.31 under dry conditions. However, the latent effectiveness increases slightly to about 0.34 when the outdoor temperature drops below freezing since the outdoor air is effectively holding no moisture. Additionally, the effectiveness remains greater across a range of flow rates for humid outdoor conditions. So, the model was updated to include three separate latent effectiveness model fits depending on the outdoor conditions relative to indoor conditions.

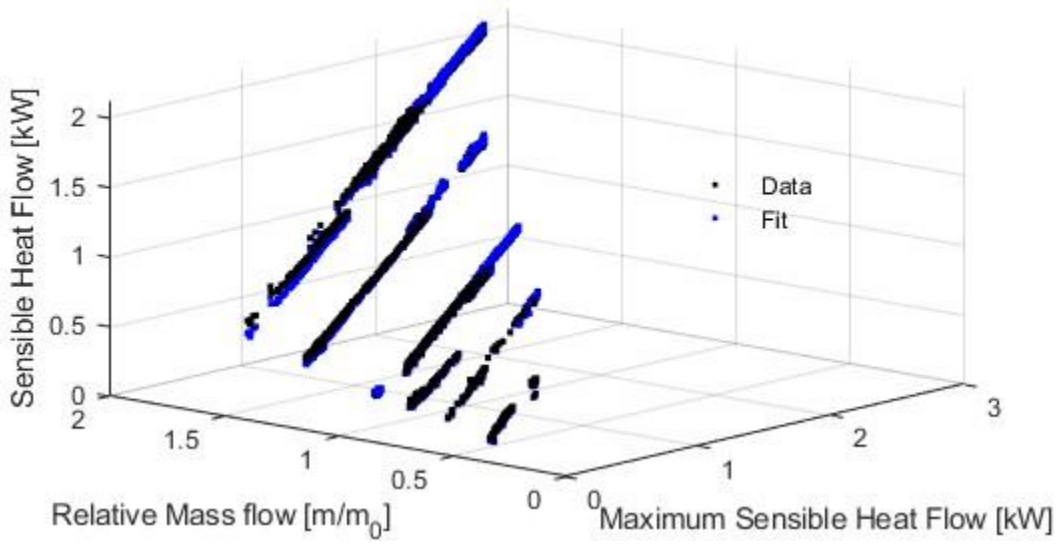

Figure 17. Sensible heat flow as a function of mass flow relative to nominal 204.8 kg h^{-1} (approximately 100 CFM) and maximum potential sensible heat flow.

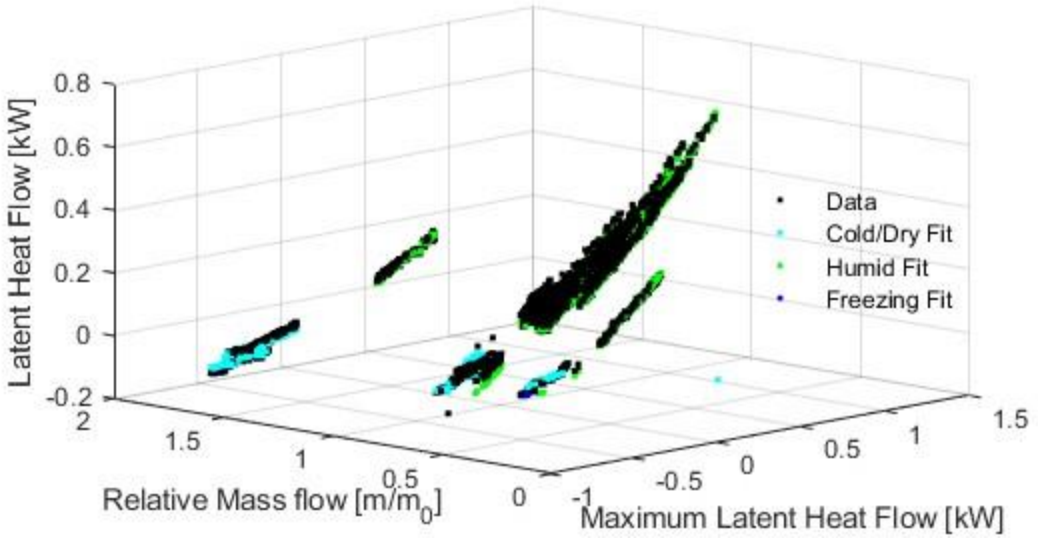

Figure 18. Latent heat flow plotted against relative mass flow and maximum potential latent heat flow.

Figure 19 shows the polynomial fits as a function of mass flow rate relative to 204.8 kg h^{-1}. The humid effectiveness data only had volumetric flow rates of about 100 CFM and 175 CFM which caused the parabolic shape. The fit was acceptable for this work since the model would only be run with flow rates in these two ranges, but it is inappropriate to extrapolate to other flow rates. The exact model fit coefficients can be found in Appendix I. These fit coefficients were entered into a new custom ERV control type 1273 in the TRNSYS model that determines the ERV state (bypass or not) and calculates the sensible and latent effectiveness values based on these coefficients and flow rate. The effectiveness values are then fed into a type 667 HRV that calculates both sensible and latent exchange. The flow rates are fed into type 111b variable speed fans to dictate the mass flow through each side of the ERV.

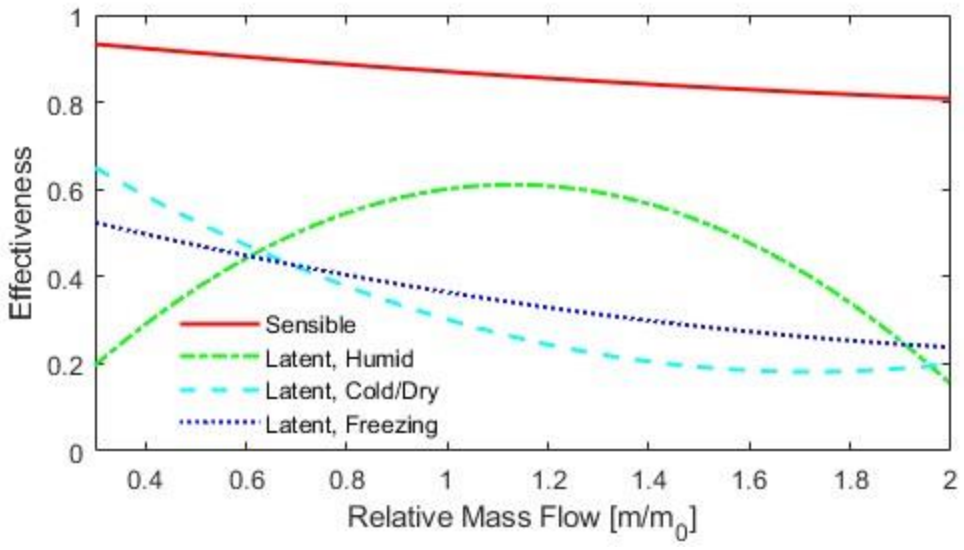

Figure 19. ERV Effectiveness as a function of mass flow rate.

2.3.5 ERV Fan Performance

The main power draw for the ERV is the fresh air and exhaust air stream fans. The same dataset from the ERV effectiveness calculations described in section 2.3.4 was used to define a correlation between the relative mass flow through each fan and the total power draw (Figure 20). Interestingly, the fit is cubic in shape instead of quadratic, according to the specification data. This data includes operating conditions with an end-of-life air filter, as can be seen by the 0.8 relative mass flow data. The power draw is about the same as the data at nominal mass flow. See Appendix I for exact fit parameters following the same form as the equation 2.

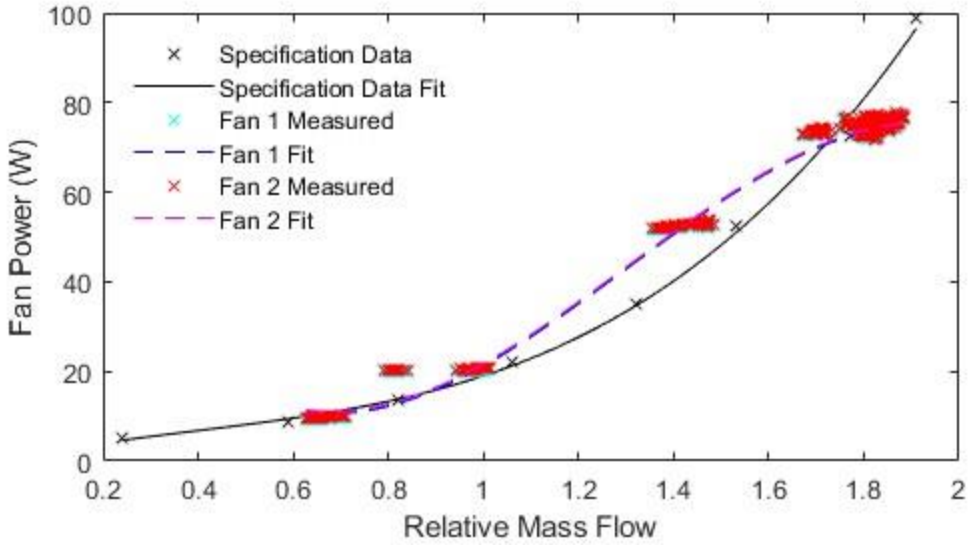

Figure 20. ERV supply and return fan fits against mass flow rate relative to nominal 204.8 kg h^{-1}.

2.3.6 Experimental Uncertainty

Each of the measured parameters outlined in the sections 2.3.1, 2.3.4, and 2.3.5 come with their own uncertainty. These 95 % confidence level uncertainties for the indoor temperature and relative humidity, as well as the heat pump total capacity, sensible capacity (for cooling), and power draw, are outlined and discussed by Davis et al. [49]. When combined and used in various equations, they propagate into larger uncertainty budgets.

Most of the thermocouple measurements at the NZERTF outlined in this work have a measurement uncertainty of ±0.2 °C, except for the heat pump supply air measurement and outdoor measurement. The supply air thermocouple has an uncertainty of ±0.5 °C and the outdoor type T thermocouple has a total uncertainty of ±0.6 °C. The supply air dewpoint measurement has an uncertainty of ±1.0 °C. The

heat pump return air and outdoor dewpoint measurement relative uncertainties are ±1.5 %. The heat pump indoor unit power meter has a total uncertainty of ±100 W while the outdoor unit power meter has an uncertainty of ±20 W. With these direct measurement uncertainties, the heat pump capacity and power draw uncertainties are on the order of 5 % for sensible capacity, 9 % for total capacity, and ±120 W for power draw at a 95 % confidence level. The percent uncertainty will naturally change depending on the magnitude of the calculation or measurement, decreasing with larger capacities and power draws, and increasing as the calculations approach zero.

When applying these measurement uncertainties and accounting for the performance fits, any total and sensible capacity estimates used in the TRNSYS model have a relative uncertainty of about 7 % and 11 %. These values do shift depending on indoor and outdoor conditions. The relative uncertainty of the power fit for the heat pump is approximately 10 % across all stages, but again, it does change depending on outdoor conditions.

The ERV measurements are performed similarly to what is described by Davis, et. al. in [49], except that the volumetric flow is measured via three pitot tube stations. The pitot tube stations that measure the volumetric flow through the outdoor air, return air, and supply air ducts have uncertainties of approximately 14 %, 7.8 %, and 7.1 %. These airflow uncertainties are mainly driven by the difference we have observed between hot wire anemometer flow measurements (uncertainty of about 0.5 %) and pitot tube flow measurements (uncertainty of 2.1 %). The thermocouples measuring the ERV air dry bulb temperatures are connected to the same system as the

NZERTF indoor conditions and therefore have the same measurement uncertainty of ±0.2 °C. These temperature uncertainties lead to a relative uncertainty of about 5 % when directly calculating the sensible effectiveness when the supply air temperature is 7 °C greater than the outdoor temperature and the return air is 8 °C greater than the outdoor air. Like with the heat pump relative uncertainty calculations, the uncertainty increases as the temperature differences decrease.

The uncertainty of the effectiveness calculated based on the maximum heat flow are more complicated. Most parameters are dominated by the outdoor airflow measurement uncertainty of 14 % since all the uncertainty contributions are added in quadrature as shown in equation 8:

$$u_{eff} = \sqrt{u_q^2 + u_{qMAX}^2 + \sum_{i=1}^{n} a_i^2 + \frac{\partial \varepsilon(\frac{\dot{m}}{\dot{m}_0})}{\partial \frac{\dot{m}}{\dot{m}_0}} u_{\dot{m}}^2} \quad 8$$

where u_q is the relative uncertainty of the measured heat transfer, u_{qMAX} is the relative uncertainty in the maximum heat flow, q_{MAX}, a_i is the standard error in the fitting coefficient, ε is the effectiveness as a function of mass flow, and $u_{\dot{m}}$ is the relative uncertainty in the mass flow rate, $\dot{m}$. With very small fitting errors and both the heat transfer and total potential heat transfer being influenced by the air's mass flow, the relative effectiveness uncertainty is mostly influenced by the mass flow uncertainty yielding an uncertainty of 21 % for the sensible effectiveness, 30 % - 32 % for the latent effectiveness humid fit, 23 % - 24 % for the latent effectiveness cold/dry fit, and 20.8 % for the latent effectiveness freezing fit.

The ERV's fan power measurement uncertainty is between 2 % and 5 % depending on the flow rate as discussed in section 3.3 of [49]. The lower flow conditions, and therefore lower power draw, lead to a 5 % uncertainty.

2.3.7 Tuning Results

The adjustments outlined in the sections 2.3.1 through 2.3.5 were added into TRNSYS and the model was run for the same three measurement periods shown in the section 2.2.4: January 24 – January 30, February 3 – February 9, and August 2 – August 5.

The stratification and Zone mixing during the January period was the first verification that model tuning was successful. The measured Zone temperatures and humidities are shown in Figure 21 compared to the TRNSYS model results. There is significantly more agreement between the two than was seen in the model pre-tuning (Figure 9). Additionally, the Zone humidities are significantly less reactive to the outdoor conditions than before. This modeling period was particularly challenging because of the large swings in outdoor humidity. Seeing the Zones simulated more accurately gives confidence that the airflow distribution and moisture capacitance adjustments are effective and accurate.

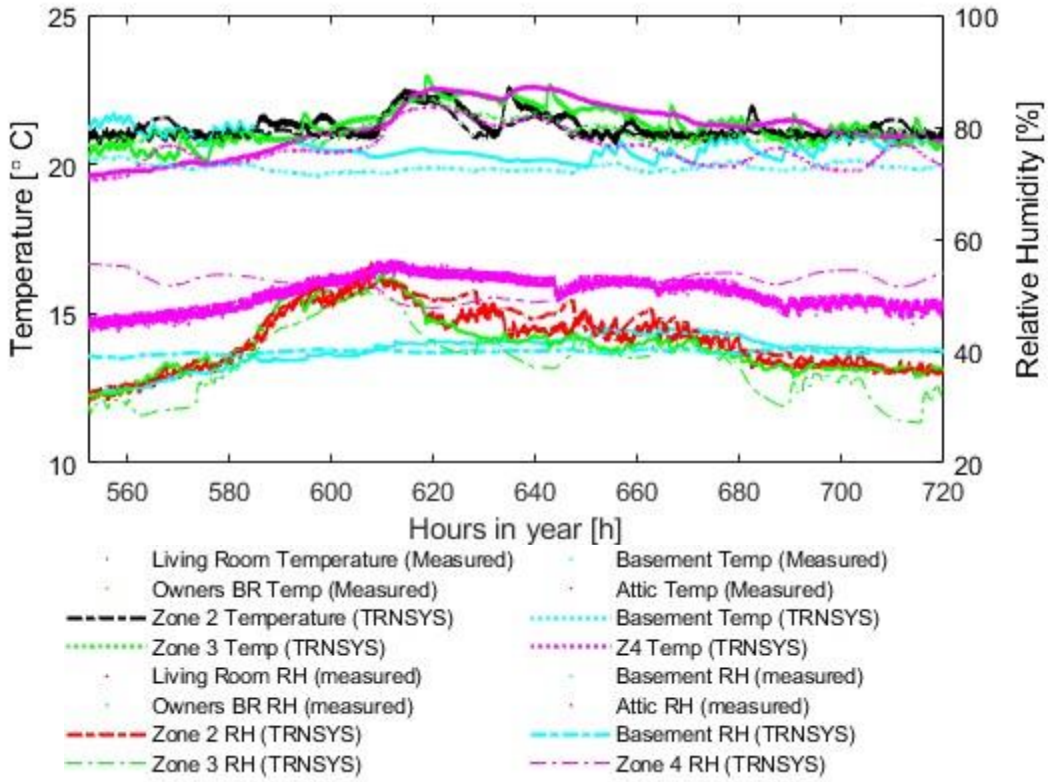

Figure 21. Comparison of Temperature and Relative Humidity across Zones 1, 2, and 3 for January 24 – January 30 tuning period with tuned model.

Figure 22 shows the measured temperature and relative humidities in the living room of the building against the tuned TRNSYS model's conditions in Zone 2. The model's Zone 2 temperature and humidity align much more closely with the measured values during all three of these time periods. This is due to a combination of revising the air distribution of the home, the moisture capacitance in the building, and the updated heat pump performance curves. The relative humidity is much less reactive to outdoor conditions. This is particularly noticeable during the January 2024 period when the indoor relative humidity no longer swings from ~ 40 % to 70 % in 30

hours. The ERV loads, shown in Figure 23, match the actual ERV loads except for when the outdoor weather data fed into the model does not match the measured outdoor air stream conditions for the ERV. These outdoor, supply, and return air conditions are shown in Figure 24.

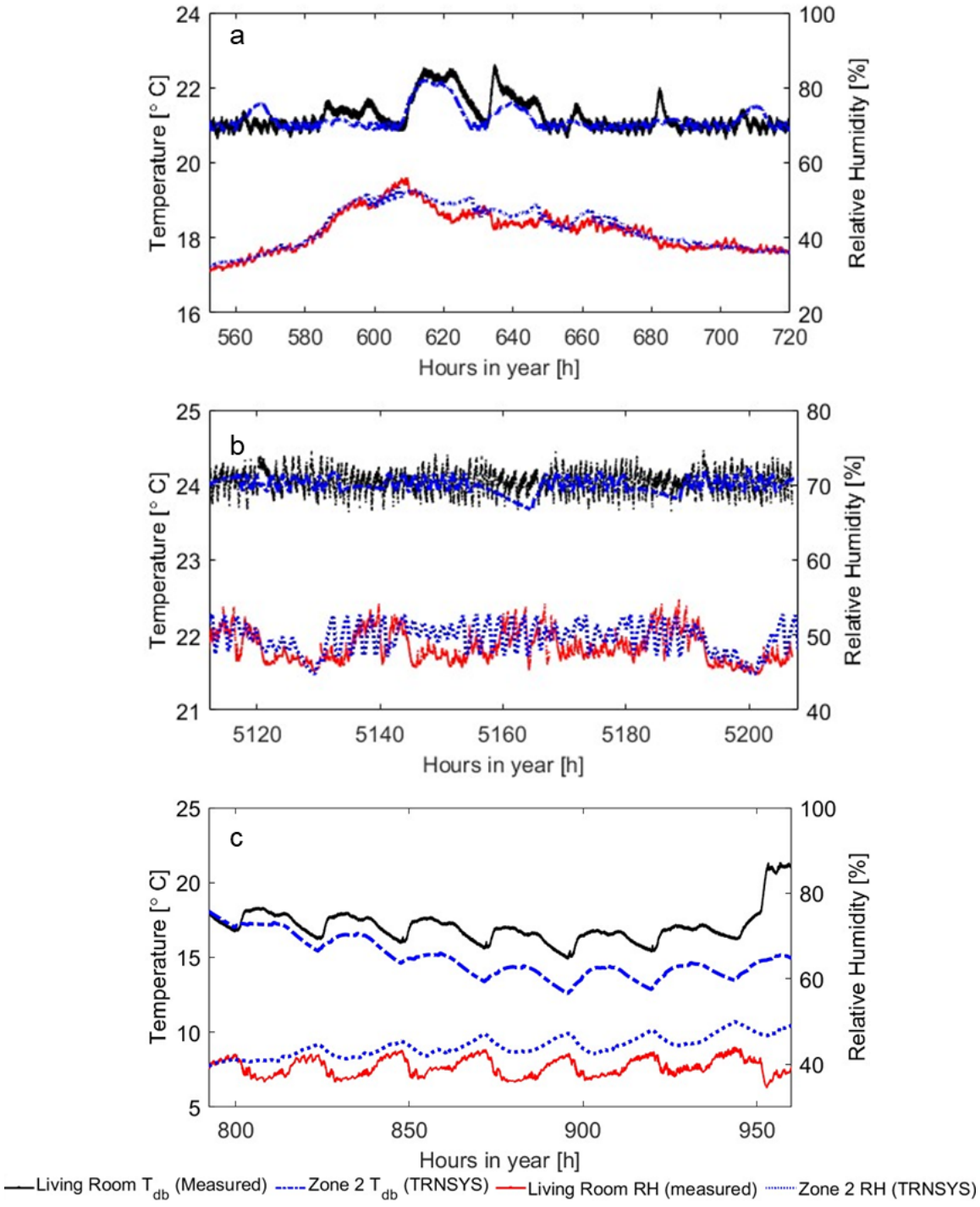

Figure 22. Measured temperature and relative humidity and Zone 2 tuned TRNSYS values for (a) 01/24/2024 – 01/30/2024, (b) 08/02/2024 – 08/05/2024, and (c) 02/03/2024 – 02/09/2024.

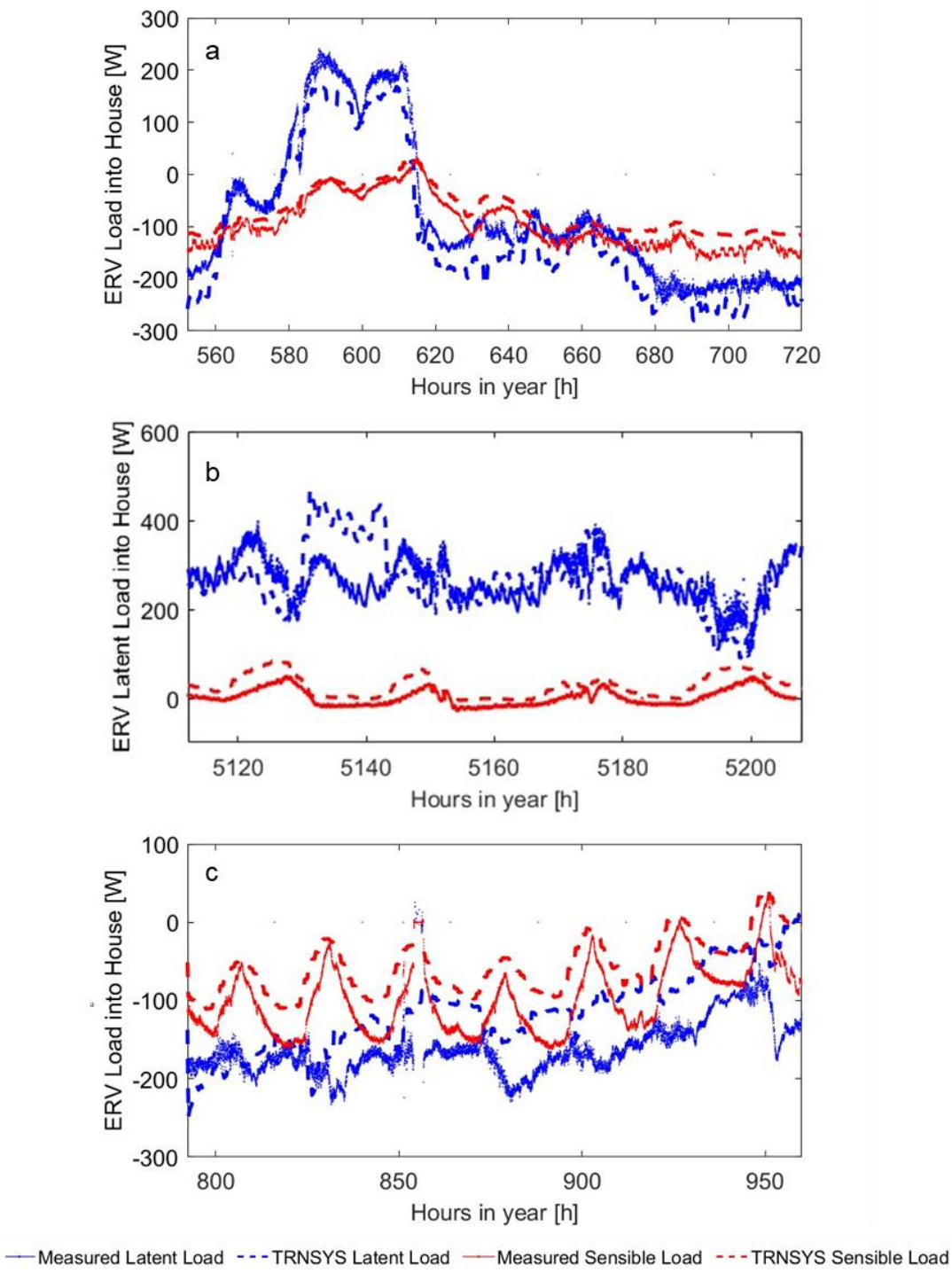

Figure 23. Measured and TRNSYS modeled sensible and latent ERV loads for (a) 01/24/2024 – 01/30/2024, (b) 08/02/2024 – 08/05/2024, and (c) 02/03/2024 – 02/09/2024.

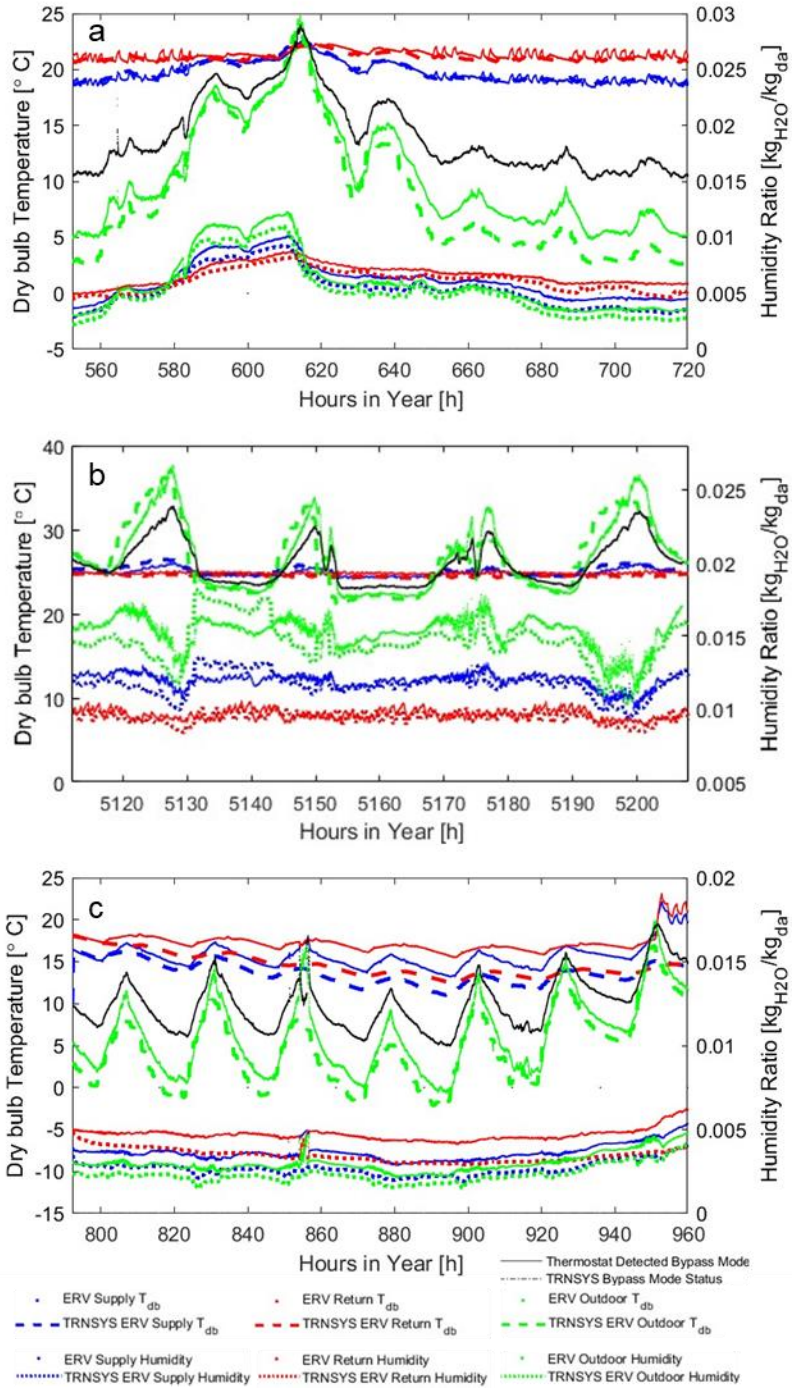

Figure 24. Measured ERV temperature (top of figure) and humidity ratio (bottom) conditions compared to tuned TRNSYS model for (a) 01/24/2024 – 01/30/2024, (b) 08/02/2024 – 08/05/2024, and (c) 02/03/2024 – 02/09/2024.

Chapter 3: Temperature-based ERV Bypass Control

3.1 Proposed Temperature-based Control

The thermostat control was devised to maximize opportunities for free cooling, reduce heat pump operation, and otherwise ventilate the building in compliance with ASHRAE 62.2. The basic flowchart for the thermostat is shown below in Figure 25. Free cooling is only maximized if the thermostat has a call for stage 1 cooling to occur when the Zone temperature exceeds the sum of the setpoint and the first stage cooling deadband of 0.56 °C. Otherwise, the standard flow rate is supplied into the house as a means of minimizing any excess latent loads added into the home. When cooling is required, the heat pump's first stage only comes on if the 2^{nd} stage deadband of 1 °C is exceeded. Second-stage cooling only comes on in emergency cases if the third-stage deadband of 1.5 °C is surpassed.

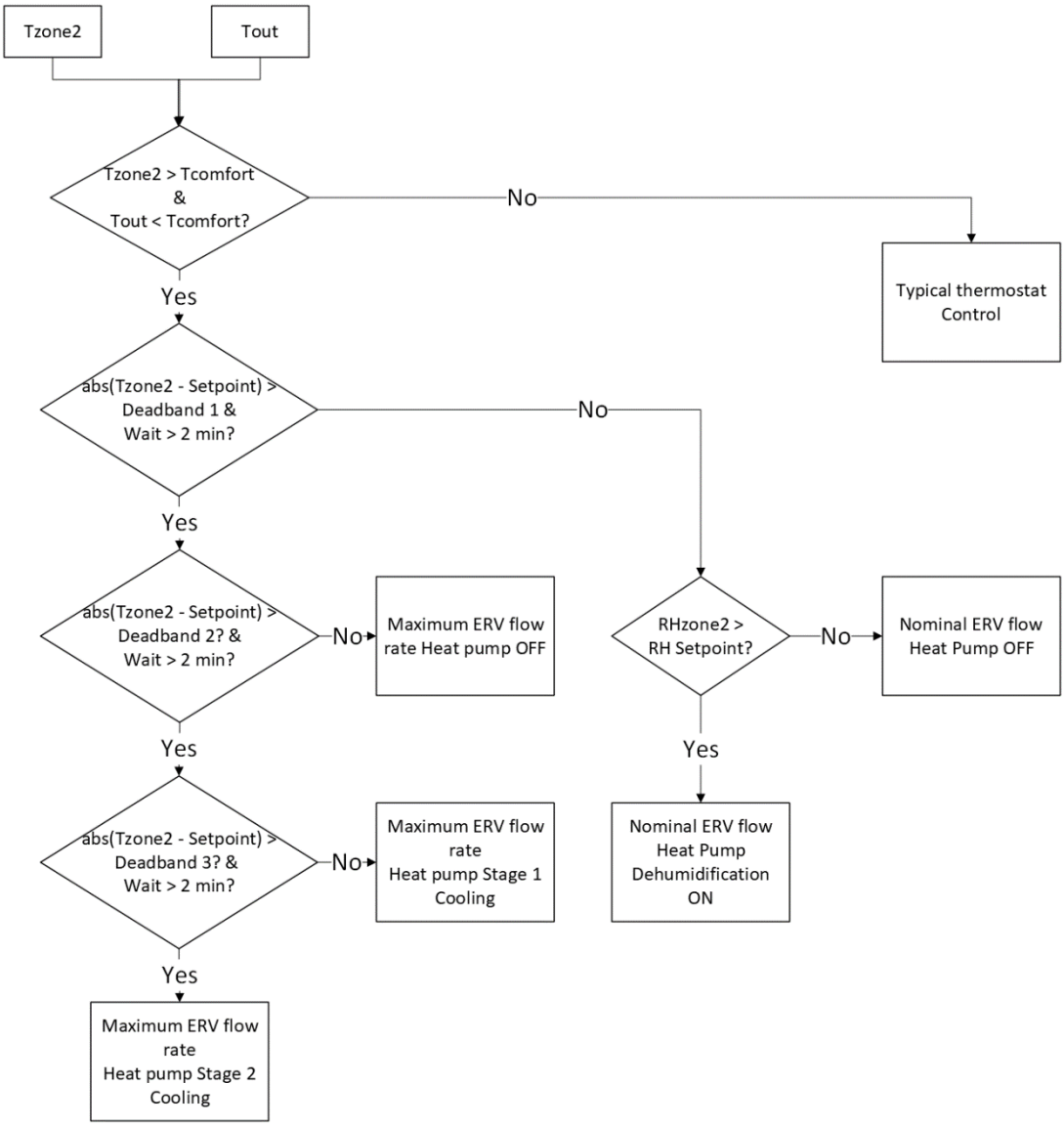

Figure 25. Thermostat control flowchart in bypass mode.

The ERV's comfort temperature was set to 23 °C to ensure that bypass mode would only be enabled if the outdoor temperature dropped below the cooling setpoint temperature of 23.9 °C / 75 °F. The Zehnder ERV uses its own proprietary controller, so our thermostat must detect and approximate if the system is in bypass mode or not. An algorithm was used to detect if bypass mode was occurring. It was designed to

intentionally underpredict bypass mode's occurrence to avoid adding excessive moisture into the house given the region's mixed humid climate. For the thermostat to register that bypass mode is in effect 5 conditions must be met: 1) the ERV return temperature must be greater than the comfort setting; 2) the ERV outdoor temperature must be less than the comfort setting ERV; 3) the ERV exhaust temperature must be greater than the supply ERV temperature indicating no sensible heat exchange; 4) the difference between the outdoor air and supply air temperatures must be between 0.2 °C and 4 °C; and 5) the flow rate must be at least 30 CFM. If all these conditions are satisfied, then the system is considered in bypass mode and the thermostat can follow the flowchart outlined in Figure 25. Condition 4 is specifically included to avoid times when the indoor and outdoor conditions are very close as the ERV does not always enter bypass mode in these instances.

3.2 Simulated Proposed Free Cooling Algorithm

The TRNSYS model's free cooling algorithm was simplified since there was no need to interpret if the ERV had entered bypass mode or not. Instead, the custom type 1273 ERV control was programmed to enter bypass mode if the outdoor temperature was less than the comfort setting and the ERV return temperature was greater than the comfort temperature. This maximizes bypass mode being in effect.

3.3 Tuning based on NZERTF Free Cooling Tests

Temperature-based ERV bypass control tests were run at the NZERTF following the control scheme outlined in 3.1 beginning in May 2024 until July 4,

2024. This data was first utilized to check the sensible and latent effectiveness when the ERV was in bypass mode. Bypass mode data was separated from the typical operation by assuming that bypass mode only occurred if the fresh air supply temperature was less than the stale exhaust air temperature if the temperature difference across the fresh air supply was less than the temperature difference between the outdoor air and stale exhaust air, and if the return air temperature was greater than the ERV comfort setting of 23 °C. After separating the data, the effectiveness was plotted and calculated in the same way as outlined in section 2.3.4. Figure 26 for sensible heat and Figure 27 for latent heat show the relationship between mass flow rate and potential heat transfer to the measured heat transfer. Intuitively, the slopes of these lines are much smaller than when the ERV is not in bypass mode indicating a very low effectiveness. The resulting effectiveness as a function of mass flow is shown in Figure 28. It is important to note that during bypass mode these relationships don't necessarily indicate a heat exchange between the two air streams but could also represent a small amount of heating or cooling occurring as the fresh air stream moves through the ductwork and system. This is further emphasized given that the nominal latent effectiveness from the curve fit is only 0.06 (see Appendix I for a summary of bypass mode effectiveness parameters). Like the latent effectiveness in humid conditions, the bypass mode latent effectiveness is only fit to two flow rates, so the shape of the curve is not representative of the physical system, but the effectiveness at the two flow rates used in TRNSYS is accurate.

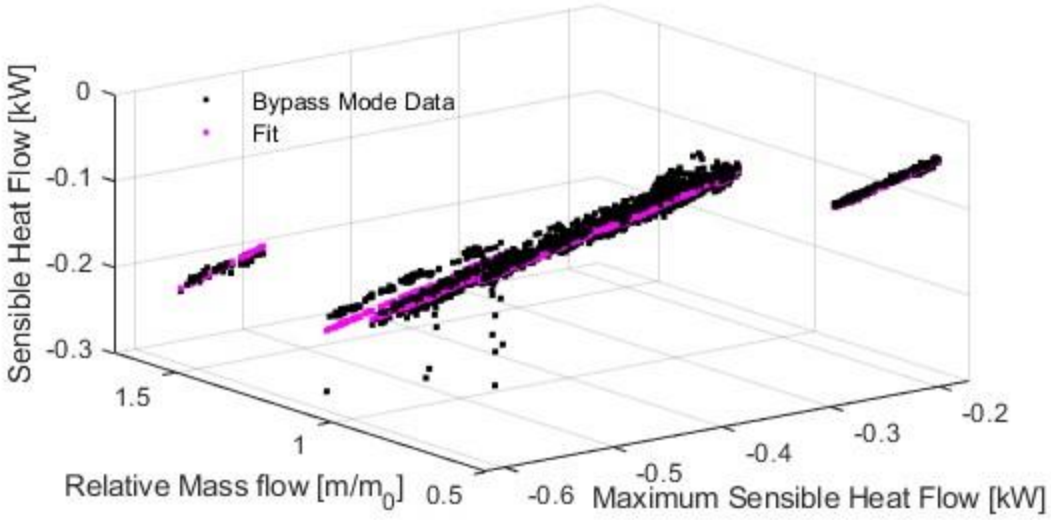

Figure 26. Sensible heat flow during bypass mode for the fresh air stream plotted against relative mass flow and the maximum possible sensible heat flow.

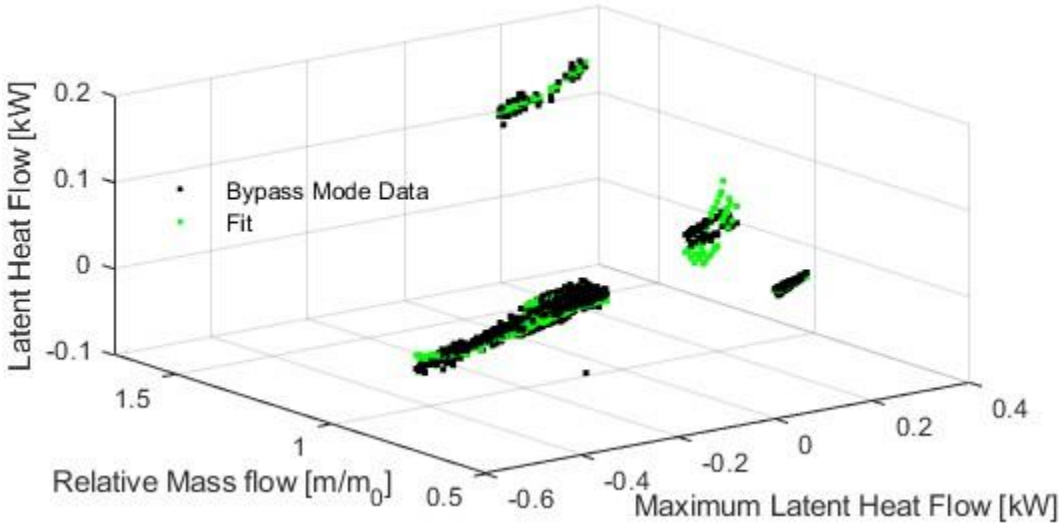

Figure 27. Latent heat flow during bypass mode for the fresh air stream plotted against the relative mass flow and the maximum possible latent heat flow.

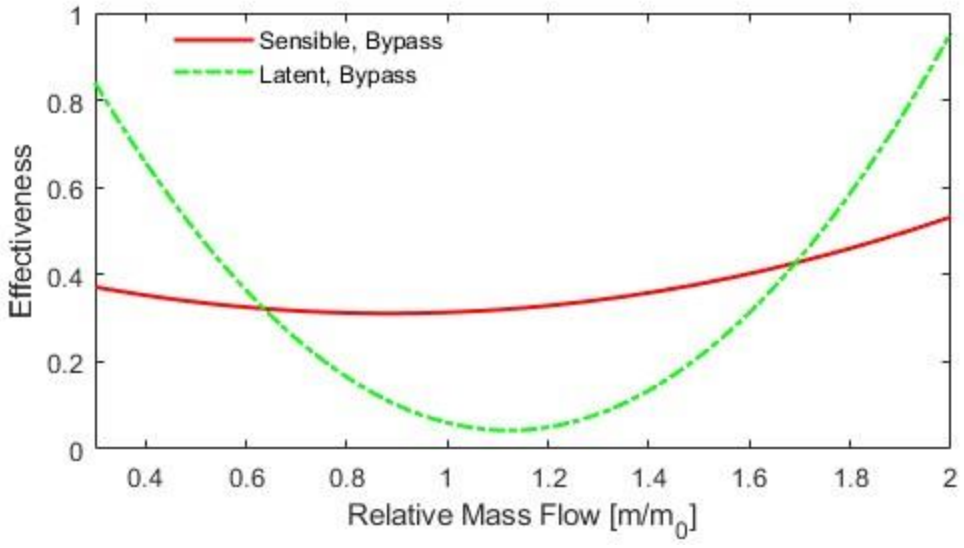

Figure 28. ERV effectiveness as a function of mass flow rate when in bypass mode.

I chose a subset of the bypass mode operation data from June 28 until July 4 to compare the actual controls to the model's attempts to implement the control scheme. Figure 29 shows the ERV's measured temperature and humidity ratios compared to the TRNSYS model for the tuning period. Overall, the temperatures match very well, indicating that both the TRNSYS models effectively model the return air temperature from the house and the sensible and latent humidity exchange between the fresh and stale air exchanges. The model also enables bypass mode at the correct times. The dashed black line indicates that the model entered bypass mode, which matches well with when the measured outdoor and supply conditions approach one another. The solid black lines indicate when the bypass mode detection algorithm described in section 3.1 flagged bypass mode as occurring. This highlights the imperfections with the detection algorithm and indicates that it will need to be refined

for any future free cooling tests at the NZERTF. For the purposes of evaluating the impact of maximizing free cooling, the TRNSYS model works very well at determining when the system is in bypass mode, so it requires no additional tuning.

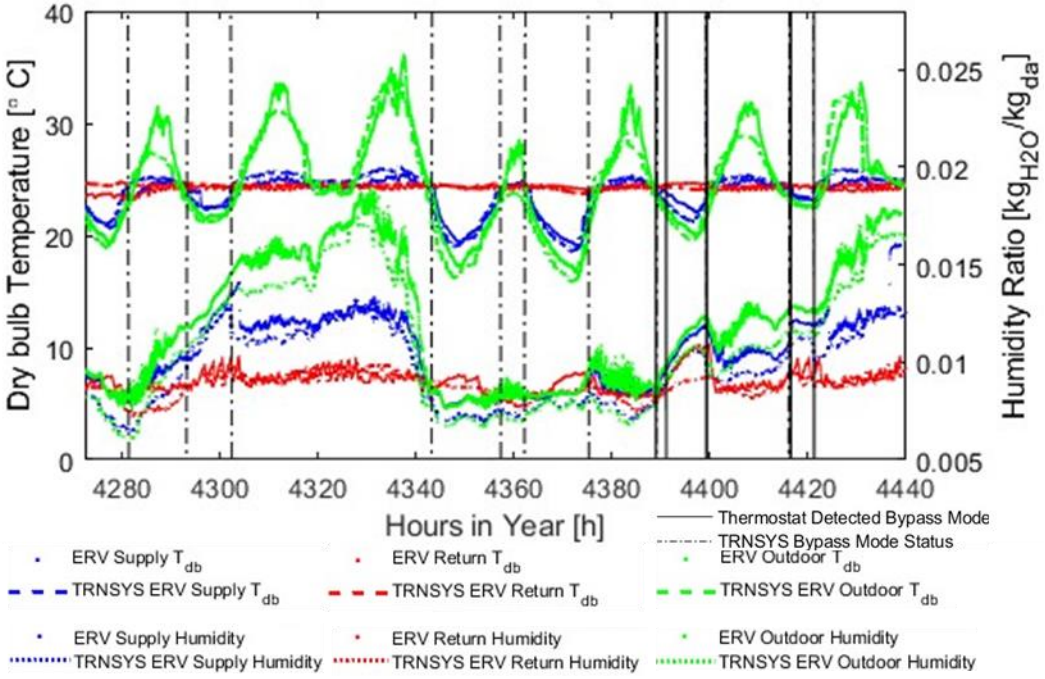

Figure 29. Comparison of measured ERV temperatures and humidity ratios to the corresponding values from TRNSYS simulation with temperature-based bypass mode implemented.

Because the model accurately predicts the temperature and humidity ratio supplied to the house, the sensible and latent loads, shown in Figure 30, are also close to the measured loads. There are a few times when the loads are under-predicted relative to measured performance. For example, the bypass mode period of hours 4390 – 4400 h shows a smaller sensible load than the measured sensible load. This discrepancy is mostly due to the difference in the modeled and measured return air

values in this time which is described in more detail below. The supply air temperatures still match very closely in Figure 29.

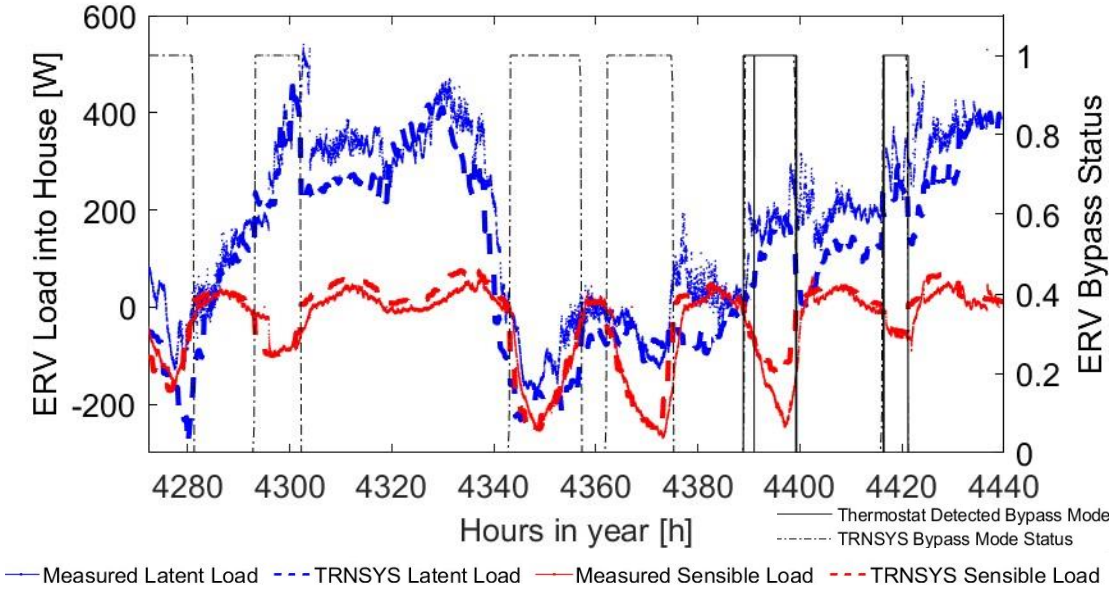

Figure 30. Comparison of measured ERV loads added to house and the corresponding loads from TRNSYS simulation with temperature-based bypass mode.

This discrepancy in return air conditions can be explained by considering the heat pump operation at this time as seen in Figure 31. Since the model enables bypass mode (dashed black line in Figure 31b) in the thermostat control more often, the cooling operation occurs less often. This limits the amount of heat pump activity apart from a couple of dehumidification operation stages since the temperature stays within the 1st deadband in these free cooling states.

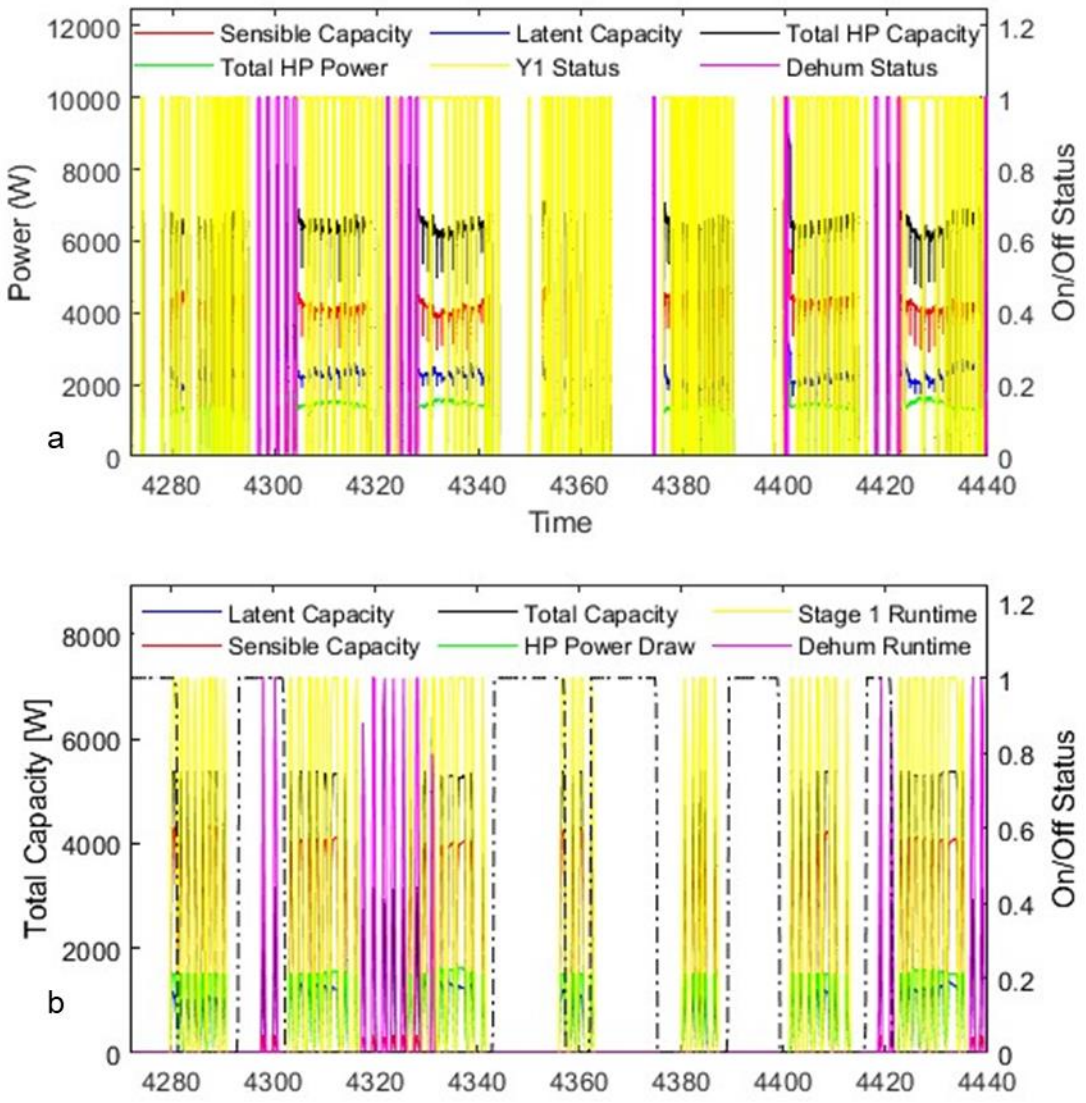

Figure 31. Comparison of (a) actual to (b) TRNSYS modeled heat pump operation during the bypass tuning period.

Figure 32 shows both the measured living room temperature and relative humidity compared with the TRNSYS model Zone 2 conditions. Overall, the conditions match very closely to the actual bypass mode performance. The main deviations are when bypass mode is enabled and the temperature drifts slightly lower

than the measured temperature. It is important to keep in mind that the model assumes a uniform temperature throughout the first floor. The humidity is generally well approximated except when the dehumidifier was correctly enabled in the model, but not in reality

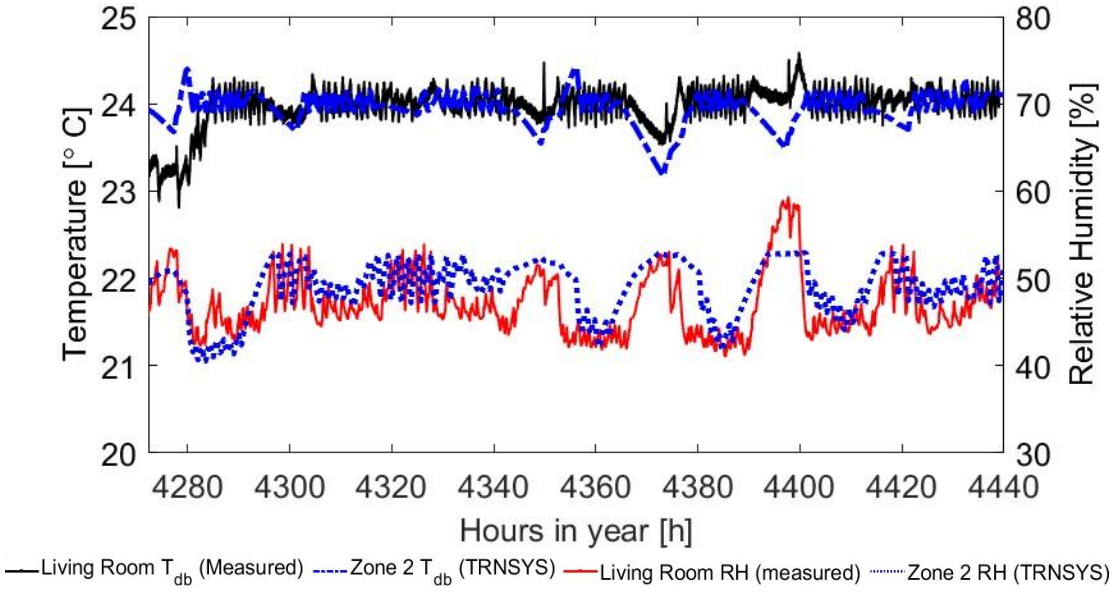

Figure 32. Comparison of measured living room temperature and relative humidity to the corresponding Zone 2 values from TRNSYS simulation with temperature-based bypass mode implemented.

Overall, the model predicts and replicates the ERV conditions and Zone 2 conditions well, indicating little need to tune the model further. Bypass mode control for the thermostat is triggered more often, but that is good as this allows for the model to evaluate the maximal effect of this control strategy instead of replicating the ineffective bypass mode detection algorithm.

3.4 Model Performance

With a well-tuned TRNSYS model of the NZERTF, the bypass control can be tested and evaluated relative to a baseline case without bypass mode. The 2024 weather data was used for a more recent representation of the local weather. However, the original water, plug load, appliance, lighting, occupancy, and moisture schedules were used to represent an occupied residential home with typical loads. This model was run for an entire simulation year to evaluate the temperature bypass control's impacts on both energy use and any difference in Zone conditions impacting thermal comfort.

3.4.1 Energy Savings

The ERV load is the critical driver in this control scheme. If the ERV sensible load can be maximized during free cooling and minimized otherwise, then the heat pump should minimize cooling operation when conditions are optimal. However, the latent load is the limiting factor for the scheme's effectiveness as a latent load that is too large will require more dehumidification cycles. Two one-week periods were selected to show the impacts of bypass mode. One in late spring, from May 23 to May 30, and the other in late summer – August 15 to August 22. Figure 33 shows both the sensible (a) and latent loads added to the facility for the baseline case of no bypass mode and the temperature-controlled bypass mode for May 23 – May 30. Where control is in bypass mode when the temperature bypass load deviates from the baseline load. In this period, the bypass control allows for up to about 350 W of free

cooling brought into the building while the baseline case adds or removes a sensible load by ± 50 W. However, the latent load added to the house can be significant. In the timeframe around hour 3480, the latent load added to the bypass control case is more than double the baseline case, negating most of the benefit of free cooling. This situation of adding cold and humid air to the building is even more significant, as shown in Figure 34b where the added latent load exceeds 500 W between hours 5,480 and 5,525 while the sensible load (Figure 34a) never surpasses 200 W of cooling in this time.

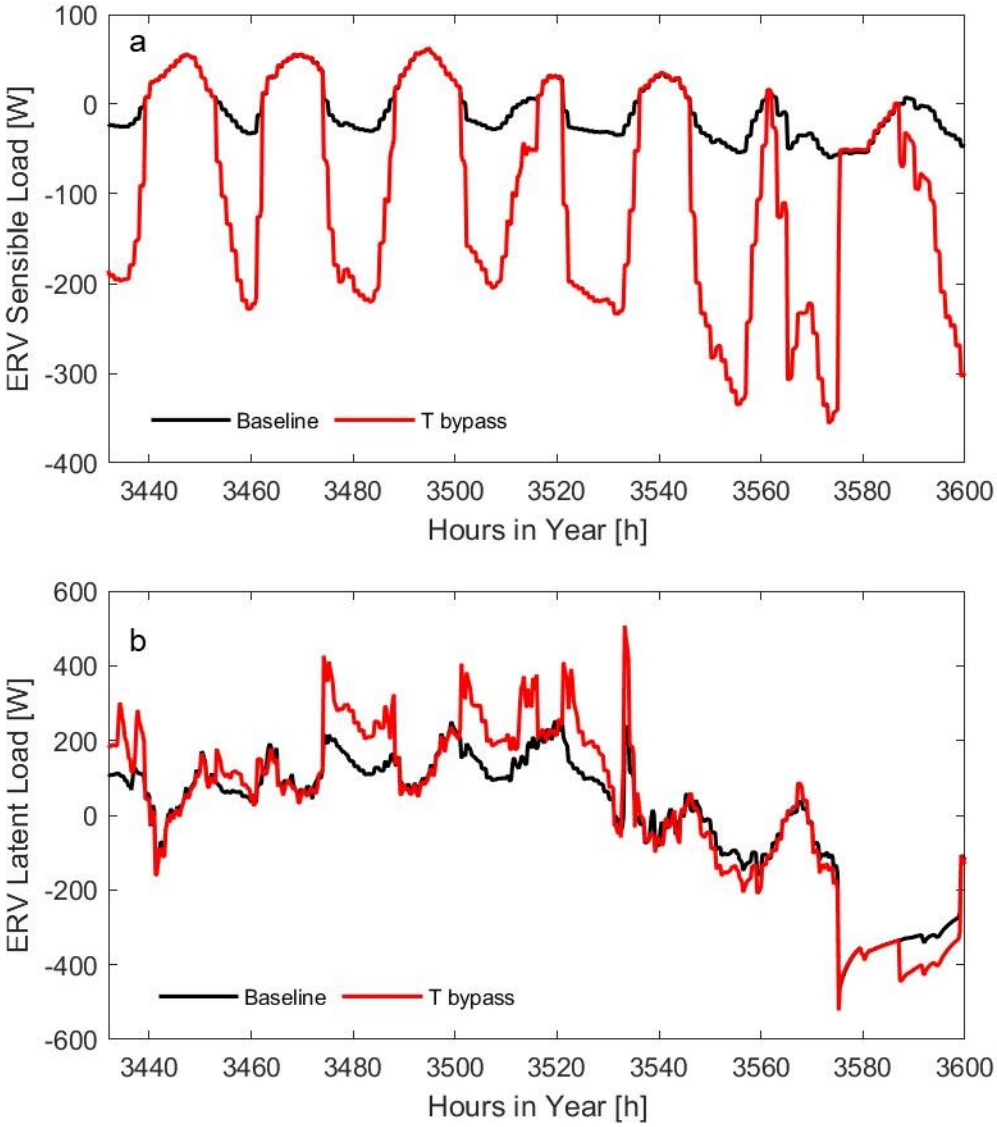

Figure 33. ERV sensible (a) and latent (b) loads added to the house through the ERV for baseline and temperature bypass conditions for hours 3432 to 3600 (May 23 to May 30).

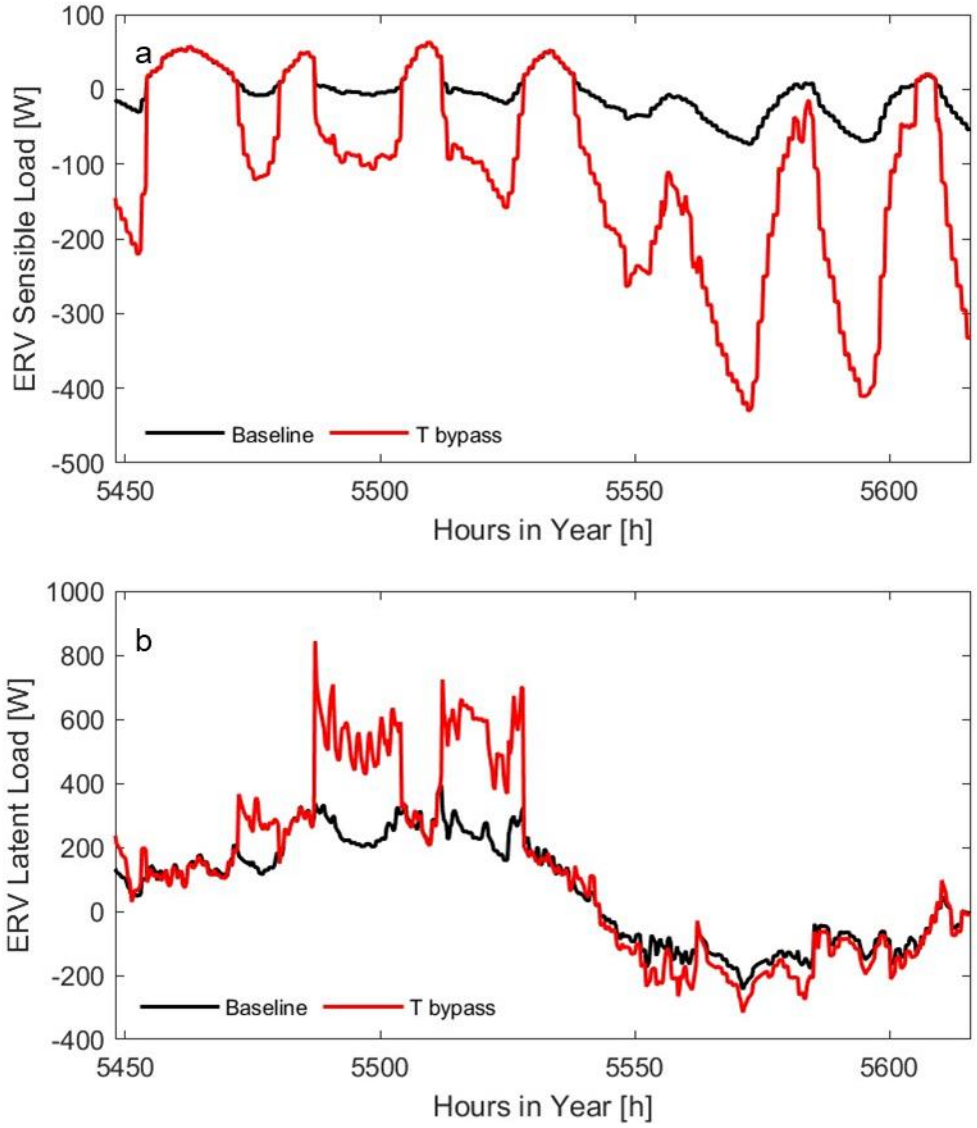

Figure 34. ERV sensible (a) and latent (b) loads added to the house through the ERV for baseline and temperature bypass conditions for hours 5548 to 5616 August 15 to August 22).

These ERV load trends from the instantaneous simulation data add up over time as shown in Figure 35. The total latent loads from April through October are higher for the bypass control than the baseline resulting in an additional 129 kWh

of latent load added to the building during this time while the sensible cooling load is reduced by 305 kWh. The total cooling load reduction by using bypass control was 176 kWh. The free cooling available is only maximized from April through mid-June and mid-August through October. There is naturally very little free cooling available during the hottest time of year.

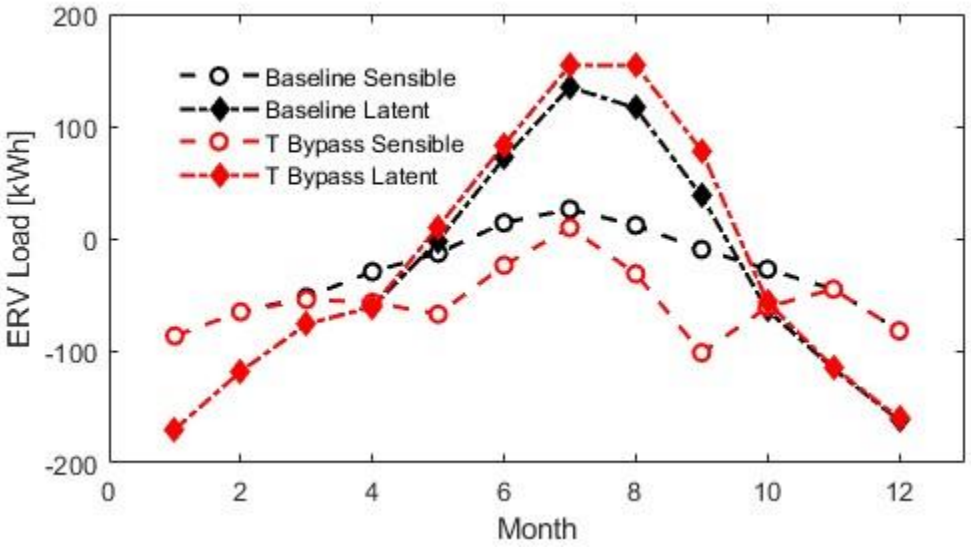

Figure 35. Monthly ERV loads added to the facility with and without temperature-based bypass control.

Since the control scheme allows for the ERV flow to be maximized when Zone 2 exceeds 24.17 °C, the ERV fan energy use can offset potential savings. Figure 36 shows the average monthly ERV fan power. The average power draw with bypass control never exceeds more than 7 % of the average in the baseline case in any month. Since the average fan power never exceeded 44 W, the excess energy use doesn't exceed 2 kWh in any given month meaning that maximizing the flow rate has minimal impact on the total savings.

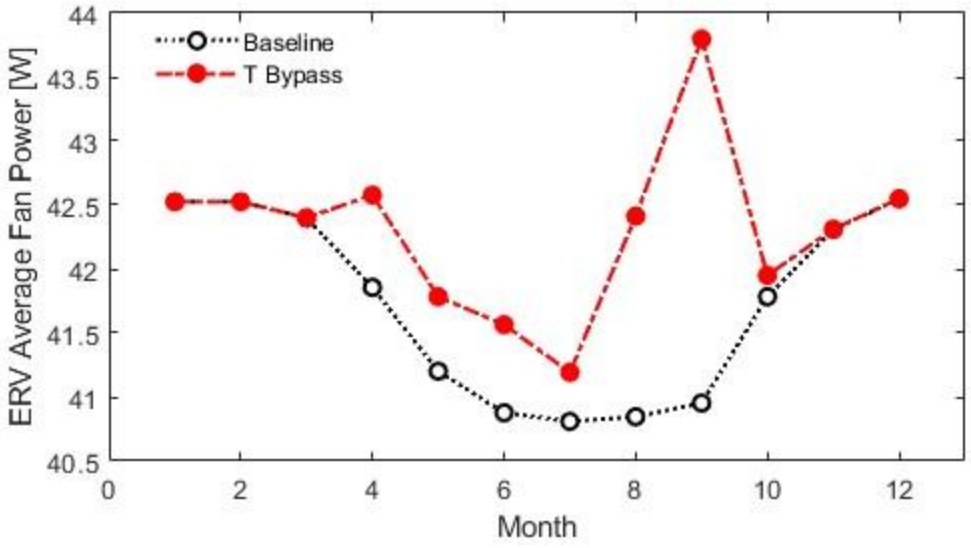

Figure 36. Comparison of ERV fan power for baseline and temperature-based bypass control.

Over the course of the year, the reduction in sensible load more than offsets the added latent load giving 38.6 kWh of heat pump load savings to the HVAC system or 0.35 % of annual heat pump loads. Figure 37 shows the monthly trends for net total heat pump energy, net sensible heat pump energy, and net latent heat pump energy using temperature-based bypass control relative to the baseline condition. June and September realized the most savings while July saw a slight loss since the added latent loads exceeded the utilized sensible free cooling. While this is a small amount of savings, it does show that a bypass control can reduce heat pump load.

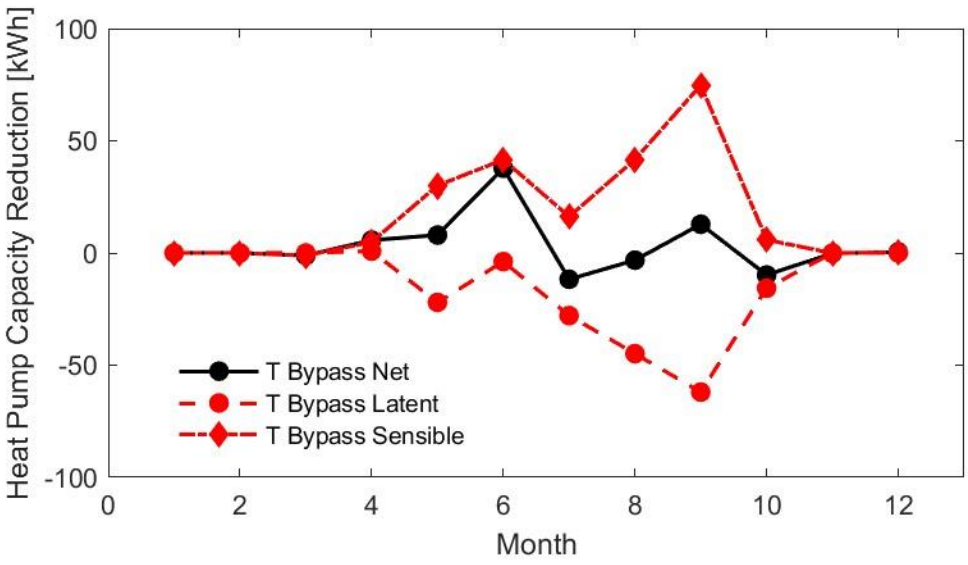

Figure 37. Net heat pump load savings with temperature-based bypass control.

Reducing heat pump capacity is undoubtedly helpful, but the end goal is to reduce electricity consumption to mitigate electrical grid draws. Figure 38 shows the monthly heat pump electricity savings. All but cooling season months are negative meaning that, unfortunately, due to the sizeable latent load that the heat pump must offset via dehumidification, an additional 82.2 kWh of electricity was needed relative to no bypass control when implementing a temperature-based control. This finding means that an energy recovery ventilator is better used in constant operation without temperature-based bypass mode being enabled for a higher humidity climate in a low-load home.

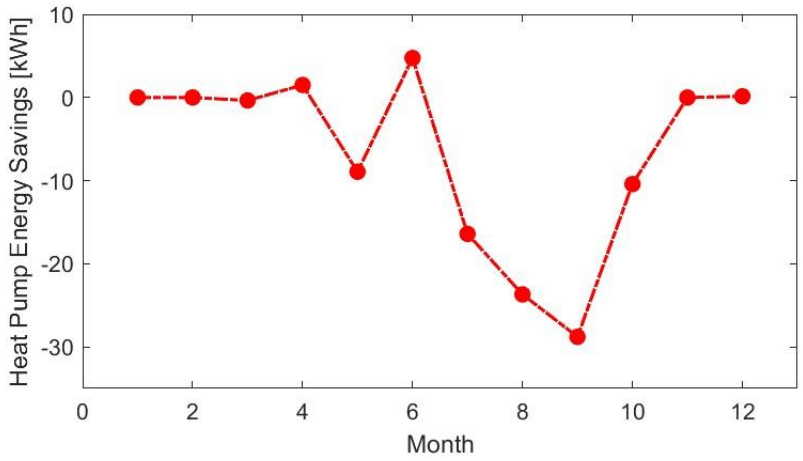

Figure 38. Monthly heat pump electricity savings for temperature bypass mode control.

3.4.2 Thermal Comfort

While energy savings are the desired outcome for this control strategy, the temperature and humidity in the home must remain comfortable for occupants. If the home becomes too humid or too cool, then the control strategy is not feasible. The temperature and relative humidity were evaluated for both the May 23 – May 30 and August 15 – August 22 time periods, as well as the monthly averages over time, to assess if implementing bypass control could make the indoor conditions uncomfortable for occupants.

Figure 39 shows how the temperature bypass control influences the Zone 2 conditions from May 23 to May 30. When the ERV enters bypass mode, the temperature generally decreases more than the baseline case, though there are a couple of instances where the temperature does increase in the Zone. These temperature increases happen in the morning or early evening when the outdoor

temperature is just below the comfort setting. The larger width of the relative humidity plateaus at 53 % for the bypass control also indicates that the dedicated dehumidifier must run more often when bypass mode is in effect to offset the added latent loads. The ERV bypass control has a similar impact in August, as seen in Figure 40.

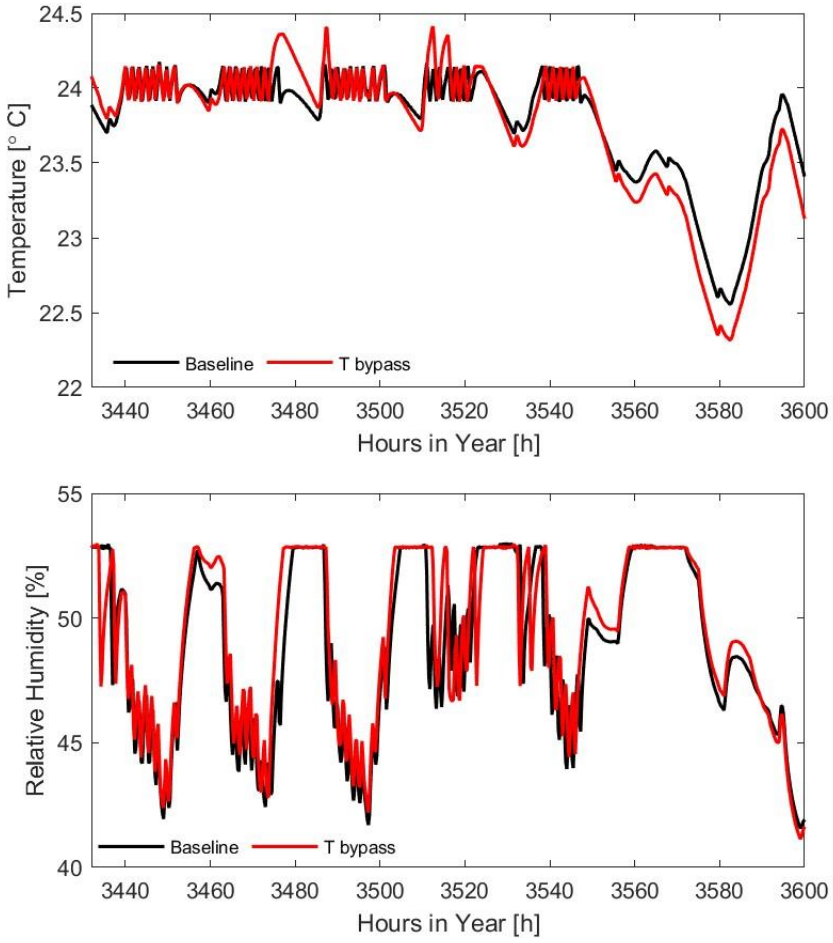

Figure 39. Comparison of Zone 2 (a) temperature and (b) relative humidity for baseline and temperature bypass control from May 23 – May 30.

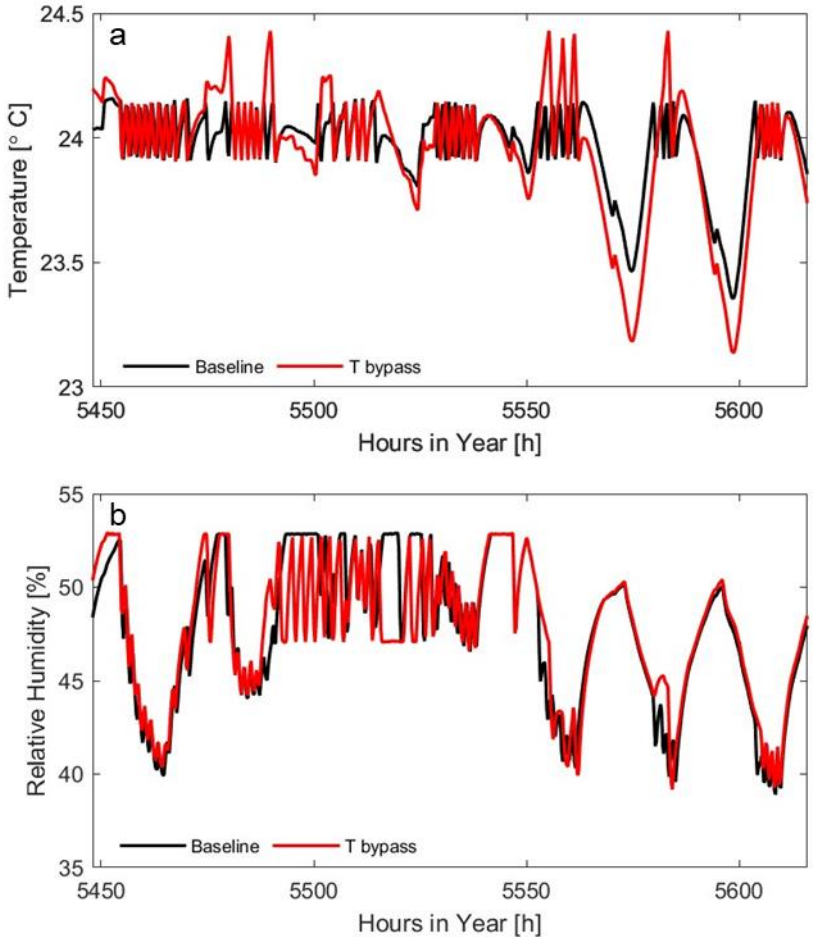

Figure 40. Comparison of Zone 2 (a) temperature and (b) relative humidity for baseline and temperature bypass control from August 15 – August 22.

These granular views help to explain the impact on the thermal comfort in the building. The average temperature and relative humidity also show the overall trends of the control. Figure 41 shows how the average monthly temperature in Zone 2 decreases by about 0.1 °C during the shoulder months when bypass mode can be operated the most, but the average relative humidity increased by up to 0.5 %.

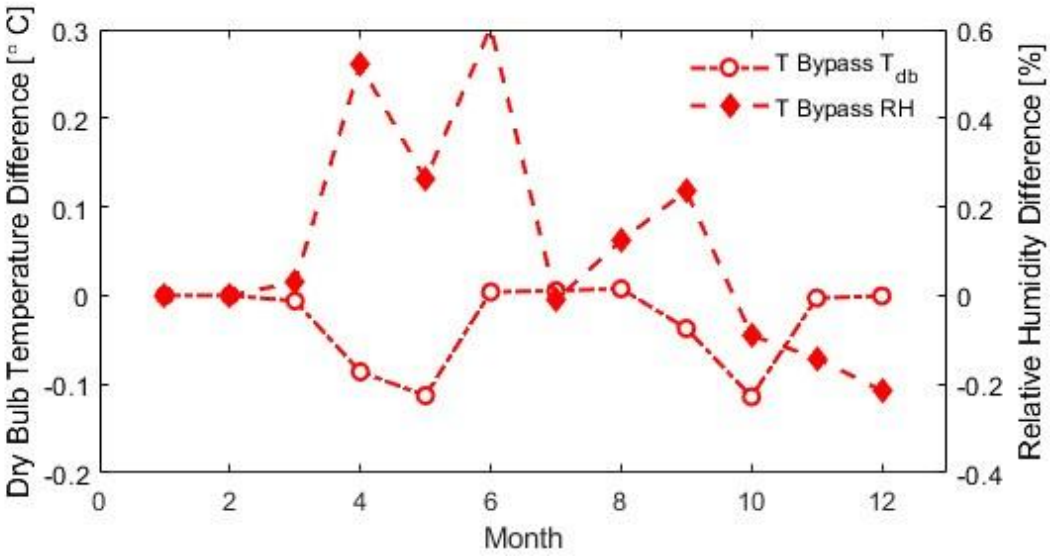

Figure 41. Difference in average monthly Zone 2 Conditions between baseline and temperature-based bypass mode ERV control.

Over the entire cooling season period from April through October, there are temperature and humidity deviations as shown in the Zone 2 and Zone 3 psychrometric plots in Figure 42. But much of the time, the Zone 2 and Zone 3 temperature deviations from the baseline model are limited to ± 0.3 °C and + 0.3 °C / -0.6 °C, respectively, and the relative humidity remains within ± 2 % for Zone 2 and ± 2.5 % for Zone 3. However, these outliers can lead to Zone 2 measuring up to 0.5 °C above the baseline and + 7.1 % to – 5.9 % in relative humidity. Zone 3 does not have any upper limit outliers, but the humidity tends to be higher, with the maximum difference being + 9.2 % to – 5.1 % compared to the baseline condition. These larger differences underscore the large latent loads allowed through during some of the free cooling periods. Despite these larger latent loads, the maximum relative humidity in the cooling season occurs in Zone 3 with a relative humidity of 61.2 % with a

corresponding dry bulb temperature of 25 °C. This air condition still lies within a summertime comfort Zone as specified by ASHRAE standard 55 [48], [50]. Note the magenta line indicating the maximum humidity ratio of 0.012 kg_{water} / $kg_{dry\ air}$. At no point does the temperature-based control exceed this line, even if it does meet it in Zone 3. The dry bulb temperature never exceeds 24.5 °C in Zone 2 and 25.9 °C in Zone 3.

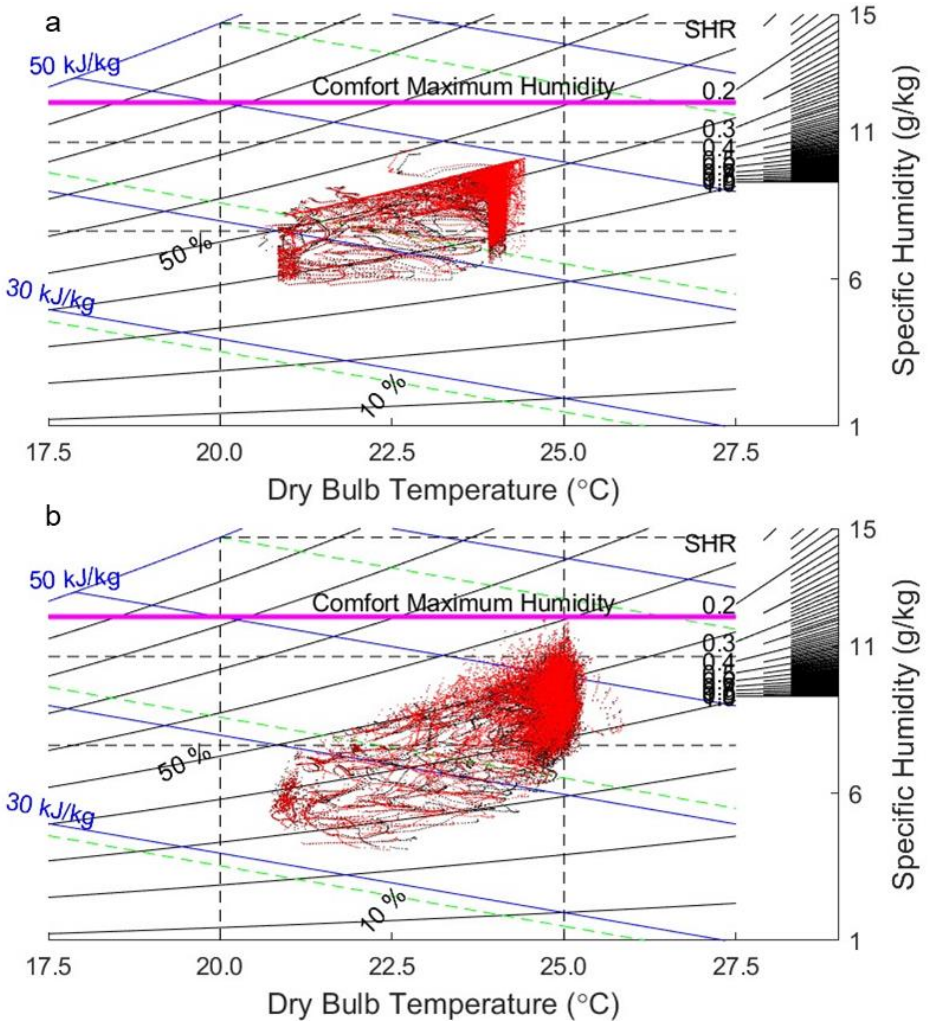

Figure 42. Psychrometric plots of (a) Zone 2 and (b) Zone 3 conditions during cooling season for baseline and temperature bypass control during cooling season.

While thermal comfort is maintained for this control strategy, it consumes more energy than the baseline case and does increase shift the Zone 3 conditions towards the upper limit of thermal comfort. All told, this strategy is not feasible for this building in a mixed-humid climate zone.

Chapter 4: Proposed Enthalpy-based Control

An enthalpy-based control can be implemented in a similar fashion to the temperature-based control. For this study, the comfort setting was 45 kJ/kg, determined from psychrometric relationships for the Zone 2 cooling setpoints of 23.89 °C and 50 % RH. The thermostat controls follow the same decision flow as described in the section 3.1, but replacing the temperatures with enthalpies. This method has not yet been implemented at the NZERTF since the ERV operates with its own controller using a temperature-based comfort setting. So, this enthalpy-based control can be utilized as a best-case scenario comparison to the temperature-based control to ideally minimize latent loads added to the house while reducing heat pump use during the swing seasons. This analysis can also answer whether it is worth pursuing these tests at the facility in the future or if this control scheme has minimal impact on the NZERTF in its mixed humid climate zone.

4.1 Performance

The main goal of this control strategy is to optimize free cooling so that sensible free cooling is maximized while minimizing any added latent loads from humid outdoor conditions. Below, the enthalpy-based control is compared to both baseline and temperature-based control for heat pump load, ERV fan energy, energy savings, and thermal comfort.

4.1.1 Energy Savings

The ERV loads, when operating in enthalpic bypass mode control, will naturally tend closer to the baseline than the temperature-based control with limited latent loads. Figure 43 highlights this for the May 23 – May 30 period. There are four periods of time when bypass mode is enabled due to a sufficient decrease in outdoor enthalpy, and in each case, very little, if any, latent load is added. This control scheme is very effective at avoiding the high latent load potential of the temperature control like in the hours of 5,480 – 5,530 shown in Figure 44. During this time, the temperature-based control allowed a latent load of up to 800 W into the building, but the enthalpic control mode limited the load since it never entered bypass mode.

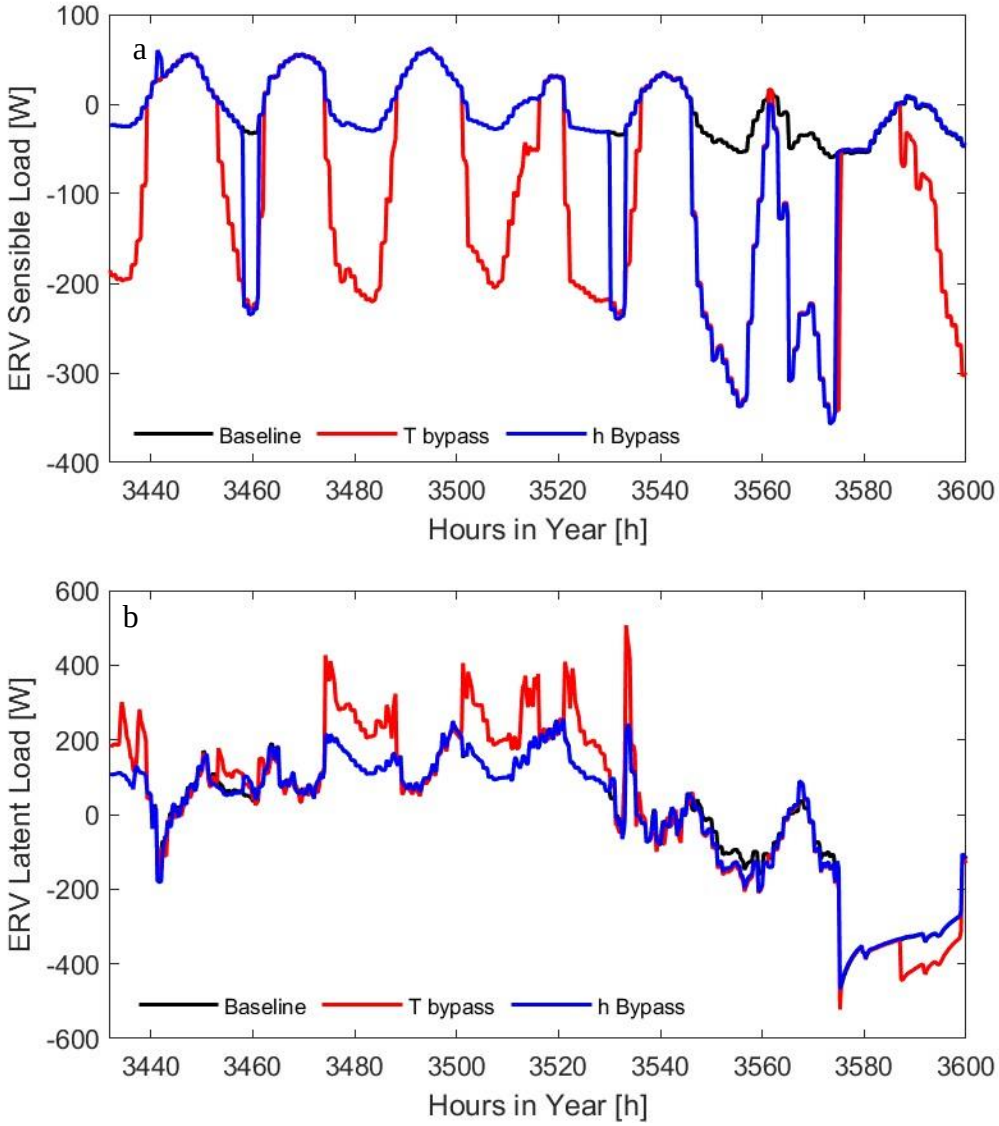

Figure 43. ERV sensible (a) and latent (b) loads added to the house through the ERV for baseline, temperature bypass, and enthalpy bypass conditions during hours 3,432 to 3,600 (May 23 to May 30).

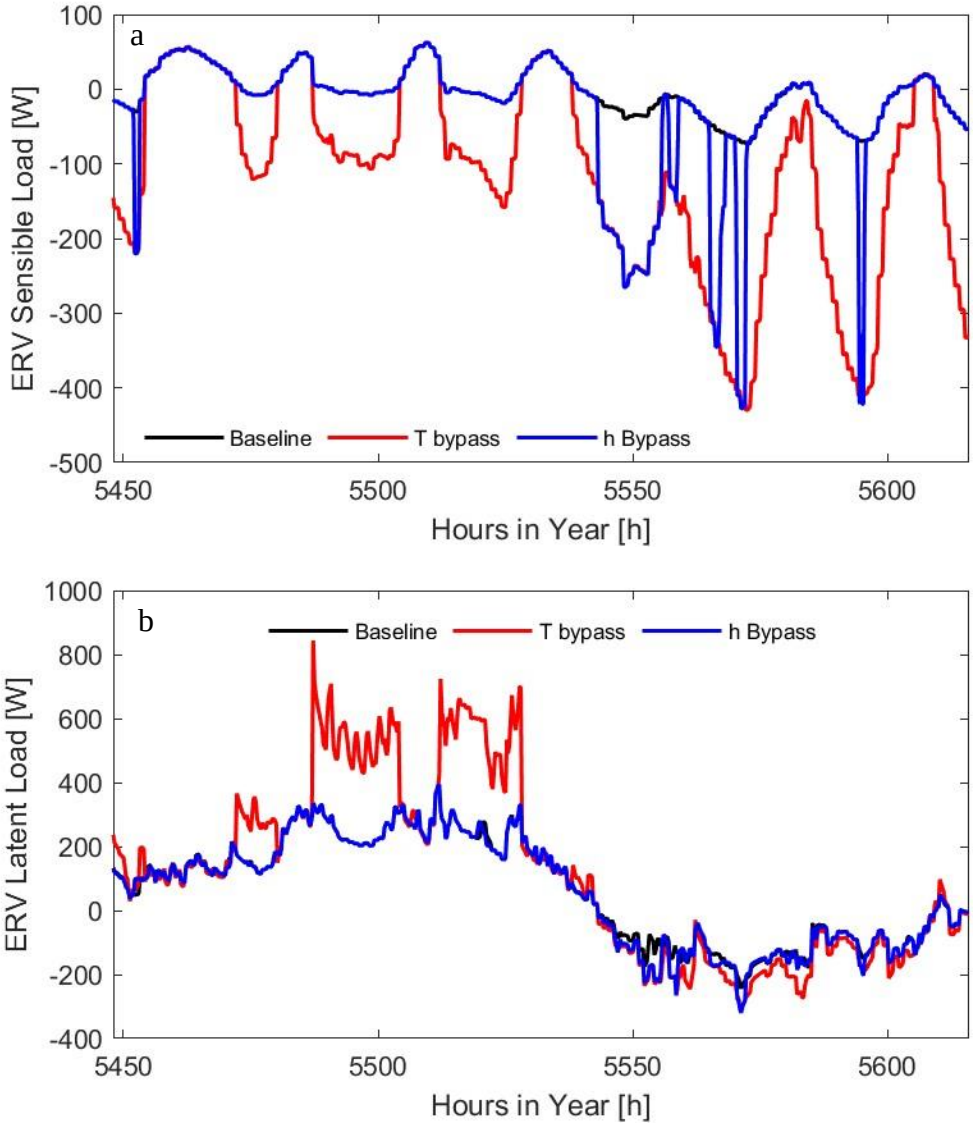

Figure 44. ERV sensible (a) and latent (b) loads added to the house through the ERV for baseline, temperature bypass, and enthalpy bypass conditions during hours 5,548 to 5,616 (August 15 to August 22).

This latent load limitation does come with the drawback of also limiting the free cooling potential, as seen by the monthly total ERV load introduced in the building shown in Figure 45. The sensible free cooling is more than halved between April and October for a total of 119.9 kWh below baseline, but the latent load is also

reduced to approximately the same level as the baseline case (+ 2.33 kWh). The reduction in loads is primarily due to a reduction in bypass mode operation, which is emphasized by the lower average ERV fan power (Figure 46) when compared to the temperature-informed control. This reduction in bypass and maximum fan flow rate allows for the enthalpic control to limit the dehumidification operation.

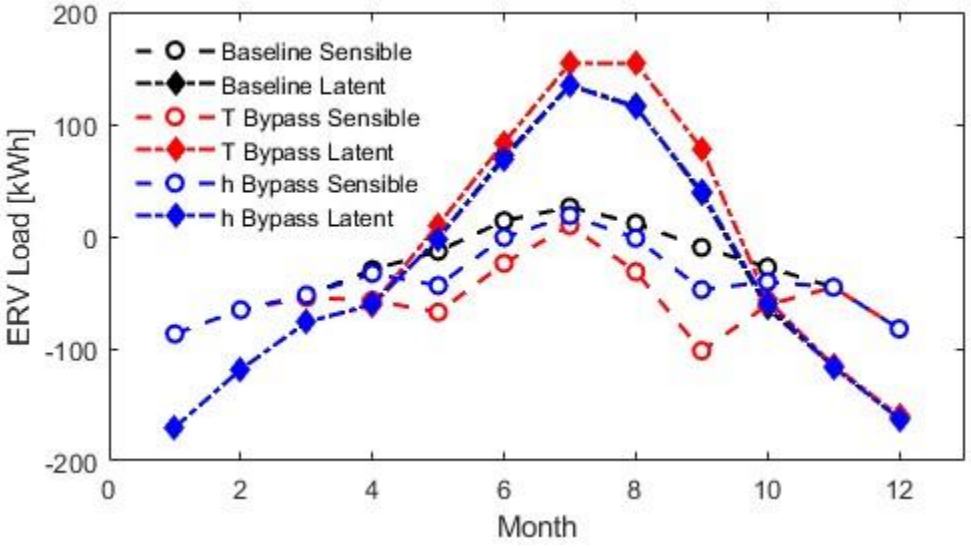

Figure 45. Monthly total ERV loads added to the facility for baseline, temperature-based bypass control, and enthalpy-based bypass control.

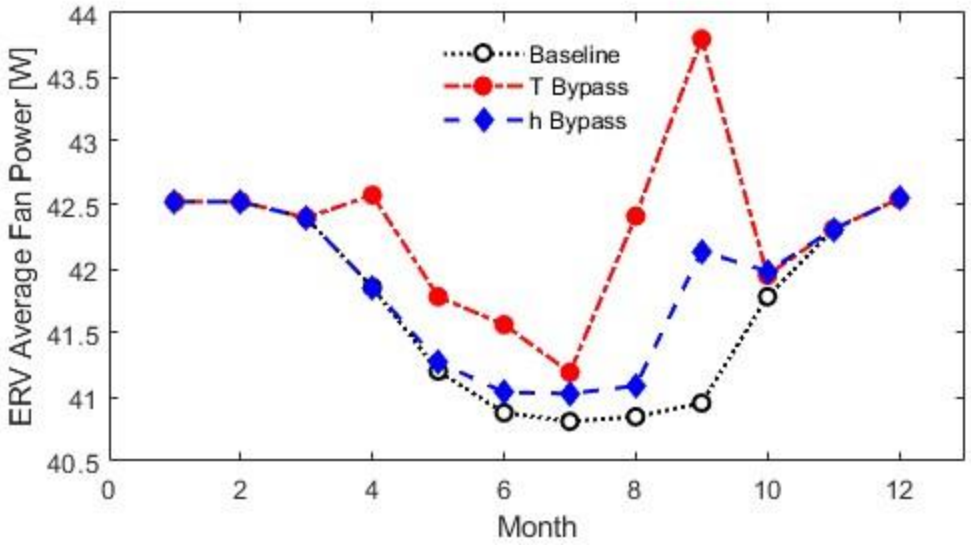

Figure 46. Comparison of ERV fan power for baseline, temperature-based bypass control, and enthalpy-based bypass control.

This reduction in ERV latent load added to the house results in a reduction of 88.5 kWh in heat pump load for conditioning the building with the monthly reductions shown in Figure 47. This is equivalent to 0.80 % annual heat pump energy savings. Since the free cooling that does occur with enthalpic bypass control minimizes latent loads, the dehumidification mode runs just barely more than the baseline case. Even though bypass mode runs less frequently, it still more than offsets the minimal latent loads added to the house yielding more significant heat pump load reduction than the temperature-based control option.

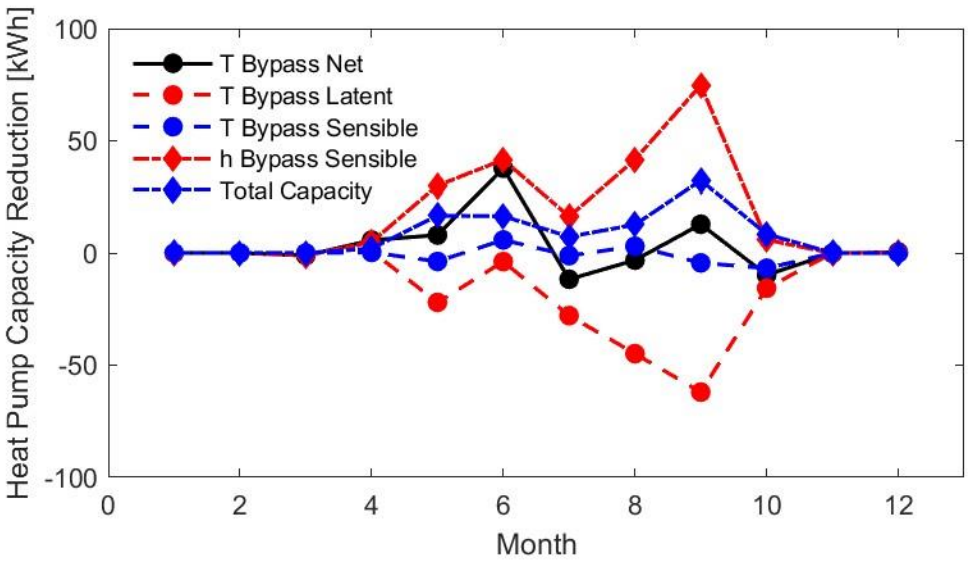

Figure 47. Comparison of net heat pump load savings for temperature-based bypass control and enthalpy-based bypass control.

While reducing the heat pump load is ideal, it is only beneficial if the electrical load is also reduced. Since the dedicated dehumidification mode runs much less often than the temperature-based control, 7.4 kWh of annual electricity is saved from heat pump operation. The savings are emphasized in Figure 48 when compared to the temperature-based control which only saw net heat pump savings in 2 months of its simulation. The enthalpic control, on the other hand, led to positive savings in every month except for July and October. The savings are small, likely due to the already very efficient home, heat pump, and very effective ERV.

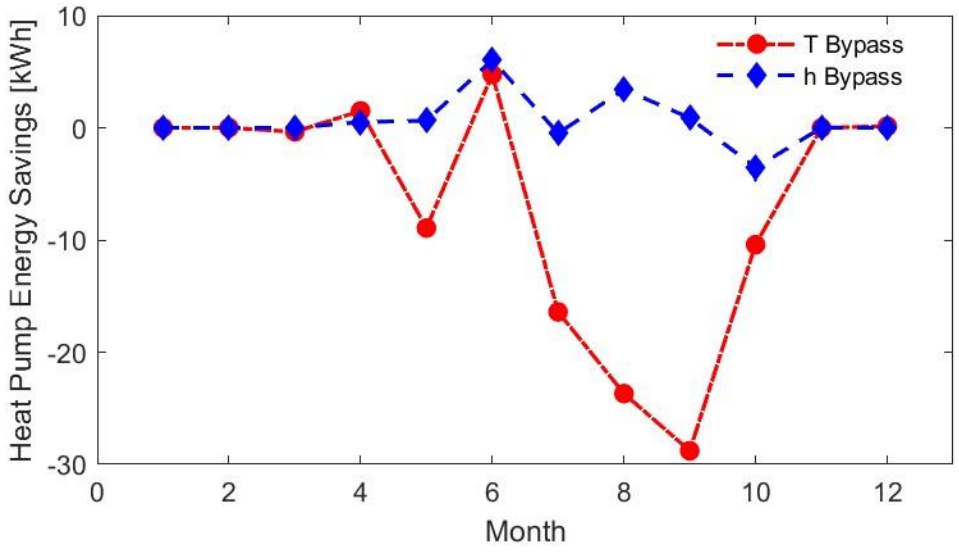

Figure 48. Monthly heat pump electricity savings for temperature and enthalpy bypass controls.

4.1.2 Thermal Comfort

Since the enthalpic control could be a feasible option due to its modest electricity savings, it is critical for the thermal comfort of the space to be satisfactory for occupants. Thankfully, the temperature and humidity do not shift as radically as the temperature bypass control. Figure 49 compares how the temperature and humidity change in zone 2 for the baseline, temperature bypass, and enthalpy bypass cases. The enthalpy bypass control optimizes enabling free cooling without adding excessive latent loads and requiring additional dehumidification. The enthalpy control also prevents the temperature spikes that occur with the temperature control method further improving the Zone conditions for occupants by reducing the magnitude of fast-changing conditions. The August timeframe (Figure 50) highlights how dehumidification runtime is significantly reduced across the 5,480 – 5,525 hours.

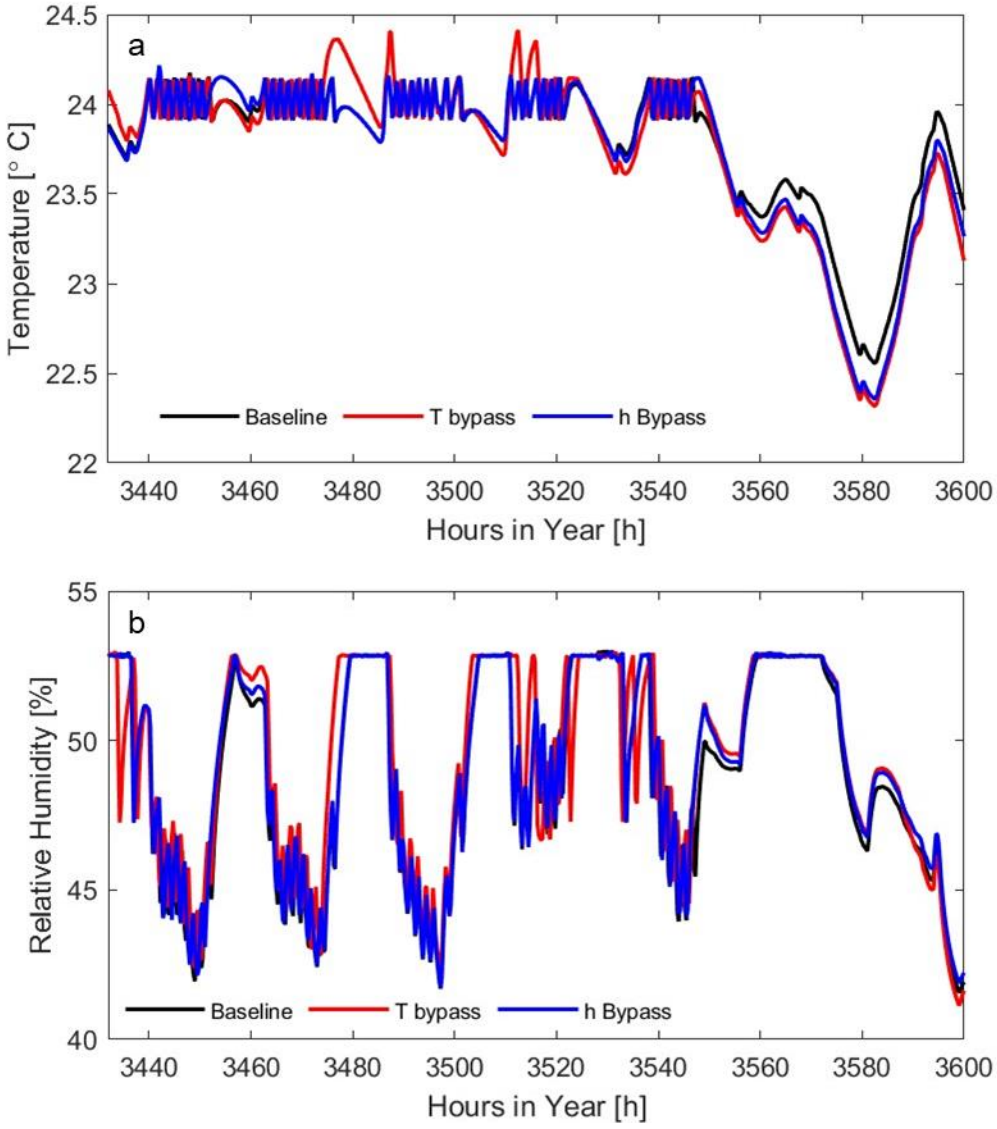

Figure 49. Temperature (a) and relative humidity (b) of the baseline, temperature bypass, and enthalpy bypass conditions for hours 3,432 to 3,600 (May 23 to May 30).

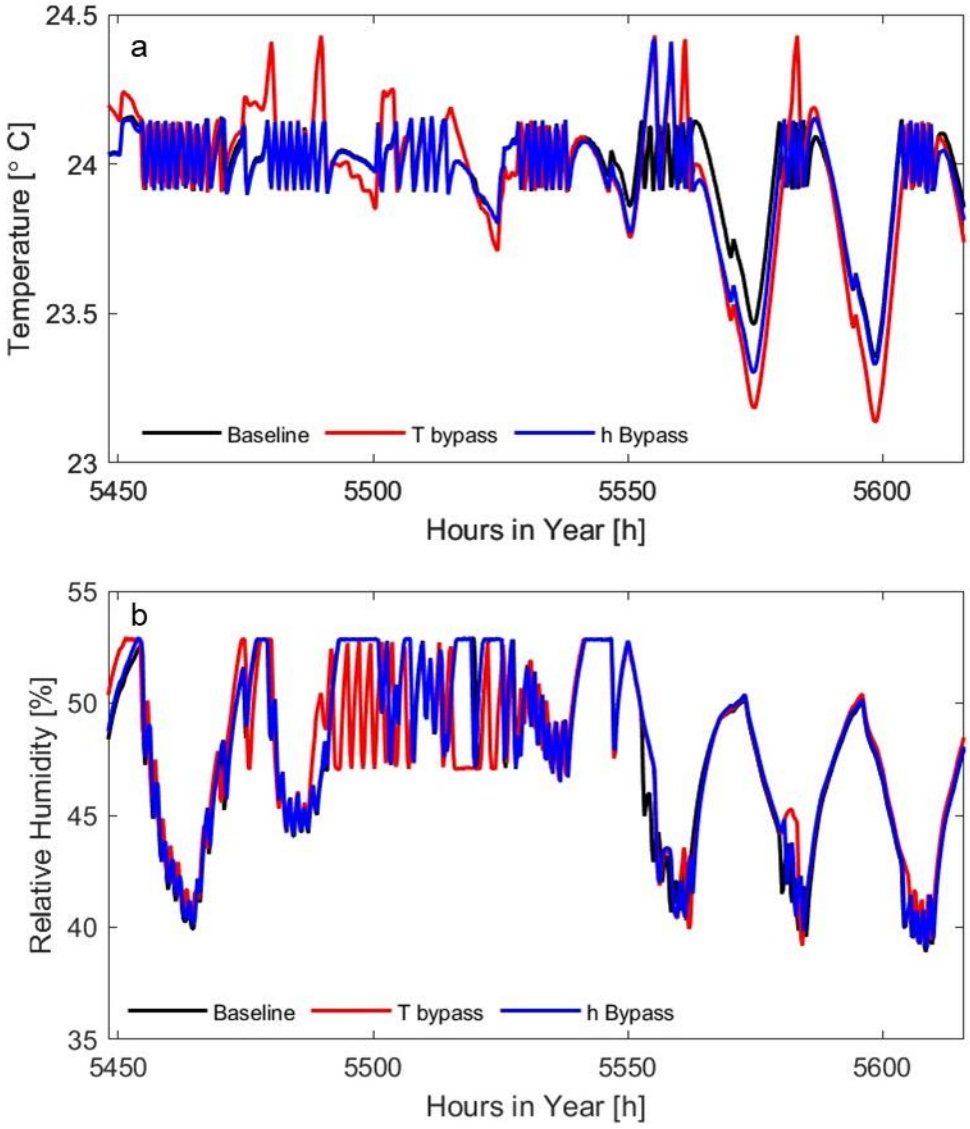

Figure 50. Temperature (a) and relative humidity (b) of the baseline, temperature bypass, and enthalpy bypass conditions for hours 5,548 to 5,616 August 15 to August 22).

These trends hold across the average monthly and relative humidity conditions during the yearlong simulation. Both the temperature and relative humidity for the enthalpy-based control scheme deviate much less from baseline conditions with only

up to 0.2 % increase in average relative humidity in any given month and the average Zone 2 temperature never deviates by more than 0.1 °C below baseline conditions as shown in Figure 51. This control scheme optimizes energy use in these periods while minimizing impacts on average thermal comfort in the space.

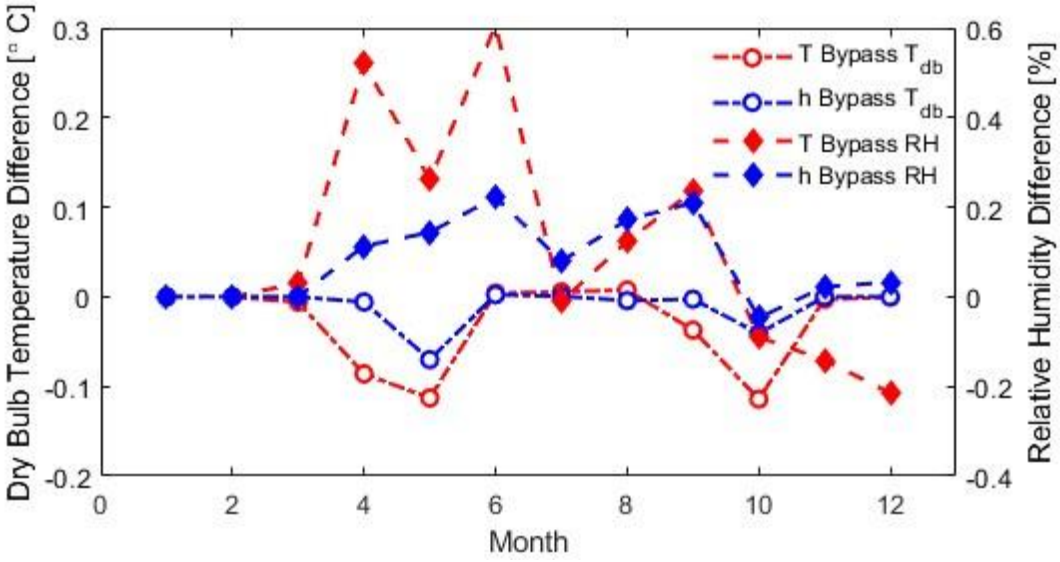

Figure 51. Difference in monthly average Zone 2 Conditions relative to baseline control for temperature-based and enthalpy-based bypass mode ERV control.

The reduced variability in transient Zone conditions for the enthalpy control case described in Figure 49 and Figure 50 are consistent when looking at the air properties on a psychrometric chart across the entirety of shoulder and cooling seasons (Figure 52). The enthalpy bypass control reduces the spread of Zone deviations from the baseline case dramatically when compared to the temperature control. The maximum temperature and relative humidity deviations are like the temperature-based control, but there is a much tighter spread of typical temperatures, which means a more reliable and consistent zone temperature. These trends are born

out of the relative humidity as well. The maximum temperature above baseline never exceeds 0.5 °C for Zone 2 and 0.3 °C for Zone 3. Meanwhile, the Zones do occasionally end up cooled to 0.4 °C and 0.6 °C below the baseline temperature. The Zone relative humidities follow a similar pattern where the enthalpy control matches the baseline conditions more closely to the temperature-based control. However, there are still times when the relative humidity is up to 6.0 % greater for Zone 2 and 5.8 % greater for Zone 3 than the humidity in the baseline simulation. Fortunately, these maximum humidities occurred when Zone 2 conditions were 22.7 °C and 59.7 % RH, and Zone 3 conditions were 24.8 °C and 58.1 % RH. These conditions are well within the psychrometric comfort Zone described in ASHRAE's Standard 55 and Chapter 9 on Thermal comfort in their Fundamentals Handbook [48], [50]. The absolute maximum humidity ratio for the enthalpy bypass is the same as the baseline: 0.015 kg_{water} / $kg_{dry\ air}$.

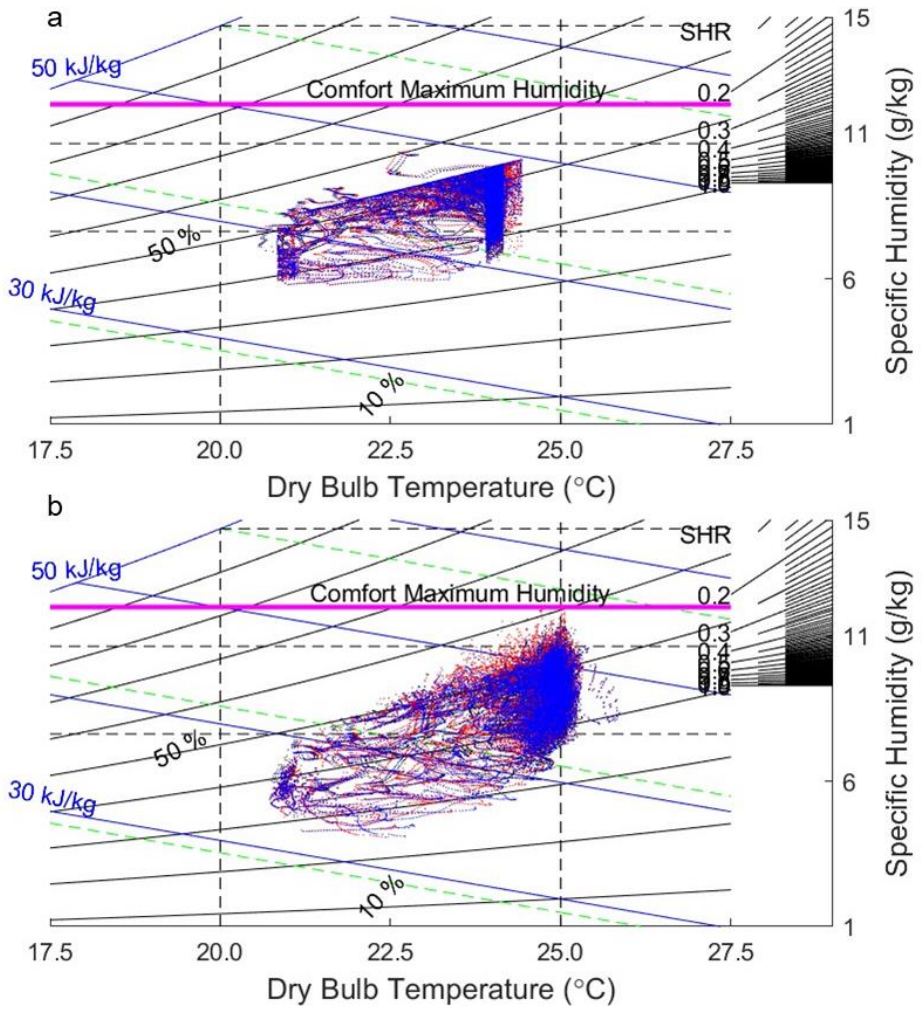

Figure 52. Psychrometric plots of (a) Zone 2 and (b) Zone 3 conditions during cooling season for baseline, temperature bypass control, and enthalpic bypass control during cooling season.

This control strategy proves effective at managing the thermal comfort of the building while reducing heat pump load demands and energy. The enthalpy control is very effective at reducing the latent loads and excessive relative humidity; otherwise, it occurs with temperature-based bypass control.

Chapter 5: Conclusions

Climate change's impact on our world is felt more acutely every day. The average global temperature continues to rise, ice caps are melting more rapidly, and it is all exacerbated by the increasing carbon dioxide concentration in our atmosphere. The need to reduce carbon emissions is paramount. Residential buildings consume nearly 15 % of the energy used in the United States annually. To curb this energy use, more and more residential buildings are being built or retrofitted with a net zero energy consumption goal to reduce total consumption and electrical grid reliance. To assist the building community with a better understanding of these buildings, NIST built its Net Zero Energy Residential Test Facility to test and accurately measure the performance of the entire building and various equipment in a typical use case of a family of four.

A recovery ventilator has been installed at the facility for over 5 years with the option of using either a heat recovery core to reduce sensible loads entering the facility or an energy recovery core that can also manage the latent loads. Preconditioning the outdoor air to reduce heat pump load can save a significant amount of energy for the building, but there are times when the outdoor air can be utilized to cool the building. When this is not done, the building load is increased. To prevent this unnecessary increase in building thermal load, the ERV has an optional bypass mode that can be enabled to allow cooler outdoor air to enter the home without exchanging with warmer indoor air during the cooling season.

This free cooling option has been run at the NZERTF for a short period of time when conditions permitted, but time availability and scheduling conflicts prevented further investigation into the control strategy. To gain a better understanding of the bypass mode's potential for saving electricity at the NZERTF, a TRNSYS model was updated, tuned, and validated compared to the 2024 measured performance.

5.1 Summary of Results

The model updates and tuning covered a wide range of model parameters. Updates included a new thermostat control scheme to match the custom thermostat installed about six years ago, updating the schedule files to represent recent sensible and latent loads and specifications for the Zehnder ERV that was installed since the TRNSYS model was last tuned. The updated model was checked for accuracy against three different periods in 2024 and found to have several deficiencies in simulating actual building operation including heat pump operation, Zone temperature and humidity conditions, and ERV loads. This necessitated additional tuning of the model based on 2024 measurements and performance.

Tuning included updating the type 56 multizone energy model to better represent the facility's moisture capacitance and the Zone air interactions. This led to more reliable Zone humidities as the moisture capacitance models were updated and refined. The HVAC airflows also assisted in the influence of Zone 1's conditions on Zone 2, which has been observed through the years. The heat pump's performance

curves, nominal capacity, and power draw were updated for dehumidification mode, stage 1 cooling, and stage 1 heating. These parameters combined helped to ensure that the Zone conditions were reliably predicted. This was particularly critical to ensure that the return air conditions were accurate so that the ERV supply air could match the measured values.

Most importantly, the ERV effectiveness was reliably characterized for a range of conditions. The effectiveness was determined by regression analysis using equations 6 and 7. The sensible effectiveness is only a function of flow rate and had a nominal effectiveness of 0.87. The latent effectiveness is dependent on the outdoor conditions as well as the mass flow rate. However, it could not be summarized into a single equation. Instead, the latent effectiveness was separated into three separate equations based on weather conditions: humid, cold-and-dry, and freezing. The nominal effectiveness for these conditions is 0.600, 0.302, and 0.364 respectively. The ERV's effectiveness was also evaluated during bypass mode. Since no actual exchange occurs in bypass mode, these values can also be considered loss coefficients for the temperature and moisture of the air. The nominal effectiveness values in bypass mode are 0.313 for sensible and 0.060 for latent representing a slight prewarming of the supply air as it goes through the ERV and barely any moisture loss from the supply air stream.

These updated parameters were used to confirm that the new model could successfully simulate the temperature-based bypass control utilized in May – July of 2024. While the actual system did not maximize free cooling since a bypass detection

algorithm could not reliably detect if the ERV went into bypass mode, the model was left to maximize free cooling. This setup allowed for a best-case scenario of free cooling because the custom type 1273 ERV control reliably predicted bypass mode in this tuning period.

A temperature-based bypass mode control and an enthalpic bypass mode control were compared to a no-bypass mode case to observe the effects on heat pump load, energy usage, and thermal comfort for occupants. The temperature-based control maximized free cooling and reduced the ERV sensible load by about 85.3 % relative to the no bypass condition. It also decreased the annual heat pump load by 0.35 % but saw a net increase in heat pump energy use of 2.4 % relative to the no bypass case due to the 32.4 % increase in ERV latent load allowed into the house. The enthalpic control significantly only increased the ERV latent loads into the building by 11.6 % above baseline. So, despite less accessible free cooling (33.3 % above baseline), the enthalpic control decreased the heat pump load by 0.80 % and saved 0.22 % of annual heat pump energy.

Both conditions still maintained thermal comfort throughout cooling season. The Zone 3 temperature drifted up to nearly 26 °C for the temperature-based control while the enthalpic control remained closer to baseline with a maximum Zone 3 temperature of 24.8 °C. The humidity ratio never exceeded the 0.012 kg_{water} / $kg_{dry\ air}$ comfort limit for either case, though the temperature-based control did reach the limit in a few cases. The enthalpic control had fewer deviations from the baseline condition

and a lower humidity than the temperature-based control with its maximum humidity ratio matching the baseline case.

5.2 Conclusions

An improved TRNSYS model of the NZERTF was developed and tuned to recent building performance. Its improvements include updated performance for the ASHP and ERV and has updated building parameters to ensure reliable Zone condition modeling. This model will pave the way for accurate simulations going forward including projections of equipment planned to be installed in the facility soon.

Regarding the bypass control schema, the NZERTF does not significantly benefit from ERV bypass control to maximize or optimize the free cooling of the building. While it did not lead to any significant thermal comfort concerns, the temperature-based scheme led to an increase in building energy consumption while the enthalpic control only saw modest energy savings. For this building in this mixed-humid climate zone, neither method is recommended. But, seeing the enthalpic control save energy means that it may have a larger impact in the region for larger buildings. For example, it may be possible to utilize a DOAS with free cooling capability in a larger multifamily residential building. Larger buildings with a smaller surface area to volume ratio end up with regions of the building requiring additional cooling even if the exterior Zones of the building have sufficient cooling.

Chapter 6: Future Work

While this work may not have led to an immediate opportunity for further research at the NZERTF, there are still several different topics to consider for this work to expand into. First, additional testing should be run throughout the summer months to gain further understanding of the latent effectiveness with and without bypass mode across a wider range of flow rates. The ERV is typically operated at 50 % of maximum or about 100 CFM, but reliably predicting the latent effectiveness could lead to finding a happy medium in terms of reducing latent loads while ensuring sufficient ventilation is supplied. Along with these tests, the same measurements could be taken for ventilation equipment's HRV core. It provides effectively no moisture transfer, but anecdotally does offer more sensible heat transfer.

Combining the updated latent effectiveness parameters with some validation testing of the enthalpic bypass control could help confirm the TRNSYS model findings of modest energy savings. This will be difficult to implement because of the ERV's proprietary controller. But it could prove useful in further refining the TRNSYS model.

These control schemes could also be tested out on the other ASHRAE climate zones to validate where they may best serve a NZEB with an installed ERV. It is clear from this work that a humid climate provides a few challenges for enabling free cooling, especially based on temperature. But what is the most humid environment

where this control scheme could be more beneficial? And how much better does the ERV perform with free cooling options than the HRV? Additional research and simulations could answer these questions.

The model is successful at simulating the return air conditions in the house and generally predicts the Zone conditions with reasonable accuracy. However, there is an opportunity to improve these components of the model further by integrating CONTAM, a multizone indoor air quality and ventilation analysis program, which comes with the capability of being coupled with TRNSYS. CONTAM can effectively model the airflows between the three occupied Zones of the NZERTF.

Appendix I: TRNSYS Model Parameters

Table I-1. Building Moisture Capacitance - Untuned

Zone	Moisture Capacitance Ratio
1 (basement)	2.2
2 (first floor)	2.2
3 (second floor)	2.2
4 (attic)	1

Table I-2. ASHP Parameters - Untuned

Type	Parameter	Value	Units
First and Second Stage Type 922	Total air flow rate – Low speed	624	CFM
	Rated Total Cooling Capacity – Low Speed	5425	W
	Rated Sensible Cooling Capacity – Low Speed	4088	W
	Rated Cooling Power – Low Speed	1440	W
	Rated Heating Capacity – Low Speed	5180	W
	Rated Heating Power – Low Speed	1398	W
	Total air flow rate – High Speed	836	CFM
	Rated Total Cooling Capacity – High Speed	7067	W
	Rated Sensible Cooling Capacity – High Speed	5360	W
	Rated Cooling Power – High Speed	2420	W
	Rated Heating Capacity – High Speed	8041	W
	Rated Heating Power – High Speed	2126	W
Dehumidification Type 922	Total air flow rate – Low speed	603	CFM
	Rated Total Cooling Capacity – Low Speed	5997	W
	Rated Sensible Cooling Capacity – Low Speed	4177	W
	Rated Cooling Power – Low Speed	1820	W
	Total air flow rate – High speed	549	CFM
	Rated Total Cooling Capacity – High Speed	1653	W
	Rated Sensible Cooling Capacity – High Speed	423	W
	Rated Cooling Power – High Speed	1230	W
3rd Stage Heating Type 922	Rated Air Flowrate	992	CFM
	Rated Heating Capacity	5056	W
	Rated Heat Power	2056	W

Table I-3. Building Moisture Capacitance - Tuned

Zone		Gradient of Sorptive Isothermal Line	Mass	Exchange Coefficient	Moisture Capacitance Ratio
Zone 1 (basement)		-	-	-	162.6
Zone 2 (first floor)	Surface Storage	0.0075	991.9	818.6	-
	Deep Storage	1	56.6	272.9	
Zone 3 (second floor)	Surface Storage	0.0075	880.5	749.5	-
	Deep Storage	1	46.3	249.8	
Zone 4 (attic)		-	-	-	1

Table I-4. ERV Type 111b Fan Power Coefficients - Tuned

Coefficient	Stale Air Fan	Fresh Air Fan
P_0	21.20	21.72
c_0	4.263	4.281
c_1	-12.55	-12.53
c_2	12.49	12.47
c_3	-3.201	-3.200

Table I-5. ERV Effectiveness Fit Parameters (no bypass mode) - Tuned

Coefficient	Sensible Effectiveness	Latent Effectiveness		
		Humid	Cold/Dry	Freezing
ε_0	0.870	0.601	0.302	0.364
c_0	1.11	-0.264	2.88	1.677
c_1	-0.129	2.27	-2.65	-0.842
c_2	0.019	-1.004	0.771	0.165

Table I. I-6. ERV Bypass Mode Effectiveness Parameters - Tuned

Coefficient	Sensible Effectiveness	Latent Effectiveness
ε_0	0.313	0.060
c_0	1.437	25.4
c_1	-1.004	-44.1
c_2	0.568	19.7

Table I-7. ASHP Parameters - Tuned

Type	**Parameter**	**Value**	**Units**
First and Second Stage Type 922	Total air flow rate – Low speed	600	CFM
	Rated Total Cooling Capacity – Low Speed	5425	W
	Rated Sensible Cooling Capacity – Low Speed	4155	W
	Rated Cooling Power – Low Speed	1351	W
	Rated Heating Capacity – Low Speed	7034	W
	Rated Heating Power – Low Speed	1379	W
	Total air flow rate – High Speed	784	CFM
	Rated Total Cooling Capacity – High Speed	7067	W
	Rated Sensible Cooling Capacity – High Speed	5360	W
	Rated Cooling Power – High Speed	2420	W
	Rated Heating Capacity – High Speed	8041	W
	Rated Heating Power – High Speed	2126	W
Dehumidification Type 922	Total air flow rate – Low speed	497	CFM
	Rated Total Cooling Capacity – Low Speed	3006	W
	Rated Sensible Cooling Capacity – Low Speed	286	W
	Rated Cooling Power – Low Speed	1531	W
	Total air flow rate – High speed	549	CFM
	Rated Total Cooling Capacity – High Speed	549	W
	Rated Sensible Cooling Capacity – High Speed	1653	W
	Rated Cooling Power – High Speed	423	W
3rd Stage Heating Type 922	Rated Air Flowrate	992	CFM
	Rated Heating Capacity	5056	W
	Rated Heat Power	2056	W

Appendix II: Heat Pump Performance Curves

Table II-1. ASHP Dehumidification Mode Curve Fits where C_0 is nominal parameter input in Appendix I.

$$Total\ Capacity\ [W] = C_0\left(0.992 + 0.224T_{in,wb} - 0.160T_{in,db}\right) \quad (9)$$

$$Sensible\ Capacity\ [W] = C_0\left(-1.17 + 0.144T_{in,wb}\right) \quad (10)$$

$$Power\ Draw\ [W] = C_0\left(0.810 + 0.018T_{in,wb} - 0.005T_{in,db}\right) \quad (11)$$

Table II-2. ASHP Low Speed Cooling Curve Fits where C_0 is nominal parameter input in Appendix I.

$$Total\ Capacity\ [W] = C_0\left(0.6386 - 0.0044T_{out,db} + 0.0285T_{in,wb}\right) \quad (12)$$

$$Sensible\ Capacity\ [W] = C_0\left(1.973 - 0.0007T_{out,db} - 0.057T_{in,wb}\right) \quad (13)$$

$$Power\ Draw\ [W] = C_0\left(0.4889 + 0.019T_{out,db}\right) \quad (14)$$

Table I. II-3. ASHP Low Speed Heating Curve Fits where C_0 is nominal parameter input in Appendix I.

$$Total\ Capacity\ [W] = C_0(0.150 + 0.0556\ln\left(T_{out,db} + 10\ °C\right) + 0.0414\ln\left(T_{out,db} + 10\ °C\right)^2 \quad (15)$$

$$Power\ Draw\ [W] = C_0(0.887 - 0.0084\ln\left(T_{out,db} + 10\ °C\right) + 0.0212\ln\left(T_{out,db} + 10\ °C\right)^2 \quad (16)$$

References

[1] "Global Temperature | Vital Signs – Climate Change: Vital Signs of the Planet." Accessed: Feb. 02, 2025. [Online]. Available: https://climate.nasa.gov/vital-signs/global-temperature/?intent=111

[2] Reinhardt Radermacher, "ENME 701 Course Lectures," Sep. 17, 2024, *College Park*.

[3] "Carbon Dioxide | Vital Signs – Climate Change: Vital Signs of the Planet." Accessed: Feb. 02, 2025. [Online]. Available: https://climate.nasa.gov/vital-signs/carbon-dioxide/?intent=111

[4] "Arctic Sea Ice Minimum Extent | Vital Signs – Climate Change: Vital Signs of the Planet." Accessed: Feb. 02, 2025. [Online]. Available: https://climate.nasa.gov/vital-signs/arctic-sea-ice/?intent=111

[5] "Sea Level | Vital Signs – Climate Change: Vital Signs of the Planet." Accessed: Feb. 02, 2025. [Online]. Available: https://climate.nasa.gov/vital-signs/sea-level/?intent=111

[6] M. K. van Aalst, "The impacts of climate change on the risk of natural disasters," *Disasters*, vol. 30, no. 1, pp. 5–18, Mar. 2006, doi: 10.1111/J.1467-9523.2006.00303.X.

[7] M. Berlemann and M. F. Steinhardt, "Climate Change, Natural Disasters, and Migration—a Survey of the Empirical Evidence," *CESifo Econ Stud*, vol. 63, no. 4, pp. 353–385, Dec. 2017, doi: 10.1093/CESIFO/IFX019.

[8] "U.S. energy facts explained - consumption and production - U.S. Energy Information Administration (EIA)." Accessed: Feb. 02, 2025. [Online]. Available: https://www.eia.gov/energyexplained/us-energy-facts/

[9] "Carbon Flow Charts | Flowcharts." Accessed: Feb. 02, 2025. [Online]. Available: https://flowcharts.llnl.gov/commodities/carbon

[10] "Summary of the Energy Independence and Security Act | US EPA." Accessed: Feb. 02, 2025. [Online]. Available: https://www.epa.gov/laws-regulations/summary-energy-independence-and-security-act

[11] A. Alajmi, S. Rodríguez, and D. Sailor, "Transforming a passive house into a net-zero energy house: a case study in the Pacific Northwest of the U.S.," *Energy Convers Manag*, vol. 172, pp. 39–49, Sep. 2018, doi: 10.1016/J.ENCONMAN.2018.06.107.

[12] A. H. Fanney *et al.*, "Net-zero and beyond! Design and performance of NIST's net-zero energy residential test facility," *Energy Build*, vol. 101, pp. 95–109, May 2015, doi: 10.1016/J.ENBUILD.2015.05.002.

[13] A. Hunter Fanney *et al.*, "Small Changes Yield Large Results at NIST's Net-Zero Energy Residential Test Facility," *Journal of Solar Energy Engineering, Transactions of the ASME*, vol. 139, no. 6, Dec. 2017, doi: 10.1115/1.4037815/379755.

[14] W. Wu and H. M. Skye, "Net-zero nation: HVAC and PV systems for residential net-zero energy buildings across the United States," *Energy*

Convers Manag, vol. 177, pp. 605–628, Dec. 2018, doi: 10.1016/j.enconman.2018.09.084.

[15] M. Shirinbakhsh and L. D. D. Harvey, "Net-zero energy buildings: The influence of definition on greenhouse gas emissions," *Energy Build*, vol. 247, p. 111118, Sep. 2021, doi: 10.1016/J.ENBUILD.2021.111118.

[16] D. D'Agostino and L. Mazzarella, "What is a Nearly zero energy building? Overview, implementation and comparison of definitions," *Journal of Building Engineering*, vol. 21, pp. 200–212, Jan. 2019, doi: 10.1016/J.JOBE.2018.10.019.

[17] "DOE Releases First Ever Federal Blueprint to Decarbonize America's Buildings Sector | Department of Energy." Accessed: Feb. 02, 2025. [Online]. Available: https://www.energy.gov/articles/doe-releases-first-ever-federal-blueprint-decarbonize-americas-buildings-sector

[18] "Zero Energy-Verified Commercial Buildings More Than Double Since 2018 - New Buildings Institute." Accessed: Feb. 02, 2025. [Online]. Available: https://newbuildings.org/news/zero-energy-verified-commercial-buildings-more-than-double-since-2018/

[19] *ANSI/ASHRAE Standard 228, Standard Method of Evaluating Zero Net Energy and Zero Net Carbon Building Performance | ashrae.org*. 2023. Accessed: Feb. 02, 2025. [Online]. Available: https://www.ashrae.org/technical-resources/bookstore/ansi-ashrae-standard-228-standard-method-of-evaluating-zero-net-energy-and-zero-net-carbon-building-performance

[20] *ANSI/ASHRAE/IES Standard 90.2-2024, High-Performance Energy Design of Residential Buildings*. Peachtree Corners, 2024. [Online]. Available: www.ashrae.org/technology.

[21] B. Pettit, C. Gates, A. H. Fanney, and W. M. Healy, "Design Challenges of the NIST Net Zero Energy Residential Test Facility", doi: 10.6028/NIST.TN.1847.

[22] W. Wu, H. M. Skye, and P. A. Domanski, "Selecting HVAC systems to achieve comfortable and cost-effective residential net-zero energy buildings," *Appl Energy*, vol. 212, pp. 577–591, Feb. 2018, doi: 10.1016/j.apenergy.2017.12.046.

[23] "Total U.S. a".

[24] S. Oh, J. S. Haberl, and J. C. Baltazar, "Analysis of zone-by-zone indoor environmental conditions and electricity savings from the use of a smart thermostat: A residential case study," *Sci Technol Built Environ*, vol. 26, no. 3, pp. 285–303, Mar. 2020, doi: 10.1080/23744731.2019.1707618.

[25] "Net Zero Energy Residential Test Facility Instrumented Data; Year 1 | Commerce Data Hub." Accessed: Feb. 02, 2025. [Online]. Available: https://data.commerce.gov/net-zero-energy-residential-test-facility-instrumented-data-year-1

[26] W. M. Healy *et al.*, "Performance Data from the NIST Net-Zero Energy Residential Test Facility," vol. 122, no. 14, 2017, doi: 10.6028/jres.122.014.

[27] B. P. Leyde, "TRNSYS Modeling of the NIST Net Zero Energy Residential Test Facility," 2014.

[28] E. C. Balke, “Modeling, Validation, and Evaluation of the NIST Net Zero Energy Residential Test Facility,” 2016.

[29] J. D. Kneifel and E. G. O’Rear, “An Assessment of Typical Weather Year Data Impacts vs. Multi-year Weather Data on Net-Zero Energy Building Simulations,” Gaithersburg, MD, Jan. 2016. doi: 10.6028/NIST.SP.1204.

[30] J. D. Kneifel, “Simulated versus Measured Energy Performance of the NIST Net Zero Energy Residential Test Facility Design,” Gaithersburg, MD, Mar. 2015. doi: 10.6028/NIST.SP.1182.

[31] “Standards 62.1 & 62.2.” Accessed: Mar. 23, 2025. [Online]. Available: https://www.ashrae.org/technical-resources/bookstore/standards-62-1-62-2

[32] L. C. Ng and W. V. Payne, “Energy use consequences of ventilating a net-zero energy house,” *Appl Therm Eng*, vol. 96, pp. 151–160, Mar. 2016, doi: 10.1016/J.APPLTHERMALENG.2015.10.100.

[33] M. Rasouli, C. J. Simonson, and R. W. Besant, “Applicability and optimum control strategy of energy recovery ventilators in different climatic conditions,” *Energy Build*, vol. 42, no. 9, pp. 1376–1385, 2010, doi: 10.1016/j.enbuild.2010.03.006.

[34] J. Li, R. Zmeureanu, and H. Ge, “Simulation of energy impact of an energy recovery ventilator in Northern housing,” in *E3S Web of Conferences*, EDP Sciences, Mar. 2021. doi: 10.1051/e3sconf/202124610005.

[35] O. Ribé, R. Ruiz, M. Quera, and J. Cadafalch, “Analysis of the sensible and total ventilation energy recovery potential in different climate conditions.

Application to the Spanish case," *Appl Therm Eng*, vol. 149, pp. 854–861, Feb. 2019, doi: 10.1016/j.applthermaleng.2018.12.076.

[36] S. Guillén-Lambea, B. Rodríguez-Soria, and J. M. Marín, "Control strategies for Energy Recovery Ventilators in the South of Europe for residential nZEB—Quantitative analysis of the air conditioning demand," *Energy Build*, vol. 146, pp. 271–282, Jul. 2017, doi: 10.1016/j.enbuild.2017.04.058.

[37] J. Lee, D. Song, J. Kim, and J. Lee, "ENERGY SAVING EFFECT OF THE ERV (ENERGY RECOVERY VENTILATOR) WITH OUTDOOR AIR COOLING."

[38] J. S. Choi, S. H. Park, B. K. Jeon, and E. J. Kim, "Simulation analysis of energy saving effect of ERV on EHP heating energy consumption in a classroom," in *IOP Conference Series: Earth and Environmental Science*, Institute of Physics Publishing, Mar. 2019. doi: 10.1088/1755-1315/238/1/012061.

[39] R. Al-Waked, D. Bani Mostafa, and M. S. Nasif, "Performance of energy recovery ventilators under different climatic regions," *Energy Effic*, vol. 14, no. 1, Jan. 2021, doi: 10.1007/s12053-020-09917-w.

[40] J. L. Zhang and A. S. Fung, "Feasibility Study of Multiple-Pass Total Energy Recovery Ventila-tor with Built-in Economizer Using TRNSYS: A Case Study for Toronto, Ontario."

[41] W. Wu, Z. Fang, W. Ji, and H. Wang, “Optimal operation condition division with profit and losses analysis of energy recovery ventilator,” *Energy Build*, vol. 124, pp. 203–209, Jul. 2016, doi: 10.1016/j.enbuild.2015.11.048.

[42] “ASHRAE 169-2021 | ASHRAE Store.” Accessed: Feb. 02, 2025. [Online]. Available: https://store.accuristech.com/ashrae/standards/ashrae-169-2021?product_id=2238548

[43] F. Omar and S. T. Bushby, “Simulating Occupancy in the NIST Net-Zero Energy Residential Test Facility”, doi: 10.6028/NIST.TN.1817.

[44] E. Wilson, C. E. Metzger, S. Horowitz, and R. Hendron, “2014 Building America House Simulation Protocols,” 2014, Accessed: Feb. 21, 2025. [Online]. Available: www.nrel.gov/publications.

[45] J. Wang, M. H. N. Yio, T. Zhou, H. S. Wong, C. T. Davie, and E. Masoero, “Water sorption isotherms and hysteresis of cement paste at moderately high temperature, up to 80 °C,” *Cem Concr Res*, vol. 165, p. 107076, Mar. 2023, doi: 10.1016/J.CEMCONRES.2022.107076.

[46] S. By and C. M. James, “Heat and Moisture Transfer in a Bed of Gypsum Boards”.

[47] “TRNSYS 16-Multizone Building modeling with Type56 and TRNBuild,” 2007, Accessed: Mar. 15, 2025. [Online]. Available: http://sel.me.wisc.edu/trnsyshttp://software.cstb.frhttp://www.tess-inc.com

[48] “ASHRAE Handbook Online - Handbook.” Accessed: Feb. 02, 2025. [Online]. Available: https://handbook.ashrae.org/Handbook.aspx

[49] M. Davis *et al.*, “Monitoring Techniques for the Net-Zero Energy Residential Test Facility”, doi: 10.6028/NIST.TN.1854.

[50] “Standard 55 – Thermal Environmental Conditions for Human Occupancy.” Accessed: Mar. 22, 2025. [Online]. Available: https://www.ashrae.org/technical-resources/bookstore/standard-55-thermal-environmental-conditions-for-human-occupancy